Effect of Brightener and Solution Temperature on the Electrodeposition Behavior of Zn-Ni alloy from Alkaline Zincate Solution

裵，聖和

Effect of Brightener and Solution Temperature on the Electrodeposition Behavior of Zn-Ni alloy from Alkaline Zincate Solution

2022

BAE SEONGHWA

Table of contents

Chapter 1. Introduction

1-1. Foreword

Electroplating is a surface treatment technology using electrolytic methods to impart a uniform and dense layer of metals or alloys onto the surface of the materials. The history of electroplating began in the 1800's when the voltaic battery was introduced, and it has been widely used to improve the surface properties of materials such as metal decoration, corrosion resistance and wear resistance.[1-3] Alloy plating has become more important in recent years. It has a higher corrosion resistance than single metal plating, and the crystal particles created through alloy plating are fine.[4-10] Therefore, the layer has excellent properties, such as local corrosion prevention and relatively good hardness. There is also the advantage that changes in the composition of an alloy can produce various properties of the plated coating. For alloy plating, it is preferable that the deposition potentials of each ion in the solution are close to each other. Usually, the deposition potentials are far apart. In such cases, metal ions complex is formed in the plating solution and additives are added to bring the deposition potentials of each metal closer together. To deposit two metals onto a cathode surface simultaneously, their deposition potentials must be the same. Therefore, if the following equation is satisfied, the two metals will be deposited simultaneously to form an alloy electrodeposition.[11-15]

$$E_1^0 + \frac{RT}{Z_1 F} ln a_1 + \eta_1 = E_2^0 + \frac{RT}{Z_2 F} ln a_2 + \eta_2$$

Here, subscripts 1 and 2 indicate the type of each ion. E_1^0 and E_2^0 are the standard electrode potential of each metal ion, and Z_1 and Z_2 are the valency of each metal ion. a_1 and a_2 represent the activity of each ion, η_1 , η_2 are the overpotential for each metal deposition, R is the gas constant, F is Faraday's constant, and T is the absolute temperature.

Cyanide has been widely used as a metal complexing agent since early times, but it is toxic and poses various difficulties in handling and wastewater treatment. Therefore, ammonia salt, EDTA, pyrophosphate, citrate, triethanolamine, etc. are also used as a metal complexing agent. The plating solution composition, such as concentrations of metal ions and complexing agent, pH and additives, and electrolytic conditions such as current density, temperature are intricately intertwined with each other in influencing alloy deposition.

The Zn-Ni alloy electroplating reviewed in this study has received much attention because of its excellent corrosion resistance and has been applied to automotive parts, home appliances and parts for building materials. Zn-Ni alloy electrodeposition is usually performed in a sulfate or chloride solution, but from the viewpoint of uniform electrodeposition on small parts, etc., a zincate solution is preferred. Many studies have been conducted on Zn-Ni alloy electrodeposition in sulfate and chloride solutions, and it is known that

electrochemically less noble Zn is preferentially deposited over nobler Ni in regions of practical current density, indicating an anomalous co-deposition behavior. The following factors have been reported for the electrodeposition of Zn-Ni alloys from zincate solutions: the effects of current density, concentrations of total metal salt and Ni complexing agent, solution composition, and stirring of solution on the Ni content in the deposited films, and the effect of current density on the current efficiency of alloy electrodeposition. However, there are few studies on the electrodeposition mechanism when using a zincate solution compared with the cases of using a sulfate solution or a chloride solution. Further, brighteners are usually added to electrodeposition from a zincate solution. It is possible that brighteners affect the electrodeposition behavior, but the effect of brightener on the electrodeposition behavior has not yet been clarified. In contrast, solution temperature is known to affect the overpotential for electrodeposition, uniform electrodeposition (throwing power), solubility of metal salts, and solution conductivity. The conductivity of the solution increases with an increase in the solution temperature. In addition, the diffusion limiting current density of metal deposition can be increased with an increase in temperature because the diffusion coefficients of ions and the solubilities of metal salts increase. When the solution temperature is decreased, the crystal grains of the electrodeposited films become finer, and the uniformity of the electrodeposition is improved due to increase in overpotential for electrodeposition. Thus, solution temperature is an extremely important factor in electrodeposition, but the effect of solution temperature on the electrodeposition behavior of Zn-Ni alloys from zincate solutions has rarely been reported.

1-2. Type of Alloy Deposition

In Abner Brenner's book ″Electrodeposition of Alloys: Principles and Practice ″,[4] the classification of alloy deposition is as follows:

  (1) Normal co-deposition

      From a theoretical point of view, this is when the deposition of noble metals is greater than that of less noble metals (Fig. 1-1).

  1) Regular co-deposition

   The deposition from hydrated ions occurs under conditions in which the deposition of the nobler metal is diffusion-dominated when the equilibrium potentials of two metals are far apart. Nobler metal is more easily depleted in the cathode layer because it deposits more easily. Therefore, the amount of nobler metal in the deposited films increases when

the electrolytic factors are changed to prevent the depletion of metal ions in the cathode layer, such as increasing the temperature and the concentration of total metal ion, agitation, and decreasing the current density.

2) Irregular co-deposition

This occurs readily when the deposition potentials of two metals are close to each other due to complexation. As the composition of deposited films is calculated from a superposition of the Tafel parts of the partial polarization curves of each metal, the effect of electrolytic factor on the composition of the deposited films is smaller than that of the regular type.

3) Equilibrium co-deposition

This is observed when each metal in deposited films and each metal ion in solution can be considered to be in equilibrium. When the standard electrode potentials are almost equal, the composition of the deposited films is identical with the concentration ratio of the metal ions in the solution. When out of equilibrium, the regular or irregular type of co-deposition behavior is observed. This is not important in practical usage because it occurs only at low current densities.

(2) Abnormal co-deposition

This is a case not based on electrochemical theory. This describes a case in which the less noble metal preferentially deposits (Fig. 1-1).

1) Anomalous co-deposition

In the metal deposition process, the metal with a less noble equilibrium potential preferentially deposits above a certain current density, and its content in deposited films becomes higher than that in the electrolytic solution. This phenomenon mainly appears in alloy electrodeposition between Fe, Co and Ni of iron group metal elements and Zn.

2) Induced co-deposition

The metals such as W and Mo that do not deposit as a single metal in aqueous solutions can co-deposit with Fe Ni and Co of iron-group metal.
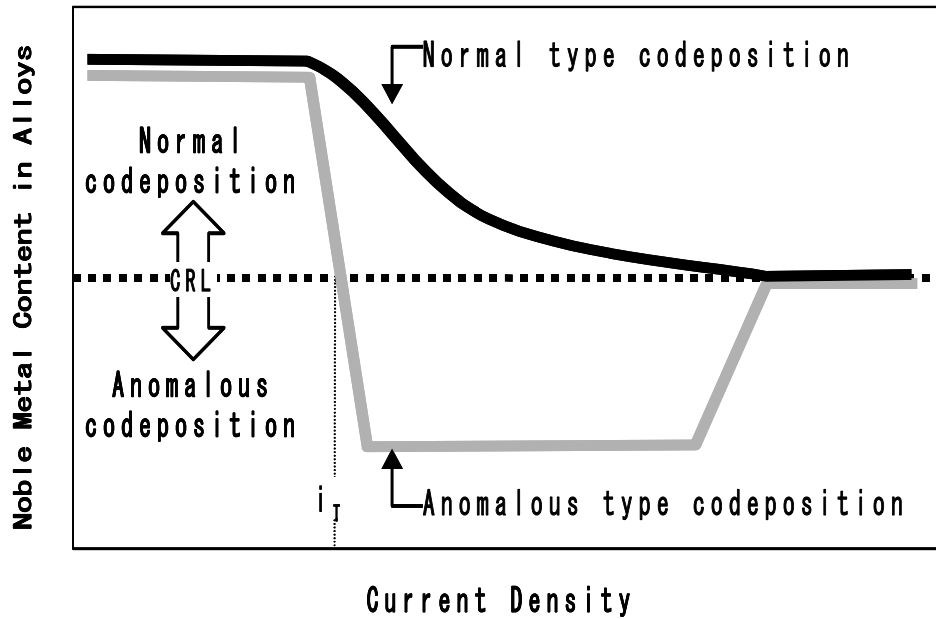
Fig. 1-1. Current density-dependence of the content of noble metal in the

alloys in the normal and the anomalous type codeposition

i_T: transition current density

CRL: concentration ratio of noble metal ions against

the total metal ions in solution

1-3. Underpotential Deposition

In electrochemistry, a metal deposition at nobler potential than its equilibrium potential calculated by the Nernst equation is known as an underpotential deposition. These underpotential depositions were first mentioned in a book by Moïse-Haïssinsky[16-19], and authors such as Haenny[20,21], Rogers[22-30], and others have described underpotential depositions using the current-potential curves (voltammograms). In 1949, Rogers interpreted the underpotential deposition using thermodynamics and suggested that the metal activity in Nernst equation must be considered to understand the underpotential deposition.[32]

Here, the equilibrium potential of metal M deposition is given by the Nernst equation as:

$$E_M^{eq} = E_M^0 + \frac{RT}{nF}\ln\left(\frac{a_{M^{n+}}}{a_M}\right)$$

Here, E_M^0: standard potential of metal M deposition, E_M^{eq} : equilibrium potential during metal M deposition, T: absolute temperature, n: metal valence, F: Faraday constant, R: gas constant, $a_{M^{n+}}$: activity of metal ions, a_M: activity of the metal, and $a_M = f_M X_M$ (f_M: activity coefficient of metal, X_M: mole fraction of metal).

- 4 -

When a metal is electrodeposited onto a metal cathode made of a different metal, the mole fraction X_M of the deposition metal is zero before the start of the deposition, so $a_M = 0$. From the above Nernst equation, it is considered that the equilibrium potential of the metal shifts infinitely to the positive region at the moment of the initial stage of electrodeposition. As a result, in the very early stage of electrodeposition, metal electrodeposition becomes possible even in a more noble potential region than the equilibrium potential calculated under steady-state conditions ($a_M = 1$ in single metal electrodeposition).

In the 1970s, Kolb et al. reported that underpotential-deposition of less noble metal atoms on noble metal materials was possible according to their experiments of Ag deposition on Pt.[32]
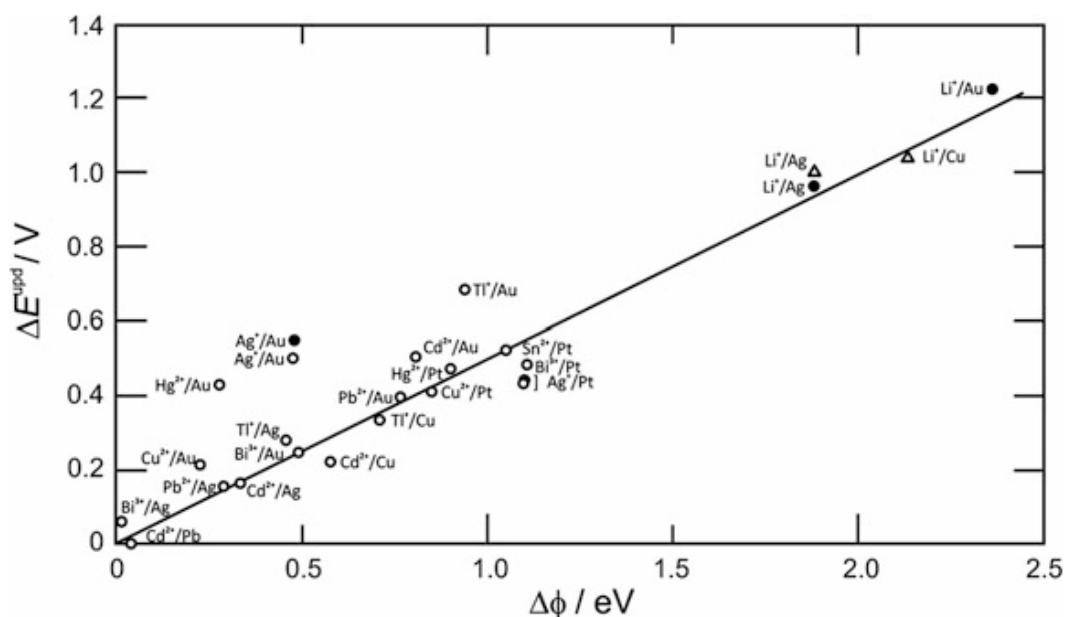
Fig. 1-2. Underpotential shift ΔE_{upd} between bulk and monolayer stripping peak as a function of the difference in work functions of the substrate and atom. The respective ions are indicated in the figure. [32] (○) aqueous solution; (●) acetonitrile; (△) propylene carbonate

A correlation between the potential shift of the substrate and the adsorbate and the difference in work functions was found, based on the experimental results.[32]

$$\Delta E = 0.5\Delta\varphi$$

ΔE: difference in potential required for bulk deposition and

monolayer deposition

$\Delta\varphi$: difference in work function between more noble bulk metals and
monolayer-deposited metals

As shown in Fig. 1-2, the slope between ΔE and $\Delta\varphi$ is close to 0.5. Using this

relationship, it seems that the underpotential deposition of less noble metal atoms on more noble metal substrates is possible. However, the underpotential deposition of Zn on Fe and Cu cathodes, which are more noble metals, does not occur in a Zn-only solution.

1-4. Previous studies on electrodeposition of Zn-Ni alloys

Shibuya and Kurimoto observed a pH increase in the cathode layer at high current density in Zn-Ni alloy deposition from a sulfate solution, and they reported that the change in relative deposition rate between Ni and Zn due to change in thickness of the Zn hydroxide layer affects the composition and the phase structure of the electrodeposited alloy (Fig. 1-3). [33]

Fig. 1-3 Electrodeposition of Ni-Zn alloys from sulfate solution.[33]
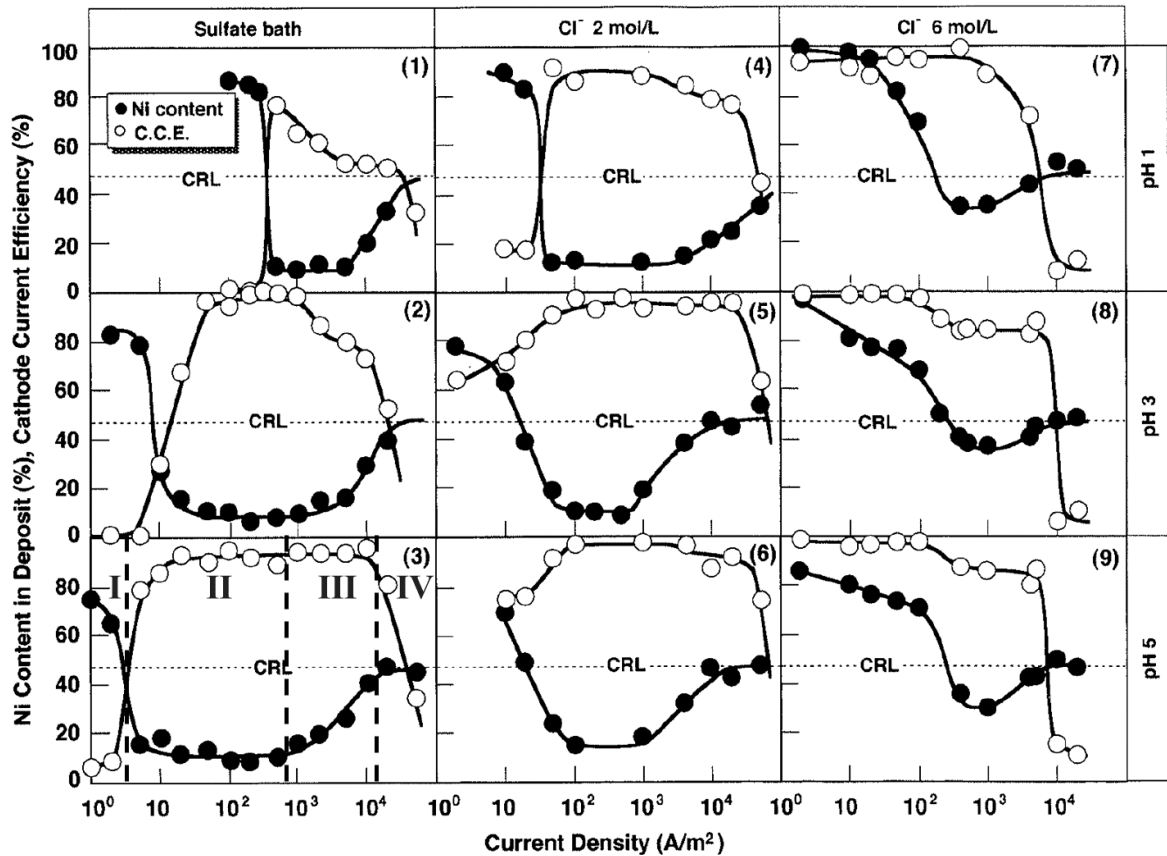
Fig. 1-4. Effect of current density on the alloy composition and the current efficiency for Zn-Ni alloy deposition from sulfate solutions with various pH values and chloride ion concentrations.[34]
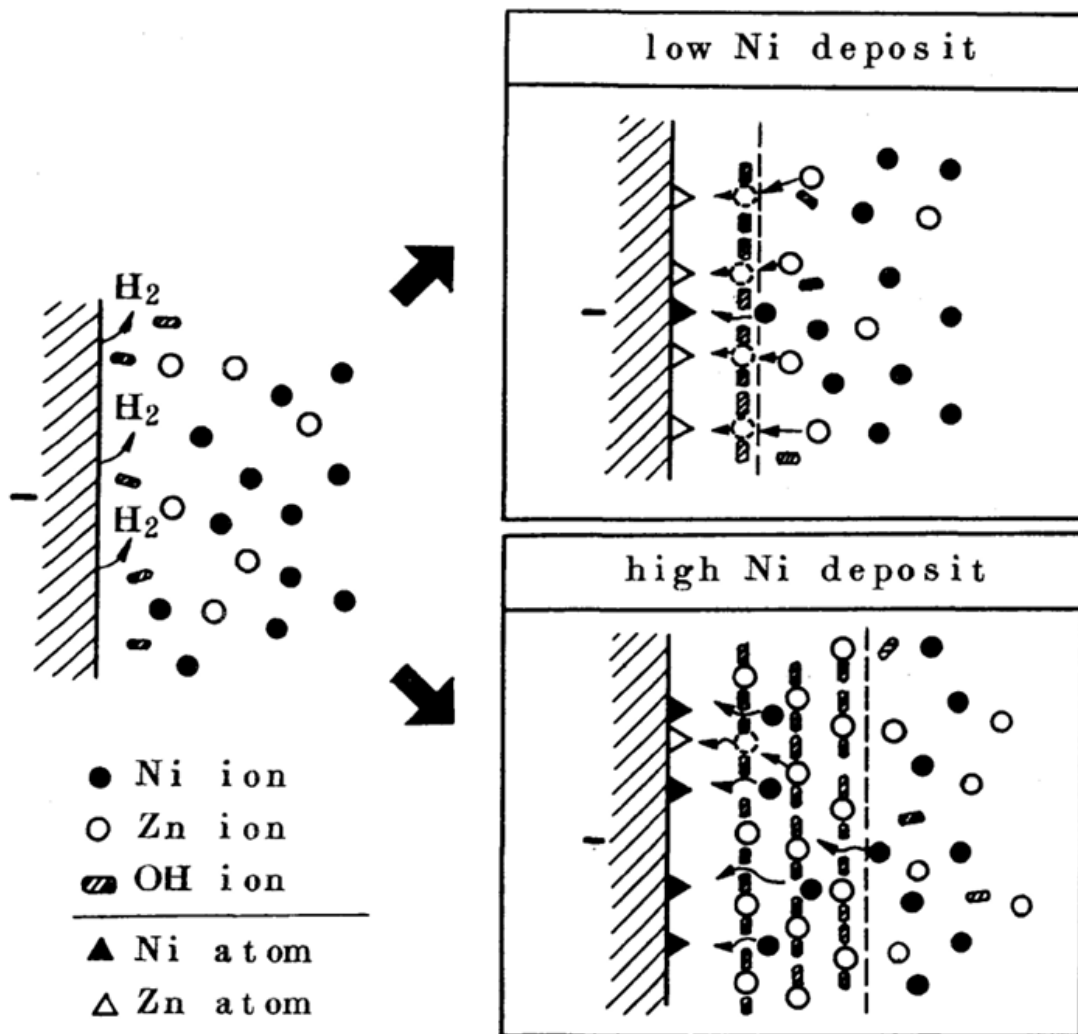
Hisaaki Fukushima[34] et al. also conducted a fundamental study on the electrodeposition mechanism of Zn-iron group metal (Fe, Co, Ni) alloys from sulfate and chloride solutions. They first clarified that the deposition behavior of Zn-Ni alloys is divided into the following four parts with respect to the current density, as shown in Fig. 1-4. In region I of Fig. 1-4, normal alloy deposition occurs with very low current efficiency. In region II, preferential deposition of less noble Zn occurs with relatively high current efficiency, but the alloy composition hardly changes. In region III, the Ni metal content of the alloy increases monotonically, and the current efficiency remains high. In region IV, the Ni metal content in the alloy increases until the metal ion concentration ratio of the Ni metal in the solution is reached, but the current efficiency decreases significantly. The boundary current densities in regions I and II are generally referred to as transition current densities, and they show that the magnitude of this transition current density is proportional to the pH buffer capacity of the electrolytic solution. Furthermore, the boundary current densities in regions II/III and III/IV correspond to the limiting current densities of the Zn and Ni metals, respectively. As the co-deposition behavior in regions II and III can be regarded as normal-type co-deposition when Zn is considered as a noble metal, they investigated the cause of the reversal of the nobility of the Zn and Ni metals.

Hisaaki Fukushima, Bockris[35] and Heusler[36] also found that the pH of the cathode surface increased to the critical pH at which Zn hydroxide ($Zn(OH)_2$) precipitates during anomalous co-deposition. Based on this finding, they proposed the following hydroxide suppression mechanism. That is, among the ions that can be discharged in the electrolytic solution, Zn initiates the deposition at its equilibrium potential. In contrast, iron group metal (Fe, Co, Ni) ions do not start electrodeposition from their equilibrium potential and require extra overpotential because the number of electrodeposited sites on the cathode is practically limited. Therefore, the deposition of iron-group metals is easily and largely suppressed by the adsorption of Zn hydroxide onto the deposition sites of iron-group metals, resulting in the preferential deposition of Zn.

$Zn(OH)_2$, which is formed by hydrolysis of Zn^{2+} ions, is reported to be an inhibitor of hydrogen evolution and Ni deposition in Zn-Ni alloy deposition from acidic solutions. However, the hydrolysis reaction of Zn^{2+} ions does not occur in a zincate solution. It has been reported that Zn electrodeposition from a zincate solution proceeds according to the multi-step reactions of equations (1), (2) and (3) shown below.

$$Zn(OH)_4^{2-} \rightarrow Zn(OH)_3^- + OH^- \qquad (1)$$

$$Zn(OH)_3^- \rightarrow Zn(OH)_2 + OH^- \qquad (2)$$

$$Zn(OH)_2 + 2\,e \rightarrow Zn + 2\,OH^- \qquad (3)$$
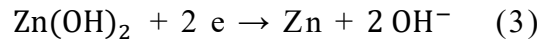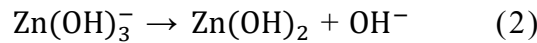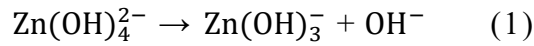
In contrast, Miranda studied the mechanism of Zn-Ni alloy deposition from acid sulfate electrolytic solution.[37] The heterogeneous reaction in their study implies the presence of four adsorbates (Fig. 1-5).

(1) $ZnNi_{ad}^+$ catalyzes the nickel deposition

(2) Intermediate H_{ad} affects the hydrogen evolution at a low polarization on nickel-rich alloy.

(3) Intermediates Zn_{ad}^+ act as a catalyst for the deposition of zinc-rich δ-phase at a highly polarization

(4) Anionic species $Zn/Ni_{4,ad}^{2-}$ inhibit the formation of the δ phase
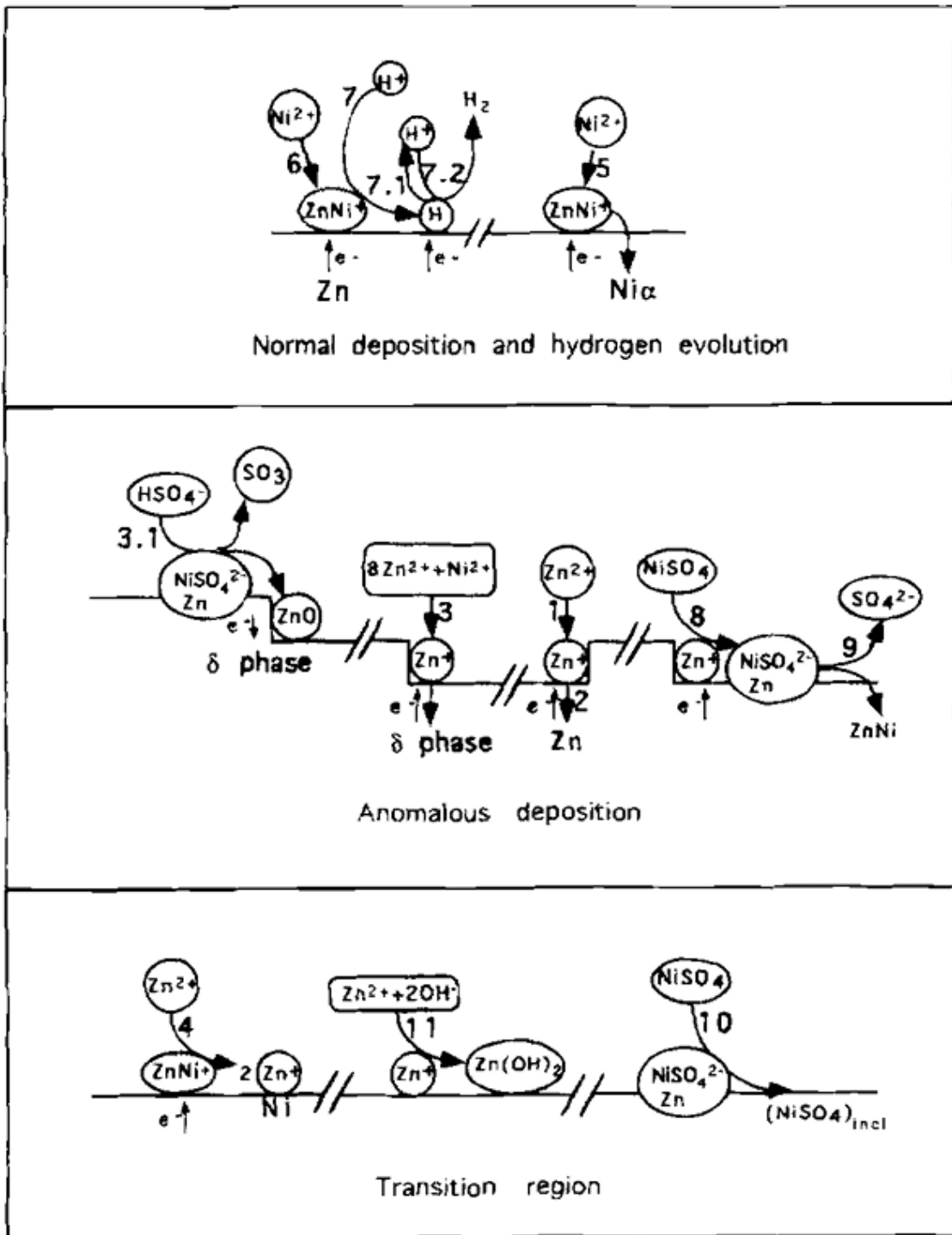
Fig. 1-5. Schematic of the reactions of predominant in the different potential domains in Zn-Ni alloy deposition from sulfate solution.[37]

In the transition region of intermediate polarization, an increase in pH at cathode layer promotes the chemical uptake of S into the deposited films catalyzed by anion adsorbates. The validity of this model is confirmed by comparison with experimental polarization curves, electrode impedance measurements, and analysis of structures and compositions of deposited films.

1-5. Effects of Additives

The purpose of additives to a plating solution is improving the uniform electrodeposition (throwing power), preventing the dendritic crystals, smoothing, brightening, and refining the crystal grains of deposited films. Common additives for sulfate and chloride solutions are gelatin, peptone, sodium sulfide, thiourea, polyvinyl alcohol, salts of aldehyde, ketone, or organic acids, etc. The smoothing the films mainly occurs due to controlling the diffusion of metal ions. In other words, pH of cathode surface rises during the plating process due to hydrogen generation. Especially, at the protrusion edge of electrode, a spherical diffusion layer is formed, and the current density is large, resulting in remarkable rise of pH. Therefore, proteins such as gelatin or soluble polyether form a thin precipitate films. The thickness of the precipitate films is determined by the current density. The precipitate films are permeable for H^+ but not for metal ions, so the electrodeposition rate at the protruding part is reduced. Therefore, the electrodeposited films are smoothed, and dendritic products are suppressed. Some smoothing agents show the leveling effects which are caused by the electrolytic depletion of the agents at plated surface. When a smoothing agent is present in solution, the smoothing agent is supplied to the plating surface through the diffusion layer of the agent at the plating surface and suppresses the deposition reaction of the plating. In this process, the smoothing agent is reduced by reduction reaction. Since the amount of smoothing agent supplied to the plating surface is inversely proportional to the thickness of the diffusion layer of agent, the amount of smoothing agent supplied to the plating surface is larger in convex areas and smaller in concave areas. As a result, the deposition in a concave area is larger than that in a convex area, resulting in smooth with increasing the thickness of deposited films.[38]

As a brightening mechanism of brightener, it is known that the crystal growth is inhibited by the adsorption of additives on the kinks and steps, and with increasing the overpotential for crystallization, the nucleation rate of crystal increases and crystal grains become finer. It is also known that the uniformity of electrodeposition is also improved by an increased polarization resistance of the electrodeposition. Winnand investigated on the microstructure of metals deposited by electrochemical methods and showed the correlation between the inhibition intensity of the electrodeposition reaction and factors related to mass transfer in solution (Fig. 1-6).[4] The inhibition intensity of the electrodeposition reaction shown in the vertical axis of Fig. 1-6 is a factor related to the easiness of metal electrodeposition. A large inhibition intensity corresponds to a small exchange current density i_0 or a large overpotential for electrodeposition. The main studies were carried out on the microstructures of deposited zinc (Zn) and copper (Cu). Figure 1-6 shows that the addition of brightener increases the inhibition intensity of the electrodeposition reaction and widens the region of non-oriented dispersed structures (UD), at which the crystals become fine and are unaffected by the substrate.[4]

Zincate solution has an advantage over sulfate and chloride solutions in that the metal ions can deposit on the substrates of complicated shapes more uniformly, but it has the disadvantage of a lower deposition rate. To negate this disadvantage, the electrodeposition rate must be increased. The electrodeposition of high speed or electrodeposition at high current density produces the dendrite-shaped deposits because the deposition proceeds under the diffusion limitation of metal ions. Therefore, it is essential to use additives to smooth the surface of electrodeposited Zn-Ni.

Fig. 1-6 Effect of ratio of current density to diffusion current density and inhibition intensity for deposition on the texture of deposited metal.[4]

Epichlorohydrin-imidazole (IME) condensates are synthesized as shown in Fig. 1-7.[39] They have been widely used as brightening agents for Zn and Zn-Ni alloy deposition, but the effect of IME on the deposition behavior and microstructure of Zn-Ni alloy has rarely been reported.

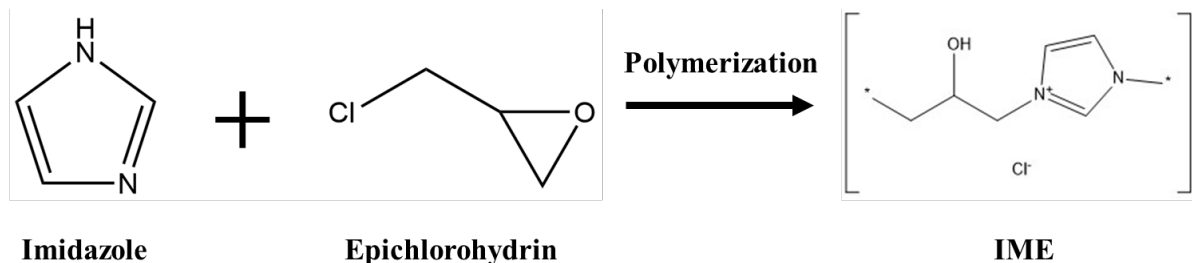**Imidazole**   **Epichlorohydrin**   **IME**

Fig. 1-7 Reaction scheme indicating the synthesis of IME.

1-6. Purpose of this thesis

As mentioned above, brightening agents are usually added to zincate solutions for the electrodeposition of Zn-Ni alloys, unlike for sulfate and chloride solutions. The relationship between the appearance quality of films deposited from zincate solutions and various brighteners has been reported a lot so far, but the effect of brightener on the electrodeposition behavior of Zn-Ni alloys has rarely been reported. In contrast, the solution temperature is an extremely important factor in electrodeposition because it affects the overpotential for electrodeposition, uniformity of electrodeposition (throwing power), solubility of metal salts, solution conductivity, etc. However, the effect of solution temperature on the electrodeposition behavior of Zn-Ni alloys from zincate solutions has not yet been reported in detail. Especially in the case of electrodeposition from electrolytic solutions containing a brightener, the effect of brightener may differ depending on the solution temperature. The synergistic effect of brightener and solution temperature on the electrodeposition behavior is expected, but the details are unknown. Therefore, in the present study, IME (Imidazole-Epichlorohydrin) was selected as a brightening agent which is reported to have brightening effect on the Zn films deposited from zincate solutions, and the effect of IME on the deposition behavior of Zn-Ni alloy was investigated. Zn-Ni alloy electrodeposition was performed in zincate solutions at different solution temperatures using IME as a brightener, and the respective and synergistic effects of IME and solution temperature on the electrodeposition behavior were discussed based on the partial polarization curves of Zn and Ni depositions and hydrogen evolution, appearance, and microstructure of the electrodeposited films.

1-7. Formation of this thesis

In Chapter 1, with respect to the background of this study as mentioned above, the previous studies on the deposition behavior of Zn-Ni alloys, and the mechanism of brightening agents, and the purpose and structure of this thesis were described.

In Chapter 2, the effect of brightener on the deposition behavior of Zn-Ni alloys from zincate solutions were described based on the partial polarization curves of Zn and Ni depositions, and hydrogen evolution. Epichlorohydrin and imidazole reactant (IME) was used as a brightener. The addition of IME decreased the transition current density at which the deposition behavior shifted from the normal to anomalous co-deposition due to suppression of hydrogen evolution. With IME, the current efficiency of alloy deposition decreased due to the suppression of both Zn and Ni depositions, while the Ni content of the deposited films decreased because the Ni deposition was more suppressed than Zn deposition.

In Chapter 3, the effect of solution temperature on the Zn-Ni deposition behavior was discussed based on the partial polarization curves of Zn and Ni depositions, and hydrogen evolution. In the region in which the charge transfer process is rate-limiting for deposition, since Ni deposition was more promoted than Zn deposition at higher solution temperatures, the Ni content in the deposited films increased with increasing solution temperature.

In Chapter 4, synergistic effect of IME and solution temperature on the electrodeposition behavior of Zn-Ni alloy was investigated by the partial polarization curves of Zn and Ni depositions and hydrogen evolution. The adsorption ability of IME on the cathode surface was expected to decrease with increasing solution temperature. The inhibitory effect of IME on the Zn and Ni depositions during alloy deposition was observed at a solution temperature of 293 K. However, the inhibitory effect on the Zn deposition decreased with increasing the solution temperature to 313 and 333 K, while that on the Ni deposition was maintained. Therefore, the Ni content in the deposited films was significantly decreased by the addition of IME at higher solution temperatures. It was also found that the adsorption ability of IME was large at a solution temperature of 293 K, and that the crystal grains of the electrodeposited films became finer and smoother.

In Chapter 5, the effect of IME addition on the corrosion resistance of deposited Zn-Ni alloy films was described based on the immersion tests in 3 mass% NaCl aqueous solution, which was a typical environment containing chloride ions. In the films electrodeposited from the solution with IME, the anodic reaction was suppressed after immersion in 3 mass% NaCl aqueous solution for 24 h, and the corrosion potential shifted to the more noble side. The plate-like crystals of zinc chloride hydroxide formed on the Zn-Ni alloy films, which was

obtained from the solution containing 5 ml·dm^{-3} of IME, were fine and uniform over the entire surface. In the films on which the corrosion products were formed after 24 h immersion in the 3 mass% aqueous NaCl solution, the suppression of anodic reaction with IME is attributed to the formation of uniform corrosion products (zinc chloride hydroxide) on the surface, in addition to the co-deposition of C.

In Chapter 6 "Conclusions," the conclusions obtained in each chapter are summarized.

1-8. References

1) G. E. Gardam: *Trans. Inst. Met. Finish.*, **23** (1947), 1.

2) L.V. Brugnatelli: *Ann. Chim. (Pavia)*, **21** (1802), 148.

3) G. R. Elkington: *Brithish patent* 8447, 1840.

4) R. Winand: *Electrochim. Acta*, **39** (1994), 1091.

5) D. Landolt: *Electrochim. Acta*, **39**, (1994), 1075.

6) D. Landolt: E.J. Podlaha and N. Zech, *J. Phys. Chem.* **208** (1999), 167.

7) C. Wagner and W. Traud: *J. Elektrochem.*, **44** (1938), 391.

8) M. Stern and A.L. Geary: *J. Electrochem. Soc.*, **104** (1957), 56.

9) J. Yahalom and O. Zadok: *J. Mater. Sci.*, **22** (1987), 499.

10) D.S. Lashmore and M.P. Dariel: *J. Electrochem. Soc.*, **135** (1988), 1218.

11) C. Bonhote and D. Landolt: *Electrochim. Acta*, **42** (1997), 2407.

12) J.J. Kelly, P. Bradley and D. Landolt: *J. Electrochem. Soc.*, **147** (2000), 2975.

13) T.E. Dinan, M. Matlosz and D. Landolt: *J. Electrochem. Soc.*, **138** (1991), 2947.

14) P. Bradley and D. Landolt: *J. Electrochem. Soc.*, **144** (1997), L145.

15) RE. Bradley and D. Landolt: *Electrochim. Acta.*, **45** (1999), 1077.

16) M. Haissinsky: *Chim. Phys.*, **30** (1933), 27.

17) M. Haissinsky: *J. Chim. Phys.*, **43** (1946), 21.

18) M. Haissinsky: *J. Chim. Phys.*, **41**(1946), 21.

19) J. Danon and M. Haissinsky: *Chim. Phys.*, **48** (1951), 135.

20) C. Haenny and P. Mivalez: *Helv. Chim. Acta*, **31** (1948), 633.

21) C. Haenny and P. Reymond: *Helv. Chim. Acta*, **37** (1954), 2067.

22) L.B. Rogers, D.P. Krause, J.C. Griess and D.B. Ehrlinger: *J. Electrochem. Soc.*, **95(2)** (1949), 33.

23) J.C. Griess, J.TByrne JT and L.B. Rogers: *J. Electrochem. Soc.*, **98(11)** (1951), 447.

24) L.B. Rogers and A.F. Stehney: *J. Electrochem. Soc.*, **96** (1949), 25.

25) L.B. Rogers, H.H. Miller, R.B Goodrich and A.F. Stehney: *Anal. Chem.*, **21** (1949), 777.

26) J.T. Byrne and L.B. Rogers: *J. Electrochem. Soc.*, **98(11)** (1951), 457.

27) J.T. Byene, L.B. Rogers and J.C. Griess: *J. Electrochem. Soc.*, **98(11)** (1951), 452.

28) L.B. Rogers: *Rec. Chem. Prog.*, **16** (1955), 197.

29) L.B. Rogers and C. Merritt: *J. Electrochem. Soc.*, **100(3)** (1953), 131.

30) R.C. De Geiso and L.B. Rogers: *J. Electrochem. Soc.*, **106(5)** (1959), 433.

31) L.B. Rogers and A.F. Stelmey: *J. Electrochem. Soc.*, **95** (1949), 25.

32) D.M. Kolb, H. Gerischer and C.W. Tobias: Advances in electro-chemistry and electrochemical engineering, vol. 11. Wiley, New York, (1978), 125.

33) A. Shibuya and T. Kurimoto: *Trans. Inst. Met. Finish.*, **33** (1982), 544.

34) H. Fukushima, T. Akiyama, M. Yano, T. Ishikawa and R. Kammel: *ISIJ Int.*, **33** (1993), 1009.

35) J. O'M. Bockris, Z. Nagy and A. Damjanovic: *J. Electrochem. Soc.*, **119** (1972), 285.

36) L. Gaiser and K.E. Heusler: *Electrochim. Acta*, **15** (1970) 161.

37) F. J. F. Miranda: *J. Electrochem. Soc.*, **144(10)** (1997), 3449.

38) H. Fischer: *Surf. Treat.*, **1** (1973) 319.

39) W. Xincheng, S. Yanlei, H. Chongpin, L. Fengbing and C. Biaohua: *Green Chem.*, **16** (2014), 4234.

Chapter 2. Effect of Reaction Product of Epichlorohydrin and Imidazole on the Electrodeposition Behavior of Zn−Ni Alloy from Alkaline Zincate Solution

2-1. Introduction

Electrodeposited Zn−Ni alloy coatings are used for automobile parts, electric household products, and building materials owing to their superior corrosion resistance.[1~3] Particularly, Zn−Ni alloy coatings are widely used for automobile engine parts, which require high corrosion resistance at elevated temperatures. Such coatings are generally produced from sulfate and chloride solutions. Alkaline solutions, such as cyanide and zincate solutions, have better throwing power of deposits.[4,5] However, since hydrogen cyanide is toxic, zincate solutions are environmentally desirable. The deposition of Zn−Ni alloys from sulfate and chloride solutions shows an anomalous co-deposition behavior, where the electrochemically base Zn preferentially deposits over Ni.[6~10]

By contrast, the deposition behaviors of Zn−Ni alloys from zincate solutions show that both normal and anomalous behaviours depend on the electrolysis conditions,[11~16] and there is an ambiguity in comparison with their behavior in sulfate and chloride solutions. Therefore, the authors investigated the deposition behavior of a Zn−Ni alloy from the zincate solution containing triethanolamine or ethylenediamine as a complex agent with Ni^{2+} ions. The results indicate that the deposition of the Zn−Ni alloys from the zincate solutions showed a normal behavior at a low current density, but its behavior became anomalous with increasing current density.[17~20] During deposition from zincate solutions, a brightener is generally added into the electrolyte. The brightener possibly affects the deposition behavior, but there is an ambiguity about this effect. Therefore, in this study, the reaction product of epichlorohydrin and imidazole,[21] which effectively provides gloss for Zn films deposited from zincate solutions, is used as the brightener. The effect of this reaction product of epichlorohydrin and imidazole on the deposition behavior of the Zn−Ni alloy is discussed from partial polarization curves of the Zn and Ni depositions and hydrogen evolution.

2-2. Experimental

Table 2-1 shows the composition of the zincate solution and the electrolysis conditions for the Zn−Ni alloy deposition. The electrolytic solutions were prepared by dissolving reagent-grade ZnO (0.15 mol·dm^{-3}), NiSO$_4$·6H$_2$O (0.016 mol·dm^{-3}), N(CH$_2$CH$_2$OH)$_3$ (0.34 mol·dm^{-3}), and NaOH (2.5 mol·dm^{-3}) in distilled and deionized water. In some experiments, the current density for hydrogen evolution was measured using a solution eliminating the Zn or Ni ions from the bath mentioned above. The brightener was a kind of polymer as shown in Fig. 2-1 that was a reaction product of epichlorohydrin and imidazole as

reported in the previous paper.[21,22)] IME shown in this paper below denotes the reaction product of epichlorohydrin and imidazole. The electrodeposition was performed in unagitated solutions under coulostatic (5×10^4 C·m^{-2}) and galvanostatic (10–500 A·m^{-2}) conditions at 293 K. Copper (1×2 cm^2) and platinum (1×2 cm^2) sheets were used as the cathodes and anodes, respectively. The cathode deposits were dissolved using nitric acid. The Zn and Ni contents of the deposited Zn–Ni alloys were quantitatively analyzed by inductively coupled plasma spectroscopy. Hence, the Ni content of the deposits and the cathode current efficiency for the Zn and Ni depositions were calculated. The partial current densities for the Zn and Ni depositions, and hydrogen evolution were calculated by multiplying the total current density by each current efficiency. The current efficiency for hydrogen evolution was calculated by subtracting the current efficiency for the Zn and Ni depositions from 100%. The cathode potentials were measured using a saturated-KCl/Ag/AgCl reference electrode (0.199 V vs. NHE, 298 K) and then plotted with reference to the NHE.

Table 2-1. Solution compositions and electrolysis conditions

ZnO	(mol·dm^{-3})	0.15	Current density (A·m^{-2})	10–500
NiSO$_4$·6H$_2$O	(mol·dm^{-3})	0.016	Temperature (K)	293
N(CH$_2$CH$_2$OH)$_3$	(mol·dm^{-3})	0.34	Amount of charge (C·m^{-2})	5×10^4
NaOH	(mol·dm^{-3})	2.5	Cathode	Cu (1×2 cm^2)
Reaction product of epichlorohy-drin and imidazole (IME)	(ml·dm^{-3})	0~5	Anode	Pt (1×2 cm^2)
			Quiescent bath	

The morphologies of the deposited films were observed by scanning electron microscopy (SEM) and the structures of the alloys were examined by X-ray diffraction (XRD). The crystallite sizes of the deposited films were calculated using the Scherrer equation[23)] from the half-width of the XRD peak corresponding to the $10\bar{1}1$ reflection. The polarization curves, which were used to evaluate the corrosion resistance of the deposited films, were measured via polarization from a less noble potential than the corrosion potential toward the anodic-potential direction using a potential-sweep method at 1.0 mV·s^{-1} in an oxygen-saturated 3% NaCl solution at 313 K.
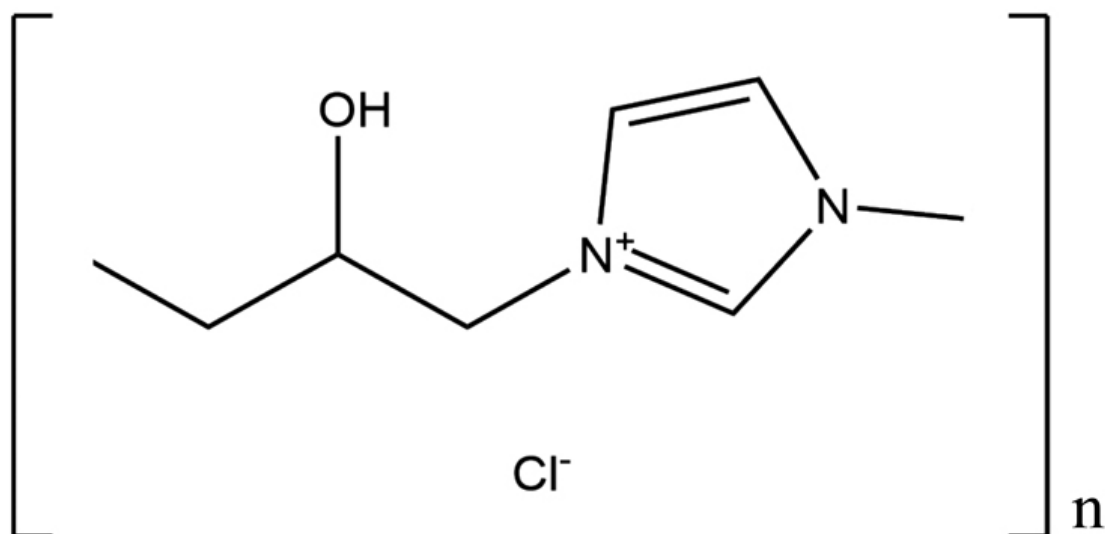
Fig. 2-1. Structural formula of reaction product of epichlorohydrin and imid-azole.

2-3. Results

2-3-1. Effect of IME on the Appearance of the Deposited Films

Figure 2-2 shows the appearance of the Zn–Ni alloy films deposited at various current densities from the solutions with and without the reaction product of epichlorohydrin and imidazole (IME). The Zn–Ni alloy films deposited at all the current densities from the IME-free solution were gray, showing no gloss. The films obtained at 20 $A \cdot m^{-2}$ from the solution containing 2 $ml \cdot dm^{-3}$ of the IME somewhat exhibited gloss, whereas those deposited at current densities above 50 $A \cdot m^{-2}$ were silver, showing gloss. The gloss of the deposited films became significant with increasing current density. Contrarily, dark dots are observed in the Zn–Ni alloy films deposited at 10 and 20 $A \cdot m^{-2}$ without IME and at 10 $A \cdot m^{-2}$ with IME. Since the current efficiency for the alloy deposition was low at 10 and 20 $A \cdot m^{-2}$ without IME and at 10 $A \cdot m^{-2}$ with IME (Fig. 2-4), the dark dots are attributed to traces of the evolved hydrogen gas.
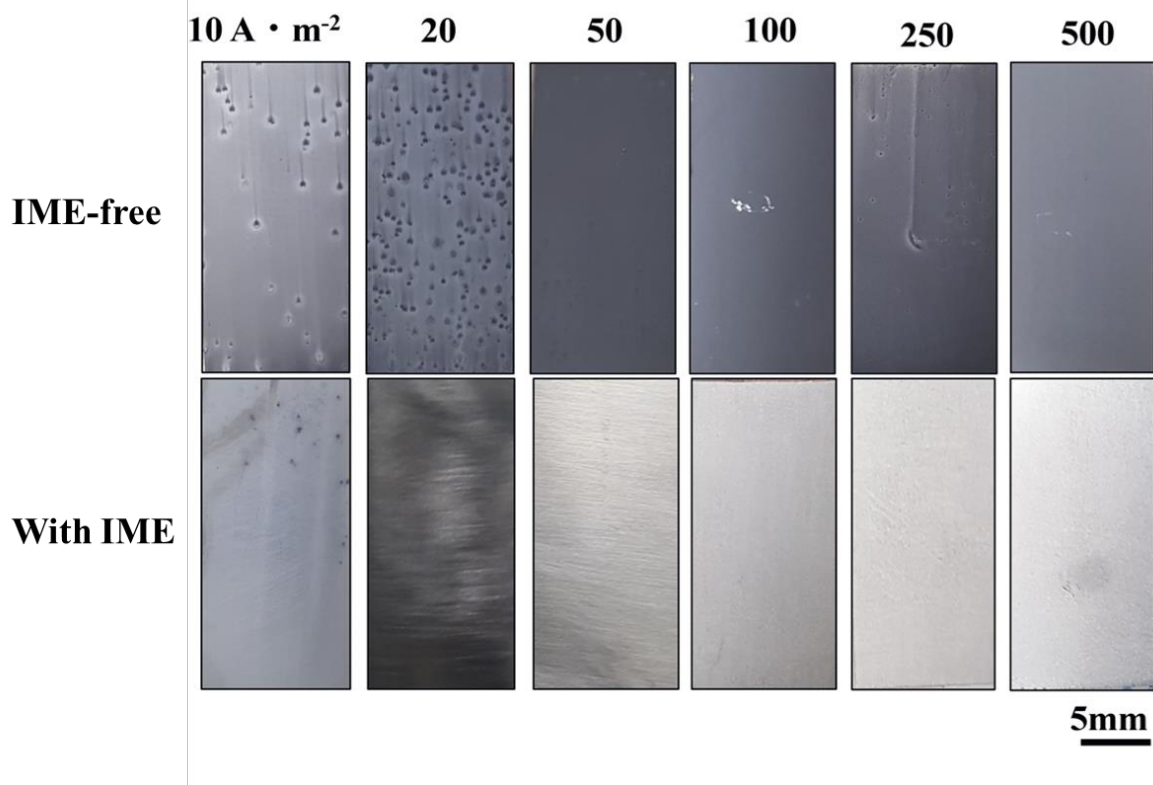
Fig. 2-2. Appearance of Zn–Ni alloy films deposited at various current densities from solutions with and without 2 ml·dm^{-3} IME.

2-3-2. Effect of IME on the Deposition Behavior of Zn–Ni Alloy

  Figure 2-3 shows the total and partial polarization curves of Zn and Ni for the Zn–Ni alloy deposition. The equilibrium potential for the Zn deposition was −1.27 V, assuming pure Zn deposition. Then, the equilibrium potential for pure Ni deposition was calculated as −0.41 V based on the complex stability constant K = $10^{4.74}$[24] which was formed by the coordination of two triethanolamine molecules toward Ni^{2+} ions, assuming pure Ni deposition. In the IME-free solution, the total polarization curve rose at approximately −0.85 V, and the cathode potential shifted rapidly to the negative direction at current densities above 50 A·m^{-2}. At potentials less noble than approximately −1.3 V, the current density rapidly increased for the second time. In the partial polarization curve for the Zn deposition, the partial current density of Zn was detected at approximately −0.9 V. Subsequently, the cathode potential rapidly shifted to the negative direction like the total polarization curve. The partial current density of Zn rapidly increased at potentials less noble than −1.27 V of the equilibrium potential for the Zn deposition. Even in the abovementioned alloy deposition, Zn substantially began to deposit at a potential less noble than its equilibrium potential. In the Zn–Ni alloy deposition, the current density for the Zn deposition was somewhat detected even at approximately −0.9 V, which

is more noble than the equilibrium potential for pure Zn deposition (−1.27 V), indicating the occurrence of an apparent underpotential deposition of Zn. Then, the partial current density for the Ni deposition began to increase at approximately −0.9 V and became almost constant at approximately 6 A·m⁻² until the equilibrium potential of Zn, and somewhat increased at potentials less noble than the equilibrium potential of Zn.

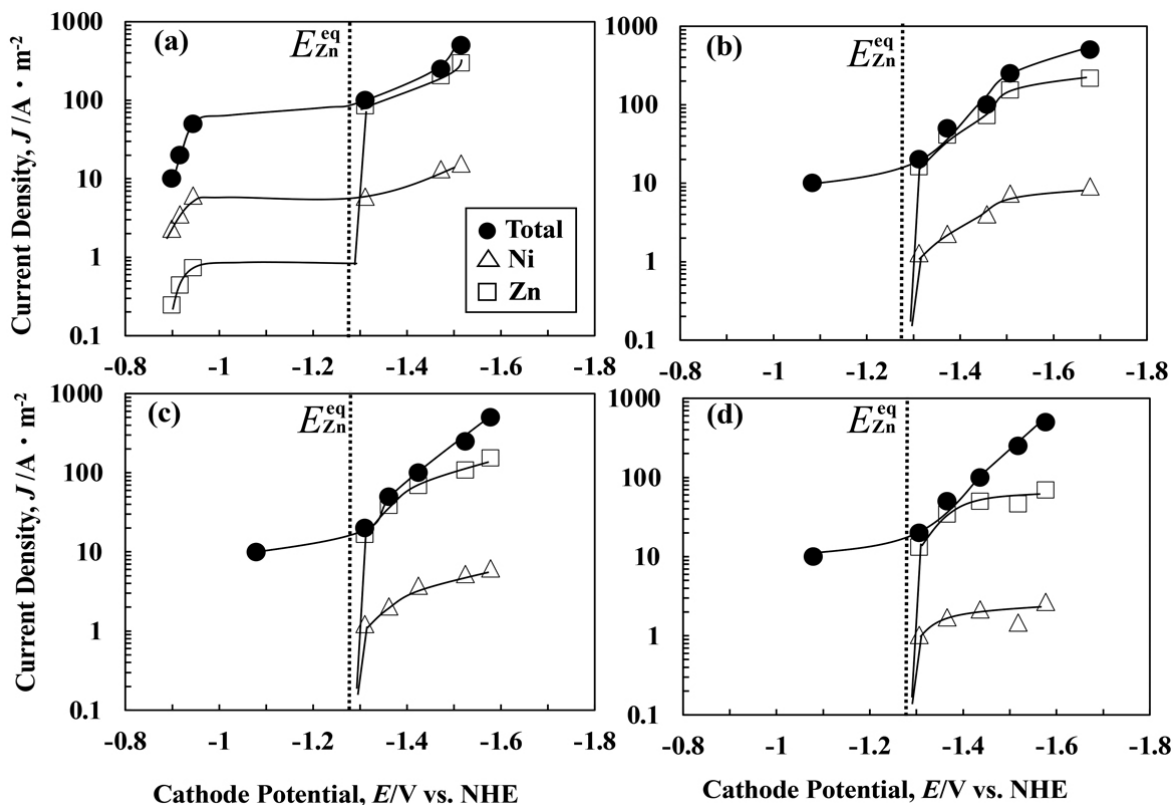Fig. 2-3. Polarization curves for Zn–Ni alloy deposition from solutions with and without IME: (a) no IME, (b) 1 ml·dm⁻³ IME, (c) 3 ml·dm⁻³, (d) 5 ml·dm⁻³.

In the deposition from the 1 ml·dm⁻³ IME-containing solution, all the total and partial polarization curves of Zn and Ni were greatly polarized compared with those from the IME-free solution (Fig. 2-3(b)). For the total polarization curves, the cathode potential rapidly polarized to the negative direction at a current density above 10 A·m⁻². The current density at which the cathode potential rapidly polarized to the negative direction was lower than that from the IME-free solution. By contrast, the partial polarization curves for the Zn and Ni depositions rose at potentials less noble than the equilibrium potential for Zn deposition, and the partial current densities of Zn and Ni approached constant values at potentials less noble than −1.5 V. This trend indicates that the Zn and Ni depositions approach the diffusion limitations of Zn²⁺ and Ni²⁺ ions at potentials less noble than −1.5 V. Although the Zn deposition occurred at approximately −0.9 V more noble than its equilibrium potential in the IME-

free solution, that is, an apparent underpotential deposition of Zn occurred, this phenomenon was not observed in the IME-containing solution. The underpotential deposition of Zn during the Zn–Ni alloy deposition was attributed to the significant decrease in the activity coefficient of Zn in the deposited films because of the formation of stable intermetallic compound Ni_5Zn_{21} during the deposition.[17,19] Thus, the co-deposition of Ni is essential for the underpotential deposition of Zn. However, the Ni deposition was considerably suppressed in the IME-containing solution in this study. Consequently, no Ni deposition occurred at the potential region more noble than the equilibrium potential of Zn, and no underpotential deposition of Zn occurred. The deposition behavior from the 3 ml·dm^{-3} IME-containing solution (Fig. 2-3(c)) showed an almost identical tendency to that from the 1 ml·dm^{-3} IME-containing solution (Fig. 2-3(b)). In particular, the partial current densities of Zn and Ni were smaller in the 3 ml·dm^{-3} IME-containing solution than in the 1 ml·dm^{-3} IME-containing solution. As the IME concentration increased to 5 ml·dm^{-3}, the partial current densities of Zn and Ni further decreased compared with those from 3 ml·dm^{-3} of the IME (Fig. 2-3(d)). Particularly, in the potential region less noble than -1.4 V, the Zn and Ni depositions reached the diffusion limitations of the Zn^{2+} and Ni^{2+} ions, suggesting that the diffusions of the Zn^{2+} and Ni^{2+} ions were suppressed by the IME. The concentration of IME in the vicinity of cathode seems to be significantly higher than that in the bulk solution because IME adsorbs on the cathode. Therefore, it is likely that the viscosity of solution at cathode layer including diffusion layer increases, resulting in suppression of the diffusions of Zn^{2+} and Ni^{2+} in the diffusion layer.
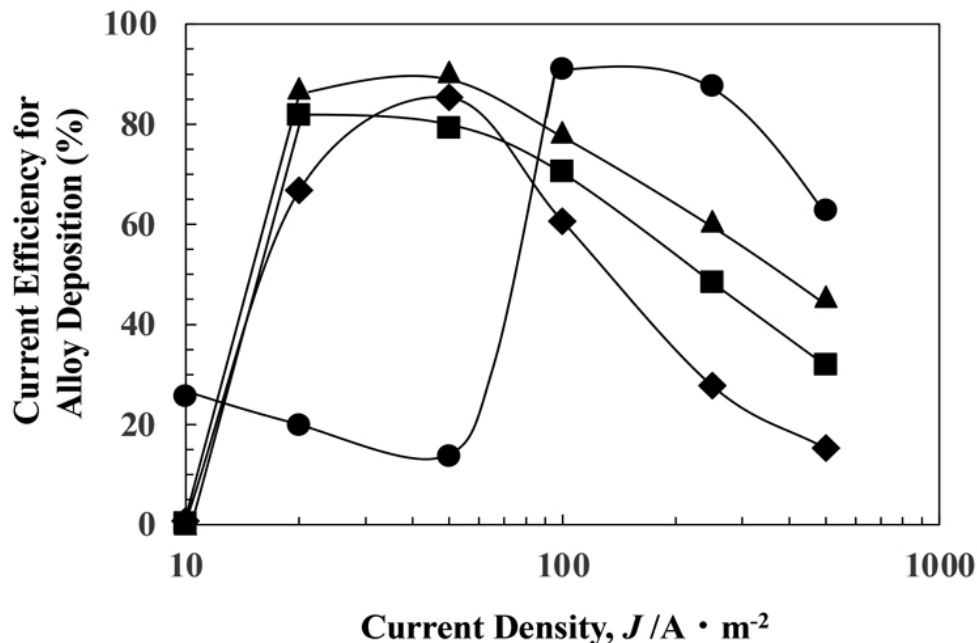

Fig. 2-4. Current efficiency for Zn–Ni alloy deposition from solutions with and without IME: ● no IME, ▲ 1 ml·dm^{-3} IME, ■ 3 ml·dm^{-3}, ◆ 5 ml·dm^{-3}.

Figure 2-4 shows the effect of current density on the current efficiency for the Zn–Ni alloy deposition. In the IME-free solution, the current efficiency for the alloy deposition was low (15%–25%) at the low current density of 10–50 $A \cdot m^{-2}$. However, the current efficiency rapidly increased at current densities above 50 $A \cdot m^{-2}$, peaked at 100–200 $A \cdot m^{-2}$, and subsequently decreased with further increasing current density. Compared with the polarization curve in Fig. 2-3(a), the cathode potential at 10–50 $A \cdot m^{-2}$ was more noble than the equilibrium potential of Zn, resulting in low current efficiency for the alloy deposition. At current densities above 50 $A \cdot m^{-2}$, the cathode potential rapidly shifted to the potential region less noble than the equilibrium potential of Zn (Fig. 2-3(a)), leading to a significant increase in the current efficiency for the alloy deposition. The decrease in current efficiency at 500 $A \cdot m^{-2}$ may be attributed to the Zn and Ni depositions approach toward the diffusion limitations of the Zn^{2+} and Ni^{2+} ions. With the addition of the IME, the current efficiency for the alloy deposition was almost zero at 10 $A \cdot m^{-2}$, increased significantly at current densities above 10 $A \cdot m^{-2}$, peaked at 20–50 $A \cdot m^{-2}$, and greatly decreased at current densities above 50 $A \cdot m^{-2}$ irrespective of the IME concentration. In the IME-containing solution, the cathode potential shifted to the potential region less noble than the equilibrium potential of Zn at current densities above 10 $A \cdot m^{-2}$ (Figs. 2-3(b)–2-3(d)). Consequently, the current efficiency for the alloy deposition increased and was significantly higher at 20–50 $A \cdot m^{-2}$ than that in the IME-free solution. Since the Zn and Ni depositions reached or approached the diffusion limitations of the Zn^{2+} and Ni^{2+} ions at total current densities above 100 $A \cdot m^{-2}$ (Figs. 2-3(b)–2-3(d)), the current efficiency for the alloy deposition seemed to decrease with increasing current density. At the current density region above 100 $A \cdot m^{-2}$, the current efficiency for the alloy deposition was lower in the IME-containing solution than in the IME-free solution and generally decreased with increasing IME concentration. This trend indicates that the Zn and Ni depositions were more suppressed than hydrogen evolution with increasing IME concentration.
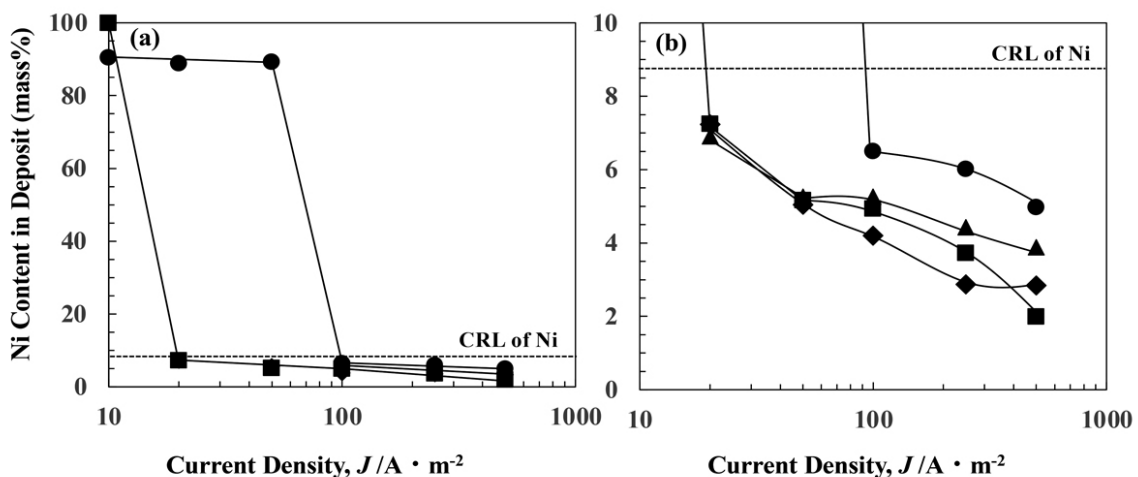

Fig. 2-5. Ni content in Zn–Ni alloys deposited at various current densities from solutions with and without IME: (b) magnified view of area of 0–10 mass% Ni content; ● no IME, ▲ 1 $ml \cdot dm^{-3}$ IME, ■ 3 $ml \cdot dm^{-3}$, ◆ 5 $ml \cdot dm^{-3}$.

Figure 2-5 shows the effect of current density on the Ni content in the deposited Zn–Ni alloy films. The broken line (CRL of Ni) shows the Ni content in the deposits predicted from the concentration ratio of Ni^{2+} ion against the total metal ions in the bath. When the Ni content in the deposited films exceeded the CRL, normal co-deposition occurred, in which electrochemically noble Ni deposited preferentially to Zn. In contrast, when the Ni content in the deposited films was smaller than the CRL, anomalous co-deposition occurred, in which base Zn deposited preferentially to Ni. In the IME-free solution, the Ni content in the deposited films changed significantly at 50–100 $A \cdot m^{-2}$ (Fig. 2-5(a)). The Ni content in the Zn–Ni films deposited at current densities below 50 $A \cdot m^{-2}$ was approximately 90 mass% above the CRL and showed normal co-deposition. However, at current densities above 100 $A \cdot m^{-2}$, the Ni content was less than the CRL and exhibited anomalous co-deposition. With the addition of the IME, the Ni content in the deposited films substantially changed at 10–20 $A \cdot m^{-2}$ irrespective of IME concentration. At current densities above 20 $A \cdot m^{-2}$, the Ni content in the deposited films was below CRL and showed anomalous co-deposition. The current density at which deposition behavior changes from normal to anomalous is called transition current density.[25] This transition current density corresponded to the current density at which the cathode potential of the total polarization curve rapidly shifted to the negative direction (Figs. 2-3(a)–2-3(d)) and at which the current efficiency for alloy deposition significantly changed (Fig. 2-4). The transition current density in the IME-containing solution was lower than that in the IME-free solution. Figure 2-5(b) shows a magnified view of the Ni content in the deposited films of the area where the anomalous co-deposition occurred at current densities above 20 $A \cdot m^{-2}$. The Ni content in the Zn–Ni alloy films obtained by anomalous co-deposition decreased with the addition of the IME and generally decreased with increasing IME concentration.

2-3-3. Effect of IME on the Microstructure of Deposited Films

Figure 2-6 shows the SEM images of the films deposited at 50, 100, and 500 $A \cdot m^{-2}$ from the solutions containing various amounts of the IME. The films deposited at 50 $A \cdot m^{-2}$ were composed of granular crystals irrespective of the presence or absence of the IME. Thus, the IME did not affect the morphology of the deposited films (Figs. 2-6(a)–2-6(d)). For the films deposited at 100 $A \cdot m^{-2}$ from the IME-free solution (Fig. 2-6(e)), a smooth granular morphology was observed; while those deposited from the solution containing 1 $ml \cdot dm^{-3}$ of the IME (Fig. 2-6(f)) were smooth and showed fewer granular crystals than that in IME-free solution. However, as the IME concentration increased to 3 $ml \cdot dm^{-3}$ (Fig. 2-6(g)), granular crystals emerged on the smooth surface. As the concentration further increased to 5 $ml \cdot dm^{-3}$ (Fig. 2-6(h)), the granular crystals decreased and the smooth area expanded. The films deposited at 500 $A \cdot m^{-2}$ from the IME-free solution (Fig. 2-6(i)) showed platelet crystals perpendicular to the substrate, which smoothed (without platelet crystals) with the addition

of 1 ml·dm^{-3} IME (Fig. 2-6(j)). With increasing IME concentration to 3 and 5 ml·dm^{-3} (Figs. 2-6(k), 6(l)), 100 nm-fine granular crystals were observed, however, the films eventually became generally smooth.
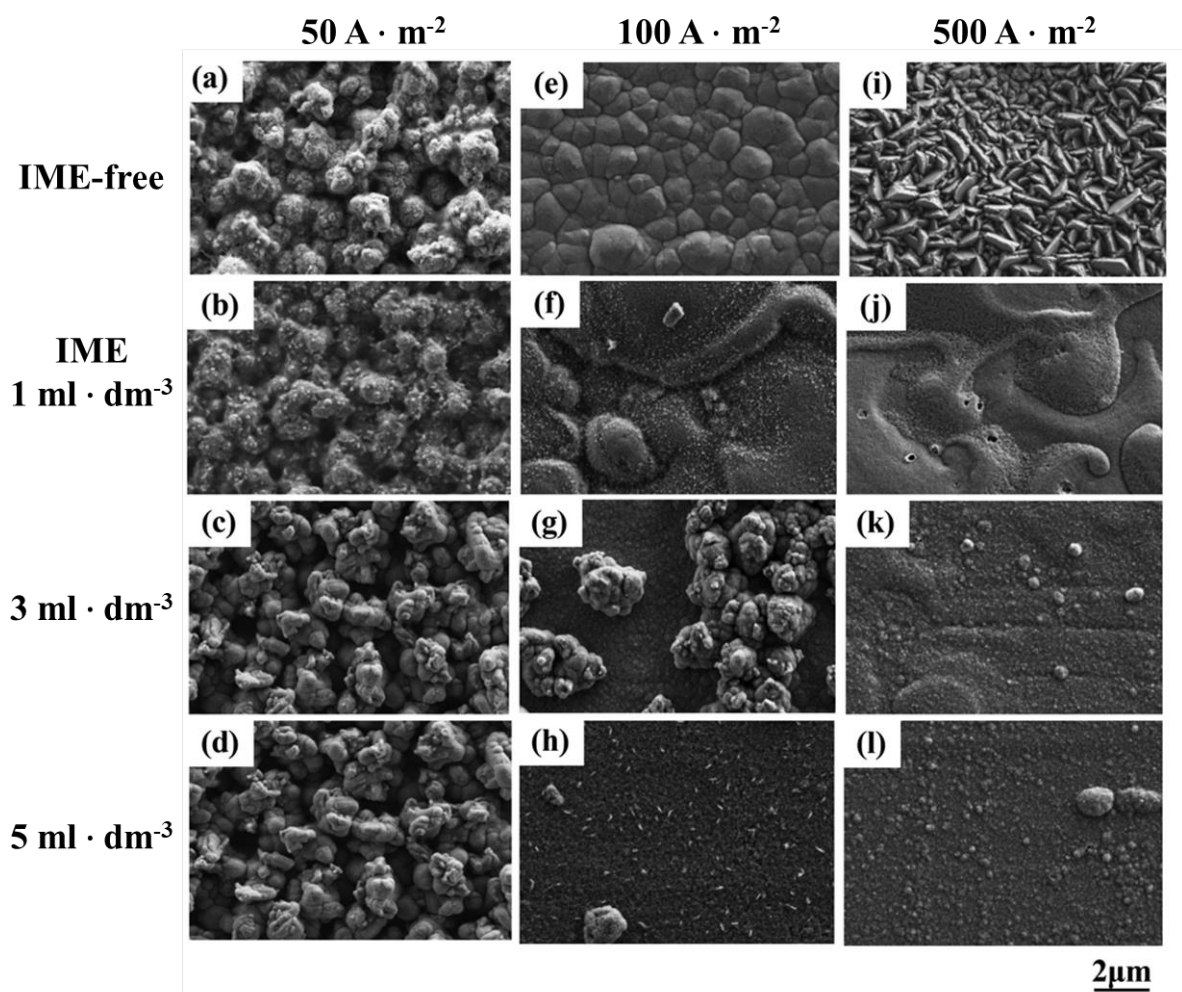

Fig. 2-6. SEM micrographs of surface of Zn–Ni alloys deposited at various current densities from solutions containing IME at different concentrations.

Figure 2-7 shows the XRD patterns of the films deposited at 500 A·m^{-2}. Only peaks resulting from the η phase, which showed a solid solution of Ni in the Zn and the Fe substrate, were detected irrespective of the presence or absence of the IME. The η phase of the films deposited from the IME-free solution was oriented mainly to the {10$\bar{1}$1} and {0001} planes (Fig. 2-7(a)), however, such orientation decreased with the addition of 1 ml·dm^{-3} of the IME (Fig. 2-7(b)). With increasing IME concentration to 3 and 5 ml·dm^{-3} (Figs. 2-7(c) and 2-7(d)), the orientation to the {10$\bar{1}$1} and {0001} planes further decreased, eventually approaching the non-orientation state. Typically, in metal deposition, the deposited film exhibits an unoriented, dispersed texture with increasing polarization, and its morphology becomes a smooth surface composed of dispersed fine crystals irrespective of the substrate and the electric field.[26] In

this study, when the polarization became large with the addition of the IME, the deposited films nearly became unoriented and dispersed in type. Then, in the Zn–Ni alloy deposition from sulfate solutions, although the γ phase of intermetallic compounds, such as $NiZn_3$ and Ni_5Zn_{21}, is reported to be present in films with 4.8 mass% of Ni content,[27] the γ phase was not detected in the films deposited from the zincate solution in this study.
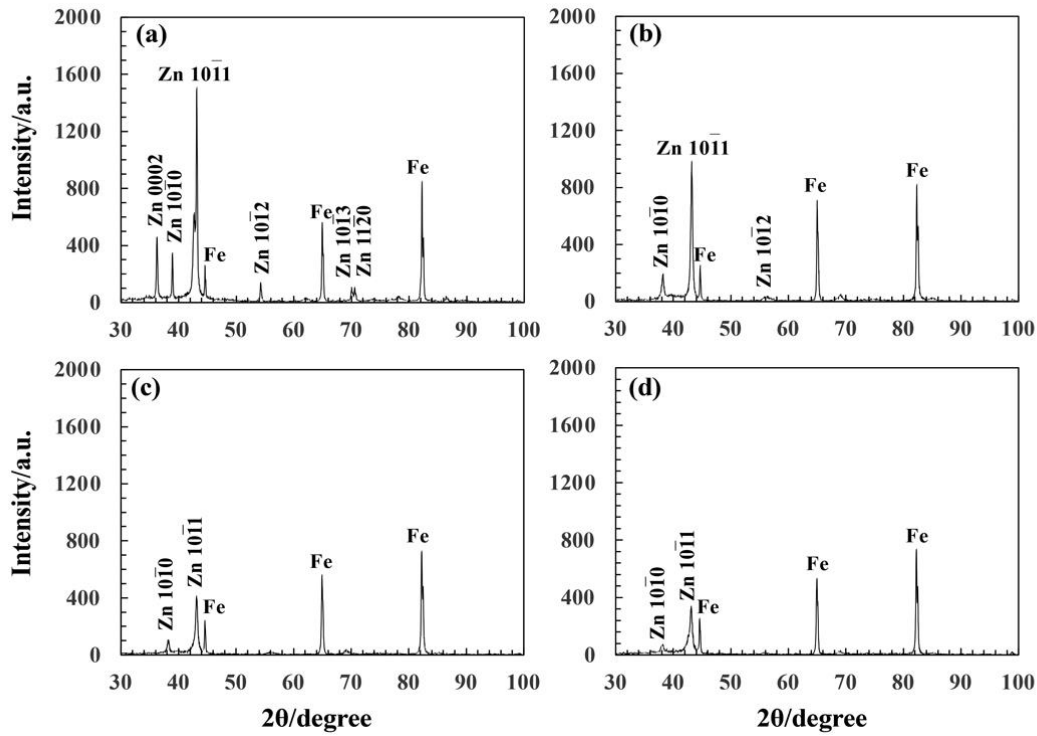

Fig. 2-7. XRD patterns of Zn–Ni alloy films deposited at 500 A·m^{-2} from solutions with and without IME: (a) no IME, (b) 1 ml·dm^{-3} IME, (c) 3 ml·dm^{-3}, (d) 5 ml·dm^{-3}.

Figure 2-8 shows the crystallite size of the films deposited at 500 A·m^{-2}. The crystallite size of the deposited films decreased with increasing IME concentration. Generally, when the overpotential for deposition increases during the metal deposition, the nucleation rate of the deposition prevails over the crystal growth, thus resulting in a decreased crystallite size of the deposits.[28~31] In this study, the decrease in the crystallite size of the deposited films with increasing IME concentration was attributed to an increase in the deposition overpotential with increasing IME concentration.
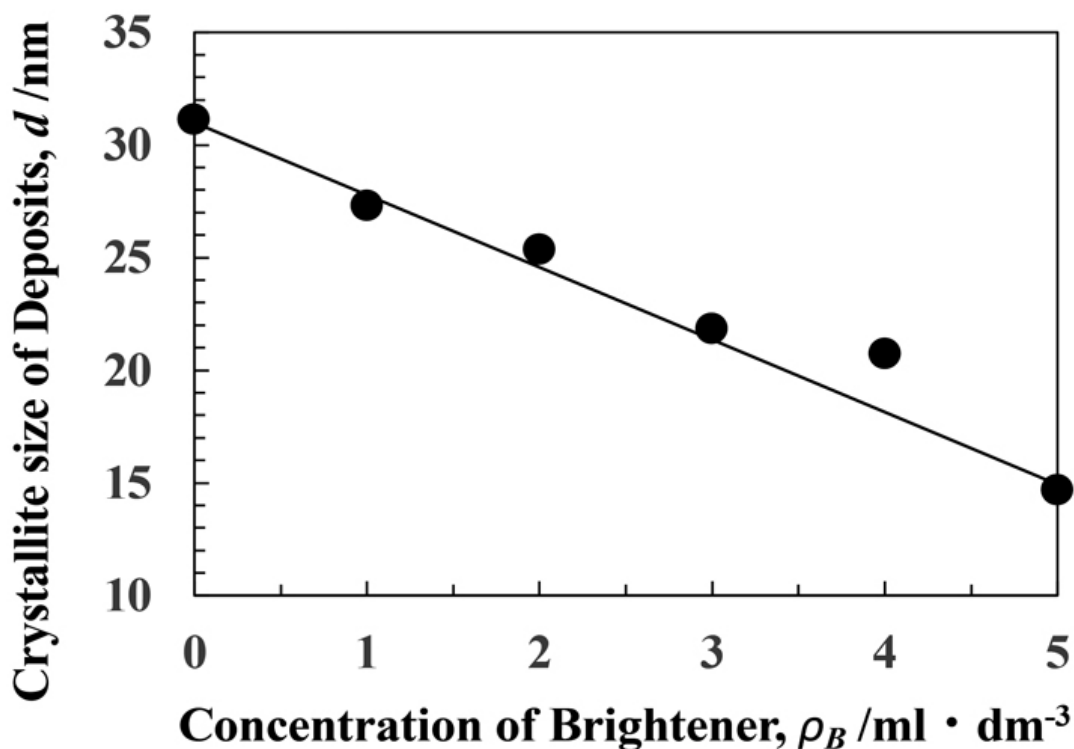
Fig. 2-8. Crystallite size of Zn–Ni alloy films deposited at 500 A·m^{-2} from solutions containing various amounts of IME.

2-3-4. Effect of IME on the Corrosion Resistance of the Deposited Films

  Figure 2-9 shows the polarization curves in a 3 mass% NaCl solution for the deposited films. For the films deposited from the IME-containing solutions, the oxidation reaction was suppressed, resulting in the shift of the corrosion potential of the deposited films to the noble direction. The degree of this shift increased with the IME concentration. In contrast, the reduction rate of dissolved oxygen, which is a cathode reaction for corrosion, rarely changed, irrespective of the presence or absence of the IME. Hence, the IME slightly affected the corrosion current density. The reason for the suppression of the dissolution reaction of the deposited films by the IME addition is unknown, but the change in the microstructure of the deposited films and the co-deposition of the IME with the deposited films seemed to affect the dissolution reaction.
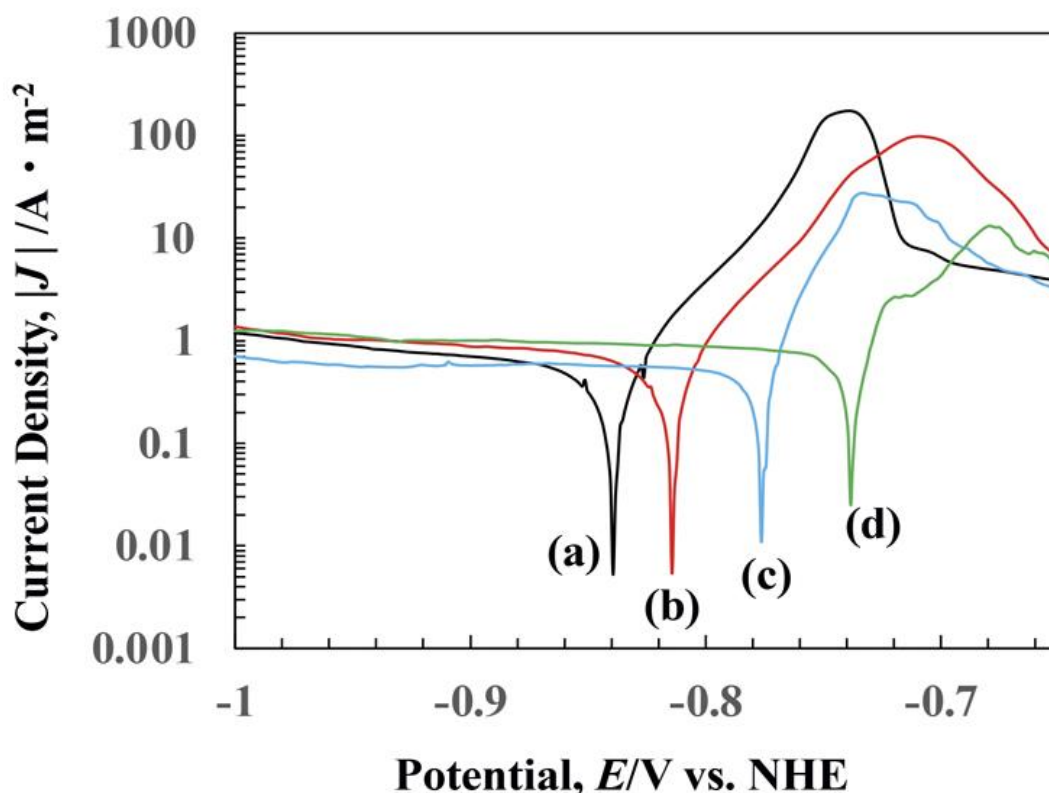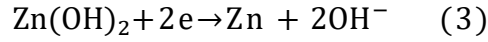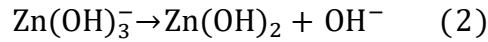
Fig. 2-9. Polarization curves in 3 mass% NaCl solution for deposits obtained at 500 A·m^{-2} from solutions with and without IME: (a) no IME, (b) 1 ml·dm^{-3} IME, (c) 3 ml·dm^{-3}, (d) 5 ml·dm^{-3}.

2-4. Discussion

  The effects of the reaction product of epichlorohydrin and imidazole (IME) on the electrodeposition behavior of Zn–Ni alloys from alkaline zincate solutions are discussed as follows. Even in the Zn–Ni alloy deposition from sulfate solutions, the anomalous co-deposition behavior where electrochemically base Zn preferentially deposits over Ni occurs in the practical current density region where the current efficiency is high.[6~10] The following hydroxide suppression mechanism (1 and 2) is proposed to explain the anomalous co-deposition from sulfate solutions. 1) The Ni deposition from hydrated ions proceeds by a multistep reduction mechanism through the adsorption of intermediate NiOH containing a hydroxyl group, and the adsorption site for NiOH is limited. 2) $Zn(OH)_2$, which results from the increase in pH at the cathode layer caused by hydrogen evolution during electrolysis, adsorbs on the cathode and obstructs the site for $NiOH_{ad}$, thereby suppressing Ni deposition.[6~10] Zn deposition from zincate solutions proceeds through the multistep reaction described by Eqs. (1), (2), and (3) based on the measurement of interfacial impedance.[32~34]

- 28 -

$$Zn(OH)_4^{2-} \rightarrow Zn(OH)_3^- + OH^- \quad (1)$$

$$Zn(OH)_3^- \rightarrow Zn(OH)_2 + OH^- \quad (2)$$

$$Zn(OH)_2 + 2e \rightarrow Zn + 2OH^- \quad (3)$$

At a high current density, Zn deposition occurs through the multistep reaction of Eqs. (1), (2), and (3), and Ni deposition seems to be suppressed by the $Zn(OH)_2$ formed at the cathode layer, resulting in anomalous co-deposition.

In the alloy deposition of Zn−Fe group metals, such as Ni, Fe, and Co, the transition current density at which the deposition behavior shifts from the normal type to anomalous has the same meaning as that at the critical current density at which Zn deposition begins in Zn single solutions.[35] Here, the transition current density for Zn−Ni alloy deposition in this study was 50−100 A·m^{-2} in the IME-free solution; it became 10−20 A·m^{-2} in the IME-containing solution, showing a significant decrease in the transition current density with the addition of the IME (Fig. 2-5(a)). As mentioned above, the transition current density corresponds to the current density at which the cathode potential of the total polarization curve drastically shifts from the more noble potential region than the equilibrium potential of Zn to the negative region, and it was similar to the critical current density for Zn deposition. The critical current density for Zn deposition decreases as the suppression for hydrogen evolution increases.[36~38] Figure 2-10 shows the partial polarization curve for the hydrogen evolution during the Zn−Ni alloy deposition. The partial polarization curve for the hydrogen evolution from the Zn^{2+}- and Ni^{2+}-free solution was compared with that from the Zn−Ni alloy solution. The current density for hydrogen evolution from the Zn−Ni alloy solution decreased once in spite of the shift in the potential to the negative direction irrespective of the presence or absence of the IME in the potential region more noble than the equilibrium potential of Zn, and it increased in the potential region less noble than the equilibrium potential of Zn. The current density for hydrogen evolution from the Zn^{2+}- and Ni^{2+}-free solution increased with the shift in the potential to the negative direction, and it did not decrease in the vicinity of the equilibrium potential of Zn. Since the hydrogen evolution reaction proceeds through a multistep reaction via the adsorption of intermediate H_{ad}[35,36] and the adsorption site for H_{ad} is limited, the formation of the $Zn(OH)_2$ on the surface may suppress the hydrogen evolution reaction by obstructing the adsorption site of H_{ad}. Therefore, the current density for hydrogen evolution from the Zn−Ni alloy solution seemed to decrease once in spite of the shift in the potential to the negative direction in the vicinity of the equilibrium potential of Zn. Focusing on the effect of IME on the hydrogen evolution, the hydrogen evolution was suppressed by the IME in the potential region more noble than the equilibrium potential of Zn. As with $Zn(OH)_2$, the IME seemingly suppressed the hydrogen evolution, due to the limitation in adsorption sites for H_{ad}. As mentioned above, the hydrogen evolution during the Zn−Ni alloy deposition was suppressed by the addition of the IME, resulting in a decrease in the transition current density for the alloy deposition.
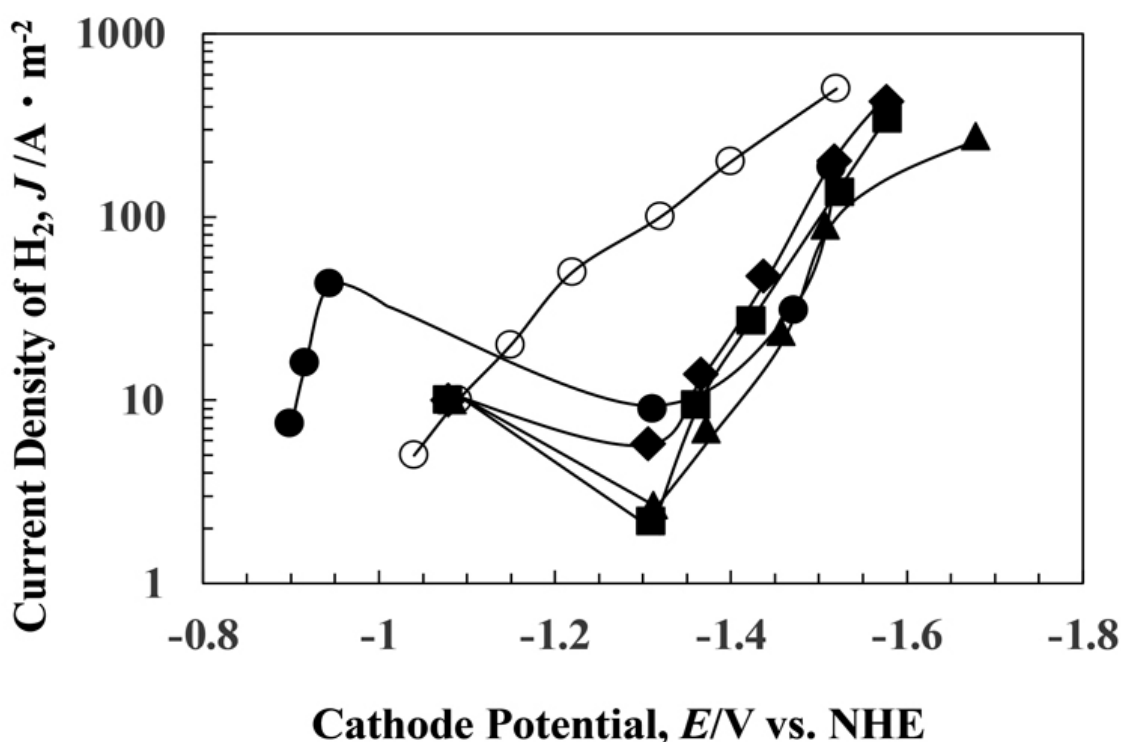
Fig. 2-10. Partial polarization curves for H_2 evolution during Zn−Ni alloy deposition from solutions with and without IME: ● no IME, ▲ 1 ml·dm^{-3} IME, ■ 3 ml·dm^{-3}, · ◆ 5 ml·dm^{-3}, ○ (Zn^{2+}, Ni^{2+}, IME)-free.

   With regard to the effect of the IME on the alloy composition and current efficiency in the Zn−Ni alloy deposition, the IME suppressed both Zn and Ni depositions (Fig. 2-3). Consequently, the current efficiency for the alloy deposition decreased with the IME in the high-current-density region (Fig. 2-4). Regarding the difference in the suppression effect between the Zn and Ni depositions, the Ni content in the Zn−Ni alloy films deposited in the anomalous co-deposition region decreased with the addition of the IME (Fig. 2-5(b)), indicating that the Ni deposition was more suppressed by the IME than Zn deposition. Assuming that the adsorption sites for intermediate $NiOH_{ad}$ during Ni deposition were limited, the limited adsorption sites of $NiOH_{ad}$ seem to be obstructed by the adsorption of the IME, resulting in greater suppression of the Ni deposition than Zn deposition. Therefore, the Ni content in the deposited alloy films decreased with the addition of the IME.

   About the effect of the IME on the appearance and crystal morphology of the deposited Zn−Ni alloy films, the films deposited from the IME-containing solution became smooth with increasing current density (Fig. 2-6), and they showed a significant gloss (Fig. 2-2). Thus, the effect of the IME on the microstructure of the deposited films increased with the current density. Since the additive used in this study was polymers composed of quaternary

ammonium cations (Fig. 2-1), the electrostatic adsorption ability onto the cathode increased with the current density or the shift in the cathode potential to the negative direction, consequently increasing the IME effect with the current density.

2-5. Conclusion

The effect of the reaction product of epichlorohydrin and imidazole (IME) on the deposition behavior of Zn–Ni alloys was investigated using polarization curves for the Zn and Ni depositions and hydrogen evolution. The IME was used as the brightener. The transition current density at which the deposition behavior shifted from the normal type to anomalous was $50-100$ $A \cdot m^{-2}$ in the IME-free solution; it became $10-20$ $A \cdot m^{-2}$ with the addition of the IME, indicating that the IME greatly decreased the transition current density. The transition current density corresponds to the current density at which the potential of the total polarization curve significantly shifts from the more noble region than the equilibrium potential of Zn to the less noble region. With the addition of the IME, the decrease in transition current density was attributed to the suppression of hydrogen evolution, and the current efficiency for the alloy deposition in the high-current-density region decreased due to the suppression of both the Zn and Ni depositions. The Ni content of the deposited films decreased with the IME, indicating that Ni deposition was more suppressed by the IME than Zn deposition. With increasing current density, the crystals of the films deposited from the IME-containing solution became smooth and showed significant brightness. The oxidation reaction of the films deposited from the IME-containing solution was suppressed. Consequently, the corrosion potential shifted to the noble direction with the IME.

2-6. References

1) L. Fellonu, R. Frratesi, E. Quadrini and G. Roventi: *J. Appl. Electrochem.*, **17** (1987), 574.

2) MF Mathias and TW Chapman: *J. Electrochem. Soc.*, **134** (1987), 1408.

3) S. Swathirajan: *J. Electronal. Chem.*, **221** (1987), 211.

4) T.Fujigaya : Electroplating, Chemical Plating & Engineering Guide, Nippon Tokin Zairyo Kyodo Kumiai, Tokyo, (2004),143 (in Korean).

5) M.Kawasaki and H.Enomoto: Mekki Kyohon (Textbook for plating), Nikkan Kogyo Shimbun, Tokyo, (1988),108 (in Korean).

6) A.Brenner : Electrodeposition of Alloys, Vols.1,2, Academic Press, New York, (1963), **221**.

7) H. Fukushima, T. Akiyama, J. Lee, M. Yamaguchi and K. Higashi: *J. Met. Finish. Soc. Jpn.*, **33** (1982), 574 (in Korean).

8) H. Fukushima, T. Akiyama, M. Yano, T. Ishikawa and R. Kammel: *ISIJ Int.*, **33** (1993), 1009.

9) H. Nakano, S. Kobayashi, T. Akiyama, T. Tsuru and H. Fukushima: *Tetsu-to-Hagane*, **89** (2003), 64 (in Korean).

10) H. Nakano, M. Matsuno, S. Oue, M. Yano, S. Kobayashi and H. Fukushima: *J. Jpn. Inst. Met.*, **69** (2005), 548 (in Korean).

11) MG Hosseini, H. Ashassi-Sorkhabi and HAY Ghiasvand: *Surf. Coat. Technol.*, **202** (2008), 2897.

12) LS Tsybulskaya, TV Gaevskaya, OG Purovskaya and TV Byk: *Surf. Coat. Technol.*, **203** (2008), 234.

13) GY Li, JS Lian and ZH Jiang: *Surf. Coat. Technol.*, **191** (2005), 59.

14) NR Short, S. Zhou and JK Dennis: *Surf. Coat. Technol.*, **79** (1996), 218.

15) C. Muller, M. Sarret and M. Benballa: *J. Electroanal. Chem.*, **519** (2002), 85.

16) HY Lee and SG Kim: *Surf. Coat. Technol.*, **135** (2000), 69.

17) H. Nakano, S. Arakawa, Y. Takada, S. Oue and S. Kobayashi: *J. Jpn. Inst. Met.*, **76** (2012), 443 (in Korean).

18) H. Nakano, S. Arakawa, S. Oue and S. Kobayashi: *Tetsu-to-Hagane*, **99** (2013), 425 (in Korean).

19) H. Nakano, S. Arakawa, Y. Takada, S. Oue and S. Kobayashi: *Mater. Trans.*, **53** (2012), 1946.

20) H. Nakano, S. Arakawa, S. Oue and S. Kobayashi: *ISIJ Int.*, **53** (2013), 1864.

21) H. Nezu, S. Fujii, N. Kaneko and N. Ofuchi: *J. Met. Finish. Soc. Jpn.*, **32** (1982), 17 (in Korean).

22) S. Konishi, S. Eguchi, N. Ozeki and M. Uesugi: *J. Met. Finish. Soc. Jpn.*, **20** (1969), 263 (in Korean).

23) T. Watanabe: *J. Surf. Finish. Soc. Jpn.*, **40** (1989), 280 (in Korean).

24) DDPerrin: Stability Constants of Metal-ion Complexes, Part B, Organic Compounds, Pergamon Press, Oxford, (1979), 466.

25) T. Akiyama, H. Fukushima and K. Higashi: *Tetsu-to-Hagane*, **72** (1986), 918 (in Korean).

26) R. Winand: *J. Appl. Electrochem.*, **21** (1991), 377.

27) A. Shibuya, T. Kurimoto, K. Korekawa and K. Noji: *Tetsu-to-Hagane*, **66** (1980), 771 (in Korean).

28) S.Haruyama: Hakumaku Zairyo no Kiso to Ohyo (Foundation and application of thin film materials), The Japan Institute of Metals, Sendai, (1987), 37 (in Korean).

29) H. Nakano, S. Oue, T. Miki, S. Kobayashi and H. Fukushima: *ISIJ Int.*, **46** (2006), 106.

30) H. Nakano, S. Oue, Y. Hamaguchi, S. Kobayashi, H. Fukushima: *ISIJ Int.*, **49** (2009), 1769.

31) H. Nakano: Trans. Nonferr. *Met. Soc. China*, **19** (2009), 835.

32) T. Yamashita and S. Toshima: Nippon Kagaku Kaishi, 1980 (1980), 1824 (in Korean).

33) K.Aotani : Gokin Mekki VI (Alloy plating VI), Nippon Plating Kyokai, Tokyo, (2005), 133 (in Korean).

34) T.Yoshida: New Engineering Review of Coating, Sangyo Gizyutsu Service Center, Tokyo, (1987), 318 (in Korean).

35) H. Fukushima and H. Nakano: *J. Surf. Sci. Soc. Jpn.*, **22** (2001), 107 (in Korean).

36) H. Nakano, T. Ohgai, H. Fukushima,T. Akiyama and R. Kammel: *Metall*, **55** (2001), 676.

37) H. Fukushima, T. Akiyama and T. Ohgai: *J. MMIJ*, **110** (1994), 967 (in Korean).

38) H. Fukushima, T. Akiyama and K. Kiyotani: *J. MMIJ*, **109** (1993), 861 (in Korean).

Chapter 3. Effect of Solution Temperature on Electrodeposition Behavior of Zn-Ni Alloy from Alkaline Zincate Solution

3-1. Introduction

Zn–Ni alloys are usually deposited in a sulfate or chloride solution; however, considering the throwing power on small parts, the use of a zincate solution is preferable. Zn–Ni alloy deposition from sulfate and chloride solutions have been studied a lot so far, and are known to lead to anomalous co-deposition behavior, in which the electrochemically less-noble Zn is preferentially deposited over noble Ni in the practical current density range.[1-7] Although the effect of current density,[8-11] total concentration of metal ions,[12] agitation of solution,[11] concentration of Ni complexing agent[19] and solution composition[9,11-13] and the effect of current density[10,12] on the current efficiency for alloy deposition were reported in Zn–Ni alloy deposition from the zincate solutions, few studies on the deposition mechanism[14] have been reported compared with those on sulfate and chloride.

Solution temperature is known to affect the overpotential, throwing power, metal salt solubility, and solution conductivity.[15] Increasing the solution temperature increases the diffusion coefficient of ions in solution and solubility of the metal salt, as well as conductivity of the solution, which consequently increases the diffusion-limiting current density. In contrast, when the solution temperature is decreased, the crystal grain of the deposits becomes finer, and the throwing power is improved, based on the increases in the deposition overpotential. Thus, solution temperature is a highly important factor in electrodeposition. However, the effect of solution temperature on the deposition behavior of the Zn–Ni alloys from zincate solutions has rarely been reported.[11] In the present study, this topic is discussed, based on the partial polarization curves of Zn and Ni depositions and H_2 evolution.

3-2. Experimental

Table 3-1 shows the zincate solution composition and electrolysis conditions for the Zn–Ni alloy deposition. The electrolytic solutions were prepared by dissolving reagent-grade ZnO (0.15 mol·dm^{-3}), NiSO$_4$·6H$_2$O (0.016 mol·dm^{-3}), N(CH$_2$CH$_2$OH)$_3$ (0.34 mol·dm^{-3}), and NaOH (2.5 mol·dm^{-3}) in distilled and deionized water at room temperature. In some experiments, the deposition behavior was investigated using a solution containing only Ni or Zn, eliminating the ZnO (0.15 mol·dm^{-3}) or NiSO$_4$·6H$_2$O (0.016 mol·dm^{-3}) from the solution noted above. Electrodeposition was carried out by the constant-current electrolysis method, without stirring, at current densities of 10–500 A·m^{-2}, an amount of charge of 5×10^4 C·m^{-2}, and solution temperatures of 293, 313, and 333 K. The amount of charge of 5×10^4 C·m^{-2} corresponded to a film thickness of 2.37 μm, assuming the deposition of pure Zn at a current efficiency of 100%. A Cu plate (1 × 2 cm) was used as the cathode and a Pt plate (1 × 2 cm) as the anode, respectively. However, when preparing samples for scanning electron

microscopy (SEM) observation and X-ray diffraction (XRD) analysis, an Fe plate (1 × 2 cm) was used as the cathode. The obtained electrodeposits were dissolved in HNO_3, and Zn and Ni were quantified by inductively coupled plasma-optical emission spectroscopy (ICP-OES) to determine the composition of the deposited alloy and the current efficiency of the Zn and Ni depositions. The current efficiency of the H_2 evolution was calculated by subtracting the current efficiencies (%) of Zn and Ni from 100, and the partial current densities of Zn and Ni depositions and H_2 evolution were calculated by multiplying the total current density by the current efficiency (%)/100. The partial current densities for Zn and Ni depositions and H_2 evolution were calculated by multiplying the total current density by their respective current efficiencies (%)/100. The current efficiencies for Ni and Zn depositions from the solution with only Ni or Zn were calculated using the same method as for alloy deposition. An Ag/AgCl electrode (saturated KCl, 0.199 V vs. NHE, 298 K) was used as a reference electrode to measure the polarization curve, but the potential was converted to a standard hydrogen electrode and displayed. The surface morphology of the deposited films was observed by SEM, and the phase identification was carried out by XRD (Cu-Kα, tube voltage = 40 kV, tube current = 15 mA).

Table 3-1. Solution compositions and electrolysis conditions.

ZnO	(mol·dm^{-3})	0.15	Current density (A·m^{-2})	10–500
NiSO$_4$·6H$_2$O	(mol·dm^{-3})	0.016	Temperature (K)	293, 313, 333
N(CH$_2$CH$_2$OH)$_3$	(mol·dm^{-3})	0.34	Amount of charge (C·m^{-2})	5 × 10^4
NaOH	(mol·dm^{-3})	2.5	Cathode	Cu (1 × 2 cm^2)
Quiescent bath			Anode	Pt (1 × 2 cm^2)

3-3. Results

3-3-1. Effect of Solution Temperature on the Deposition Behavior of Zn–Ni Alloys

Figure 3-1 shows the total polarization curve of the Zn–Ni alloy deposition and the partial polarization curves of Zn and Ni depositions and H_2 evolution. The equilibrium potential, E_{Zn}^{eq}, of the Zn deposition （$ZnO_2^{2-} + 2H_2O + 2e^-$ $\rightarrow Zn + 4OH^-$） was −1.27 V, assuming pure Zn deposition.[16] The total polarization curve (Fig. 3-1(a)) rose in the nobler potential region compared with the equilibrium potential of Zn (−1.27 V), regardless of the solution temperature. Furthermore, it significantly shifted to the less-noble potential region when the current density exceeded 50–100 A·m^{-2}, and rose again when the potential reached the equilibrium potential of Zn. At all the potential region nobler and less noble than the equilibrium potential of Zn, comparing the potential at the constant total current density, the potential shifted to noble direction with

increasing solution temperature. At solution temperatures of 293 and 313 K, the current density range in which the cathode potential shifted significantly from the region nobler than the equilibrium potential of Zn to the equilibrium potential was 50–100 A·m^{-2}. At 333 K, it was as high as 100–200 A·m^{-2}.

The partial polarization curve of the Zn deposition (Fig. 3-1(b)) rose in the nobler potential region than the equilibrium potential of Zn, as with the total polarization curve, regardless of the solution temperature. It then shifted to the less-noble potential region, before sharply rising when it reached a potential less-noble region than the equilibrium potential of Zn (−1.27 V). In both potential regions, the partial polarization curve of the Zn deposition shifted in the noble direction as the solution temperature increased. For the Zn−Ni alloy deposition, the current density for Zn deposition was only slightly detected, even at approximately −0.9 V, a value nobler than its equilibrium potential. Comparing the current density at a constant potential of −0.9 V, the current density of Zn deposition increased with increasing solution temperature.

The equilibrium potential, E_{Ni}^{eq} for Ni deposition (Ni(TEA)$_2^{2+}$ + 2e$^-$→Ni + 2TEA) was −0.41 V. This was calculated by assuming that pure Ni had been deposited, based on the complex stabilization constant K = 10$^{4.74}$,[17] which was formed by the coordination of two triethanolamine molecules toward Ni^{2+} ions. Similar to the total polarization curve, the partial polarization curve of the Ni deposition (Fig. 3-1(c)) also rose in the potentially nobler region compared with the equilibrium potential of Zn, regardless of the solution temperature. It then shifted to the less-noble potential region and rose again at potentials less noble than the equilibrium potential of Zn (−1.27 V). In both potential regions, the partial polarization curve of the Ni deposition shifted to nobler potential direction as the solution temperature increased.

The H$_2$ evolution in the Zn−Ni alloy solution (Fig. 3-1(d)) rose in the region nobler than the equilibrium potential of Zn, decreased once (despite the shift in the potential to the negative direction), and increased again in the region that was less noble than the equilibrium potential of Zn. The partial polarization curve of the H$_2$ evolution did not differ significantly at solution temperatures of 293 and 313 K. In contrast, at 333 K, it was clearly depolarized (i.e., the electrode potential shifted to a nobler value when comparing the electrode potential at a constant-current density), and the current density at which the potential sharply shifted to in the less-noble direction was higher than those measured at 293 and 313 K.
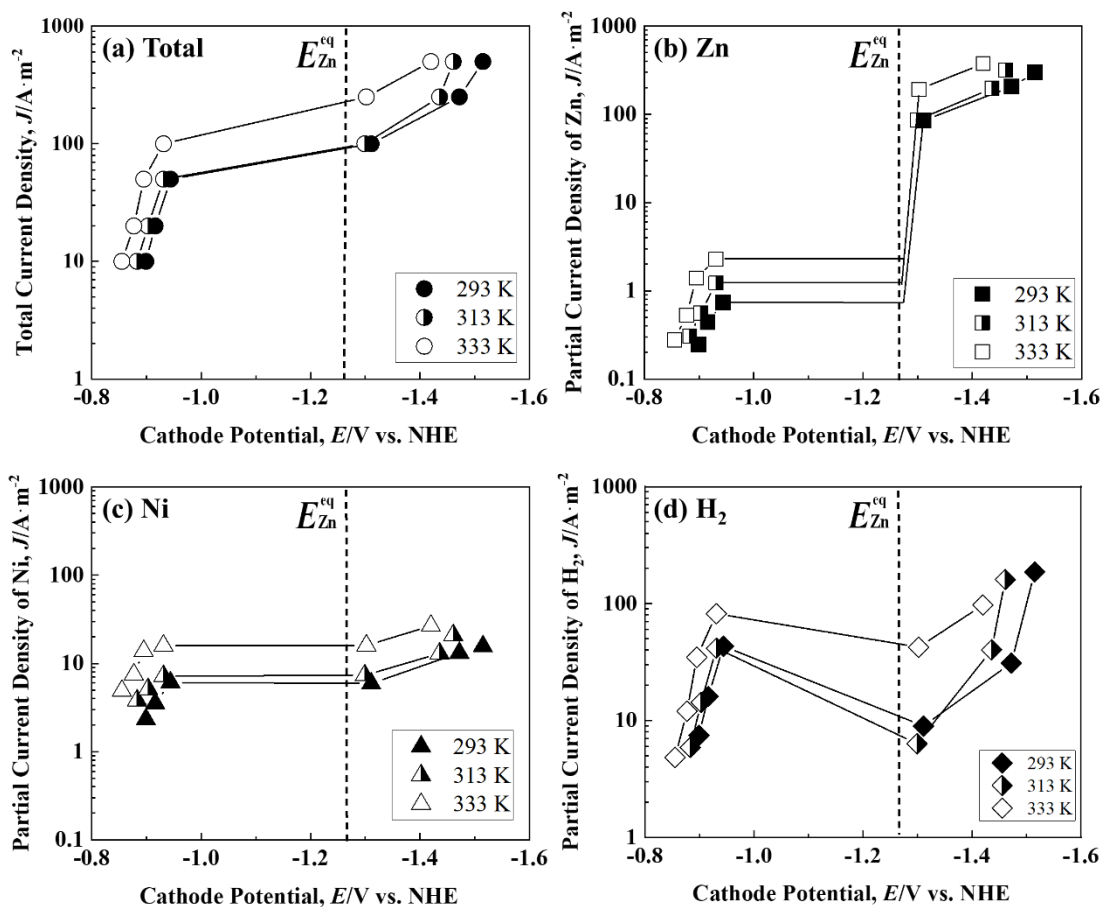
Fig. 3-1. Polarization curves for Zn–Ni alloy deposition at 293, 313 and 333 K. [(a) Total polarization curves, partial polarization curves of (b) Zn, (c) Ni and (d) H$_2$]

Figure 3-2 shows the correlation between the current efficiency and current density for Zn–Ni, Zn, and Ni depositions and H$_2$ evolution during Zn–Ni alloy deposition at different temperatures. The current efficiency of Zn–Ni alloy deposition is the sum of the current efficiencies of Zn and Ni depositions. As shown in Fig. 3-2(a), the current efficiency of the alloy deposition at a solution temperature of 293 K was low, ranging from 14% to 26% in the low-current density range of 10–50 A·m^{-2}. However, it sharply increased when the current density exceeded 50 A·m^{-2} and reached a maximum at 100 A·m^{-2}. It then decreased as the current density further increased. A similar trend was observed at 313 K, although the current efficiency was slightly higher in the low and high-current density ranges of 10–50 A·m^{-2} and 500 A·m^{-2}, respectively. Contrastingly, at a solution temperature of 333 K, the current efficiency was low, ranging from 18% to 52% in the low-current density range of 10–100 A·m^{-2}, although it significantly increased when the current density exceeded 100 A·m^{-2} and reached a maximum at 250 A·m^{-2}. The current efficiency rarely decreased, even when the current density was increased to 500 A·m^{-2}. At solution temperatures of 293 and 313 K, the current efficiency of Zn deposition during alloy deposition (Fig. 3-2(b)) was very low in the low-current density

range of 10–50 A·m^{-2}, and it was also very low in the range of 10–100 A·m^{-2} at 333 K. However, it increased sharply when the current density exceeded 50 and 100 A·m^{-2}, respectively. The current efficiency of Ni deposition during alloy deposition (Fig. 3-2(c)) also decreased with increasing current density, regardless of the solution temperature. Furthermore, the current efficiency of Ni deposition was higher at higher solution temperature. In the low-current density range of 10–50 A·m^{-2} at solution temperatures of 293 and 313 K, and in the range of 10–100 A·m^{-2} at 333 K, H$_2$ evolution had the highest current efficiency (Fig. 3-2(d)), followed by Ni deposition. However, in the high-current density range above 50–100 A·m^{-2}, the current efficiency of Zn deposition was the highest. Thus, the current efficiency of Zn–Ni alloy deposition reflected the current efficiency of Ni deposition in the low-current density region and that of Zn deposition in the high-current density region.

The current efficiency of Zn deposition (Fig. 3-2(b)) was also compared with the total polarization curve shown in Fig. 3-1(a). The range of 10–50 A·m^{-2} was nobler than the equilibrium potential of Zn at solution temperatures of 293 and 313 K, and the current efficiency of Zn deposition was thus considered as being low. When the current density exceeded 50 A·m^{-2}, the potential shifted to the less-noble region compared with the equilibrium potential of Zn (Fig. 3-1(a)), therefore, the current efficiency of Zn seems to increase sharply. At a solution temperature of 333 K, the potential was nobler than the equilibrium potential of Zn in the range of 10–100 A·m^{-2}. However, when the current density exceeded 100 A·m^{-2}, the potential shifted to a potential range less noble than the equilibrium potential of Zn (Fig. 3-1(a)), resulting in a sharp increase in the current efficiency of Zn. Thus, the current densities at which the current efficiency sharply changed, at all measured temperatures, corresponded to those at which the cathode potential changed from the potential region nobler than the equilibrium potential of Zn to that of the equilibrium potential of Zn in the total polarization curve. The decrease in the current efficiency at 500 A·m^{-2} at solution temperatures of 293 and 313 K appeared to have been caused by the fact that the Zn deposition approached the diffusion limit of the Zn ions.
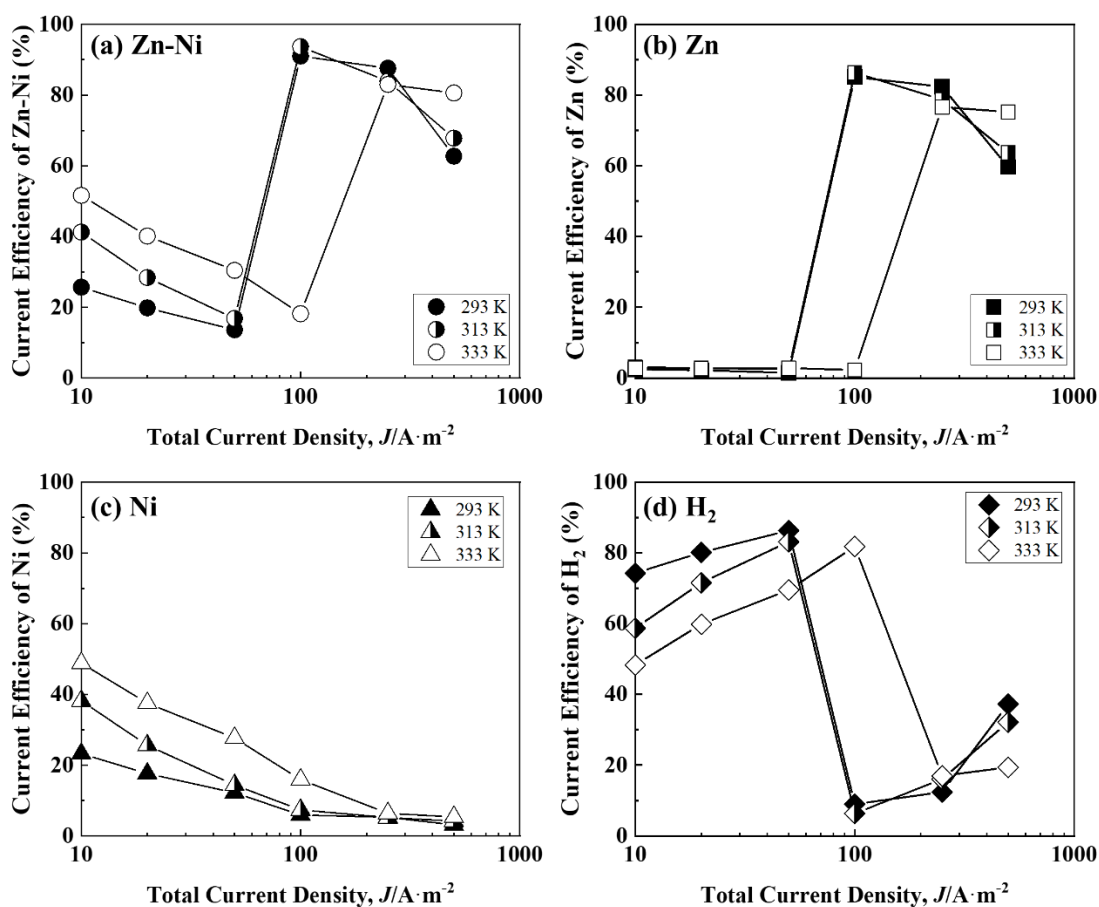
Fig. 3-2. Current efficiencies for Zn–Ni alloy deposition at 293, 313 and 333 K. [(a) Zn-Ni, (b) Zn, (c) Ni and (d) H_2]

Figure 3-3 shows the effect of the current density on the Ni content of the Zn–Ni alloy films. The broken line (the compositional reference line [CRL] of Ni) represents the Ni content in the deposits predicted from the concentration ratio of Ni ions against the total metal ions in the solution. When the Ni content in the deposited films exceeded the CRL, a normal co-deposition occurred, with electrochemically noble Ni being preferentially deposited over Zn. In contrast, when the Ni content in the deposited films was lower than the CRL, an anomalous co-deposition occurred, with base Zn being deposited preferentially over Ni. As shown in Fig. 3-3, the Ni content in the deposited films altered significantly in the range of 50–100 $A \cdot m^{-2}$ at solution temperatures of 293 and 313 K. At current densities below 50 $A \cdot m^{-2}$, the Ni content in the deposited films was approximately 90 mass% above the CRL, indicating normal co-deposition, while at current densities above 100 $A \cdot m^{-2}$, the Ni content in the deposited films was below the CRL, indicating anomalous co-deposition. In contrast, at 333 K, the Ni content in the deposited films was significantly altered in the region from 100 to 250 $A \cdot m^{-2}$. Below 100 $A \cdot m^{-2}$, the Ni content in the deposited films was above the CRL, indicating the normal co-deposition. Above 250 $A \cdot m^{-2}$, the Ni content in the deposited films was below the CRL, indicating the

anomalous co-deposition. The current density at which the deposition behavior shifts from normal to anomalous is called the transition current density.[18-20] At all the solution temperatures, the transition current density corresponded to the current density at which the potential of the total polarization curve shown in Fig. 3-1(a) abruptly shifted to the less-noble potential region, or to the current density at which the current efficiency significantly changed (Fig. 3-2(b)). As described above, the transition current density at 293 K was almost identical to that at 313 K, although it was higher at 333 K. The Ni content in the films increased with increasing solution temperature in the low-current density range, where normal co-deposition was observed. The Ni content in the deposited films also increased slightly with an increasing solution temperature in the current density range above 250 $A \cdot m^{-2}$ at which the anomalous co-deposition occurred (Fig. 3-3(b)).
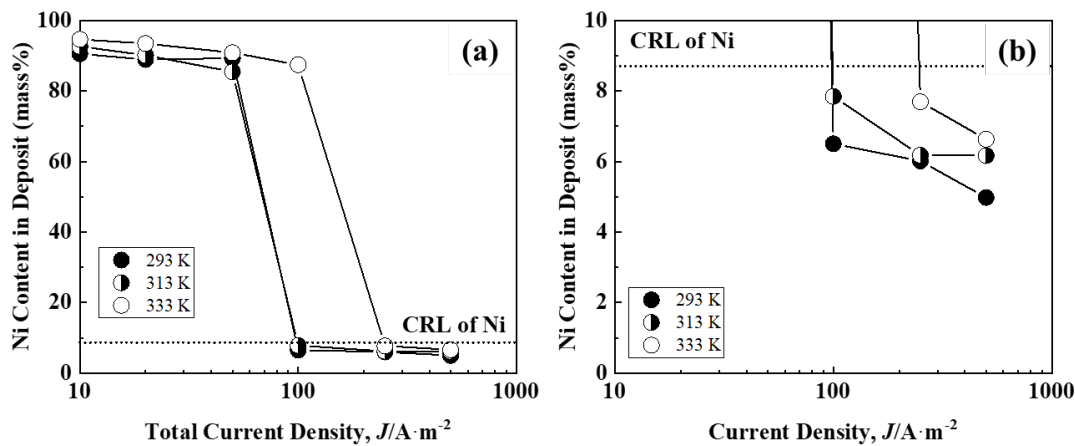

Fig. 3-3. Ni contents in the Zn–Ni alloys deposited at various current densities from different temperatures. (b) Magnified view of the area of 0–10 mass% of the Ni content.

3-3-2. Effect of Solution Temperature on the Microstructure of Deposited Films

Figure 3-4 shows the X-ray diffraction patterns of the films obtained at various current densities from the solutions at different temperatures. Three main peaks were observed in the films obtained at 10 $A \cdot m^{-2}$ (Figs. 3-4(a)–(c)). The diffraction angles of the substrate Fe and α-Ni phases (solid solution of Zn in the Ni) overlapped at 44.7°, making it difficult to identify the α-phase. Therefore, we investigated the XRD pattern of the substrate Fe only and confirmed that the peak intensity at a diffraction angle of 44.7° was smaller than that at 65.0°. However, it was larger than that at 65.0° for the deposited film obtained at 10 $A \cdot m^{-2}$, regardless of the solution temperature; it was thus concluded that the α-phase existed in all the deposited films. Weak peaks indicating the presence of the α-phase were also detected at diffraction angles other than 44.7° in the deposited films obtained at 333 K. The deposition at 10 $A \cdot m^{-2}$ exhibited the normal co-deposition, regardless of the solution temperature, and the Ni content in the deposited films was above 90 mass%. As a result, only the α-

phase was thought to be detected. No peaks related to Zn, obtained by underpotential co-deposition, were detected. In the deposited films obtained at 100 A·m^{-2}, the η-phase (solid solution of Ni in the Zn) and γ-phases (intermetallic compound Ni$_2$Zn$_{11}$), were detected at solution temperatures of 293 and 313 K (Figs. 3-4(d) and (e)), whereas only peaks of the α-phase and Fe were detected at 333 K (Fig. 3-4(f)). At 100 A·m^{-2}, the deposition behavior differed significantly, based on the solution temperature. In particular, the depositions at 293 and 313 K exhibited the anomalous co-deposition, resulting in a high Zn content (approximately 93 mass%) in the films, while the deposition at 333 K exhibited the normal co-deposition, resulting in a high Ni content (approximately 87.4 mass%; Fig. 3-3). The XRD patterns of the deposited films obtained at 100 A·m^{-2} reflected this same deposition behavior. In contrast, the η- and γ-phases were detected in the deposited films obtained at 500 A·m^{-2} (Figs. 3-4(g)–(i)), and the formation of the γ-phase was dominant at higher solution temperatures. Since the Ni content in the deposited films increased with increasing solution temperature (Fig. 3-3(b)), the formation of the γ-phase seems to become easy with increasing temperature. At 100 A·m^{-2}, the main peak of the γ-phase was higher at 313 K than at 293 K, indicating that the γ-phase had increased with temperature. These results indicated that the γ-phase increased with increasing solution temperature in the case of the anomalous co-deposition of deposited films with a high Zn content.

Figure 3-5 shows the SEM images of the deposited films obtained from the solutions at different temperatures and current densities. The films deposited at 10 A·m^{-2} were smooth at 293 K (Fig. 3-5(a)) but became slightly coarse at higher solution temperatures (Figs. 3-5(b) and (c)). The films obtained at 10 A·m^{-2} comprised the α-phase and had an Ni content of greater than 90 mass% at all the solution temperatures, while the grain size was thought to be increased as the solution temperature increased, due to a decrease in the overpotential for deposition. In the films deposited at 100 A·m^{-2}, the agglomerations consisting of fine crystals were observed at 293 and 313 K (Figs. 3-5(d) and (e)), while at 333 K, the morphology was similar to that of the deposited films obtained at 10 A·m^{-2} (Fig. 3-5(f)). As noted above, for the deposition at 100 A·m^{-2}, an anomalous co-deposition was observed at 293 and 313 K, and the deposited films with approximately 7 mass % of Ni content in deposits comprised η and γ-phases, while a normal co-deposition was observed at 333 K, and the deposited films with 87.4 mass % of Ni content in deposits comprised an α-phase. The surface morphology of the films obtained at 100 A·m^{-2} seem to reflect the phase structure noted above. In contrast, that of the films obtained at 500 A·m^{-2} where an anomalous co-deposition was observed at all the temperatures, exhibited the plate-like crystal characteristics of the η-phase at a solution temperature of 293 K (Fig. 3-5(g)). However, this plate-like structure disappeared with increasing solution temperatures (Fig. 3-5(i)), and a smooth surface was observed. The films deposited at 500 A·m^{-2} comprised η and γ-phases, and the γ-phase became dominant with increasing solution temperature, as a result, the surface morphology seems to change.
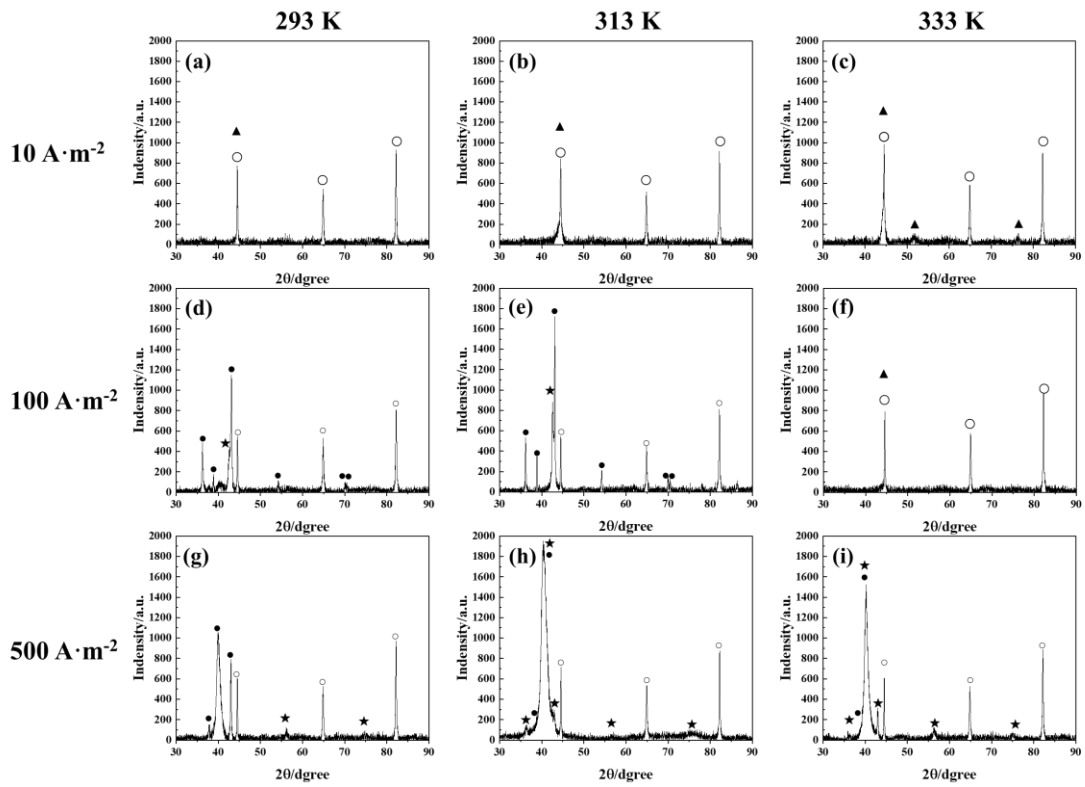
Fig. 3-4. X-ray diffraction patterns of the Zn−Ni alloy films deposited at various current densities from different temperatures. (▲ Ni[α] PDF # 87-0712, ○ Fe PDF # 65-4899, ● Zn[η] PDF # 87-0713, and ★ Ni_2Zn_{11}[γ] PDF # 65-5310)
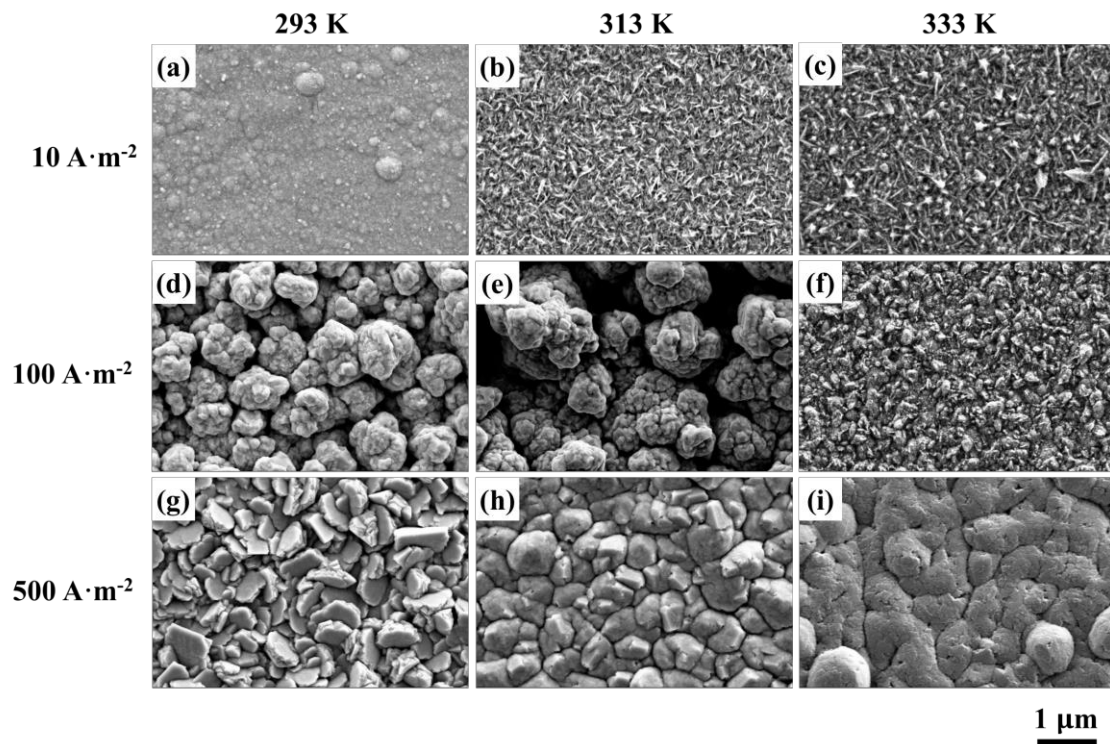

Fig. 3-5. SEM images of the surface of the Zn−Ni alloys deposited at various current densities from different temperatures.

3-4. Discussion

The effect of solution temperature on the deposition behavior of the Zn−Ni alloys from alkaline zincate solutions was investigated. The transition current density at which the deposition behavior shifted from the normal to anomalous, the current efficiency of the alloy deposition, and the composition of the deposited films changed depending on the solution temperature. The reasons for these effects are discussed as follows.

The partial polarization curve of Ni deposition in the alloy deposition (Fig. 3-1(c)) is first explained. This partial polarization curve rose at approximately −0.9 V, regardless of the solution temperature, which was a nobler value than the equilibrium potential of Zn, and then sharply shifted to a less noble potential region (Fig. 3-1(c)). The partial current density at which the cathode potential changed sharply to a less noble potential region was similar to the diffusion-limiting current density[15] of the Ni deposition. However, if this current density was assumed as the diffusion-limiting current density of Ni, the Ni content of the deposited films would be above the CRL in the entire current density range,[21-23] which would contradict the results of the present study. In fact, it has been reported that in the normal type deposition, the deposition of the noble metal becomes the diffusion-limiting current density, and the content of the noble metal in the films will be above the CRL in all the current density range.[21-23]

In the present study, the partial current density of Ni deposition at which the cathode potential changed sharply to a less noble potential region shown in Fig. 3-1(c) was not the diffusion-limiting current density because the anomalous co-deposition was observed in the high-current density region.

It was reported that the transition current density in Zn−Ni alloy deposition from a sulfate solution corresponded to the current density that generated the overpotential for H_2 evolution η_H^{Inh}; this is represented by Eq. (1) as follows:[24-26]

$$E_H^{eq} - \eta_H^0 - \eta_H^{Inh} = E_{Zn}^{eq} \qquad (1)$$

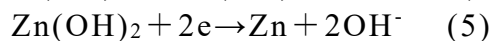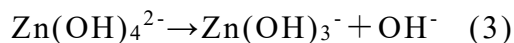Here, E_H^{eq} and E_{Zn}^{eq} denote the equilibrium potentials for H_2 evolution and Zn deposition, respectively; η_H^0 is the minimum overpotential for H_2 evolution, and η_H^{Inh} is the overpotential for H_2 evolution in the presence of its inhibitor. In the case of Zn deposition from an acidic solution, the reaction intermediate $Zn(OH)_2$ will be formed by hydrolysis of the Zn^{2+} ions ($Zn^{2+} + 2H_2O \rightarrow Zn(OH)_2 + 2H^+$), caused by the increase in pH due to H_2 evolution reaction ($2H^+ + 2e^- \rightarrow H_2$) at the cathode layer. This $Zn(OH)_2$ appears to create the overpotential for H_2 evolution, i.e., η_H^{Inh}.[32-34] In Zn−Ni alloy deposition from a sulfate solution, Ni deposition is suppressed by $Zn(OH)_2$ and becomes almost zero in the normal co-deposition region, resulting in H_2 evolution only.[18] Therefore, to complete Eq. (1), the transition current density is defined as the H_2 evolution current density that is required to generate the overpotential, i.e., η_H^{Inh}.[24-26] However, in Zn−Ni alloy deposition from zincate solutions, Zn and Ni are deposited in the region of the normal co-deposition at potentials nobler than the

equilibrium potential of Zn (Figs. 3-1(b),(c)), and the potential of Ni deposition shifts significantly to the equilibrium potential of Zn at the transition current density. Therefore, the transition current density in the zincate solution is considered to be the sum of the current densities of the H_2 evolution and Zn and Ni depositions required to satisfy both Eqs. (1) and (2).

$$E_{Ni}^{eq} - \eta_{Ni}^0 - \eta_{Ni}^{Inh} = E_{Zn}^{eq} \qquad (2)$$

Here, E_{Ni}^{eq} denotes the equilibrium potential for Ni deposition, η_{Ni}^0 is the minimum overpotential for Ni deposition, and η_{Ni}^{In} is the overpotential for Ni deposition in the presence of its inhibitor.

It was reported that the inhibitor of H_2 evolution and Ni deposition in Zn–Ni alloy deposition from acidic solutions was $Zn(OH)_2$, which was formed by the hydrolysis of Zn^{2+} ions.[26] However, no hydrolysis reaction of the Zn^{2+} ions occurs in zincate solutions. Generally, Zn deposition from a zincate solution has been reported to proceed by the multistep reactions shown in Eqs. (3)–(5),[27-29]

$$Zn(OH)_4^{2-} \rightarrow Zn(OH)_3^- + OH^- \quad (3)$$
$$Zn(OH)_3^- \rightarrow Zn(OH)_2 + OH^- \qquad (4)$$
$$Zn(OH)_2 + 2e \rightarrow Zn + 2OH^- \qquad (5)$$

In Zn–Ni alloy deposition from a zincate solution, the $Zn(OH)_2$ formed during the multistep reactions is thought to act as an inhibitor for the H_2 evolution and Ni deposition. In this study, the current density for H_2 evolution from the Zn–Ni alloy solution decreased once, despite a shift in the potential to the less noble direction in the region that was nobler than the equilibrium potential of Zn (Fig. 3-1(d)); this was attributed to suppression by $Zn(OH)_2$, formed through the multistep reactions of Zn deposition. The transition current densities at solution temperatures of 293 and 313 K were almost identical but they significantly increased at 333 K (Fig. 3-1(a)). Focusing on the effect of solution temperature on the partial current densities of Zn and Ni depositions and H_2 evolution in the transition current density region, it was found that the partial current densities of the H_2 evolution and Ni deposition were almost identical at solution temperatures of 293 and 313 K but clearly increased at 333 K (Figs. 3-1(b)–(d)). That is, because the H_2 evolution and Ni deposition were promoted at 333 K, the current density that was required to complete Eqs. (1) and (2), i.e., the transition current density, seems to increase with solution temperature.

In Zn–Ni alloy deposition, a competition reaction between the Zn and Ni depositions and H_2 evolution occurs. Hence, deposition was performed with solutions including only Ni or Zn to compare the effect of the solution temperature on each reaction. Figure 3-6 shows the effect of solution temperature on the partial polarization curve for Ni deposition and H_2 evolution for the Ni solution. Both Ni deposition and H_2 evolution were depolarized with increasing solution temperature. At a partial current density of 3 $A \cdot m^{-2}$ for Ni deposition, the potential shifted to the noble direction by approximately 0.2 V, when the

solution temperature was raised from 293 to 333 K. At a partial current density of 100 A·m^{-2} for H$_2$ evolution, the potential shifted by approximately 0.06 V with increasing solution temperature, and the degree of depolarization was greater for Ni deposition. Here the overpotential for metal deposition, i.e., η_M, is defined by the following equation:

$$\eta_M = |E_M^{eq} - E_M| \quad (6)$$

where E_M^{eq} is the equilibrium potential of metal deposition, and E_M is the electrode potential for metal deposition. Comparing the overpotential for Ni deposition with that for H$_2$ evolution, the one for Ni deposition was larger. Figure 3-7 shows the effect of solution temperature on the current efficiency of Ni deposition from the Ni solution. The current efficiency for Ni deposition increased with increasing solution temperature at all current densities. Particularly, in the low-current-density region of 10–20 A·m^{-2}, the current efficiency for Ni deposition significantly increased with solution temperature. Based on Figs. 3-6 and 7, it was found that both Ni deposition and H$_2$ evolution were promoted with increasing solution temperature, while increase in solution temperature had a stronger promotional effect on the Ni deposition.
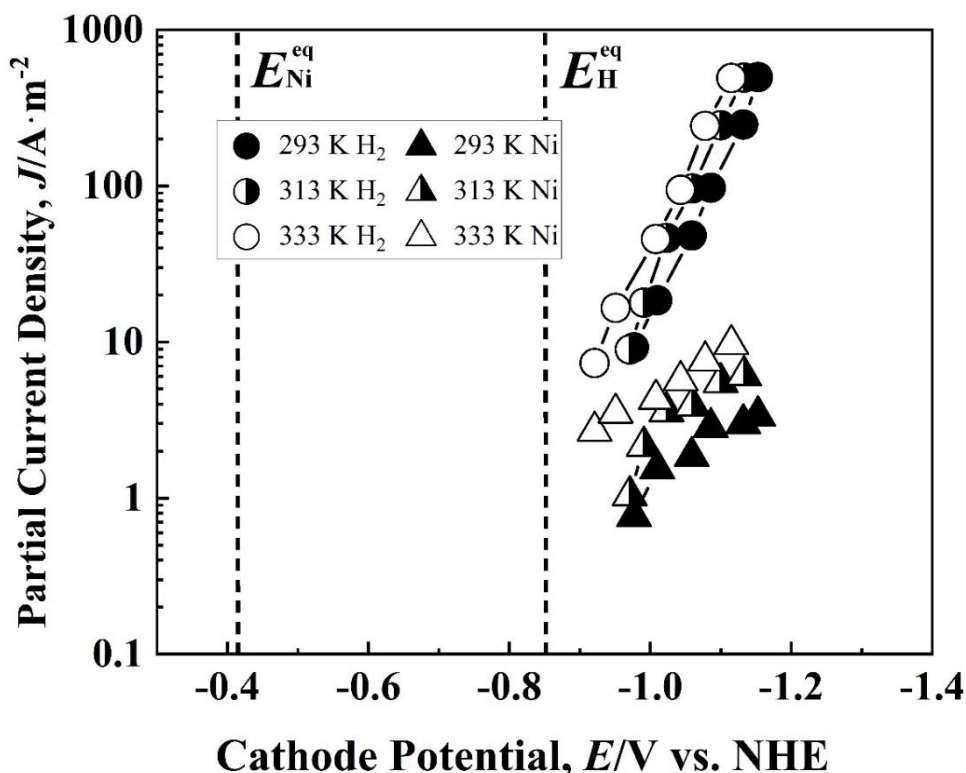

Fig. 3-6. Partial polarization curves for Ni deposition and H$_2$ evolution from the Ni only alkaline solutions at 293, 313 and 333 K.
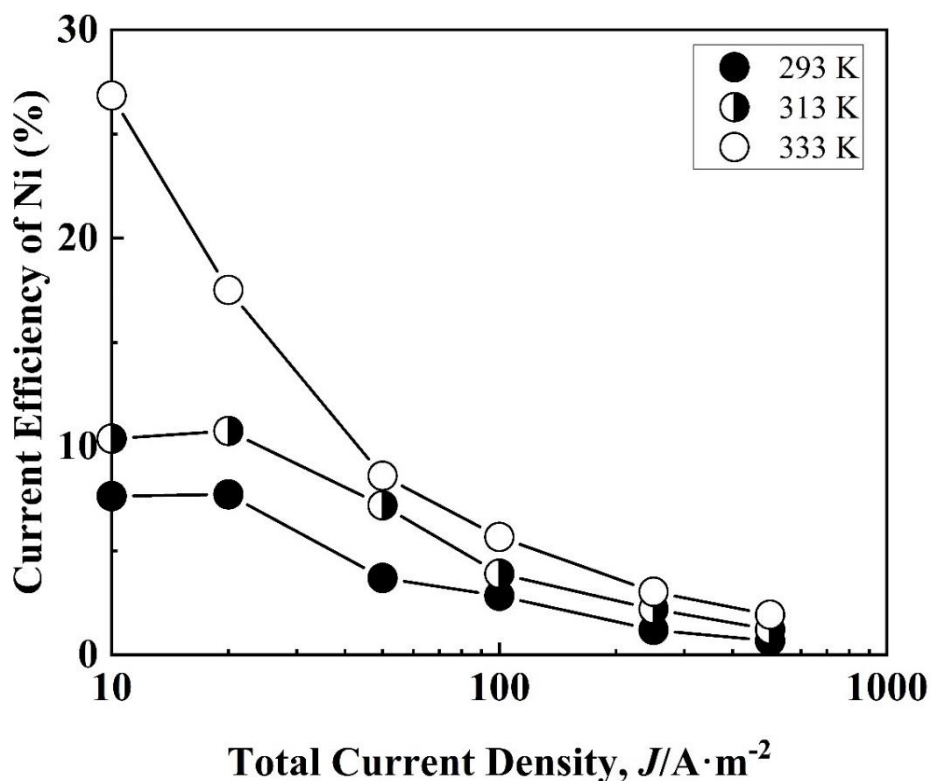
Fig. 3-7. Current efficiencies for Ni deposition from Ni only alkaline solutions at 293, 313 and 333 K.

Figure 3-8 shows the effect of solution temperature on the partial polarization curve for Zn deposition from the Zn solution. The partial polarization curves for Zn deposition depolarized with increasing solution temperature. At 313 and 333 K, the Zn began to deposit near its equilibrium potential, indicating that the deposition overpotential was small. At a solution temperature of 293 K, the Zn deposition approached the diffusion limitation of Zn ions at approximately -1.6 V. Figure 3-9 shows the effect of solution temperature on the current efficiency of Zn deposition from the Zn solution. In the low-current-density range of 10–20 $A \cdot m^{-2}$, the current efficiency for Zn deposition decreased with increasing solution temperature, indicating that and increase in solution temperature had a stronger effect on H_2 evolution. Comparing the effects of solution temperature on the Zn and Ni depositions and H_2 evolution (Figs. 3-6~3-9), in the low-current density range, where the charge transfer process was rate-limiting, the degree of promotion with increasing solution temperature followed the order Ni deposition > H_2 evolution > Zn deposition. Zinc deposition from an aqueous solution is known to occur in the case where there is a small overpotential for deposition, whereas Ni deposition and H_2 evolution occur when there is a large overpotential for deposition since they proceed in the multistep reactions via adsorption intermediates $NiOH_{ad}$ and H_{ad}, respectively and slow elementary process is present. As shown in Figs. 3-6 and 8, the overpotential for Zn deposition was small, even from the zincate solution,

while that for Ni deposition was large. Since Ni deposition and H_2 evolution had an inherently large overpotential, the promotional effect of increasing the solution temperature on the Ni deposition and H_2 evolution appeared to have been stronger than that on the Zn deposition. In the deposition from the Ni solution, the promotional effect of increasing the solution temperature on the Ni deposition was larger than that on the H_2 evolution, which was attributed to the fact that the overpotential for Ni deposition was larger than that for H_2 evolution on Ni. Contrastingly, in the high-current density region of 500 A·m^{-2}, the current efficiency for Zn deposition increased with increasing solution temperature (Fig. 3-9). Since the diffusion of Zn ions became the rate-limiting step of the Zn deposition in the high-current density region, the current efficiency for Zn deposition seems to increase with increasing solution temperature due to the promotion of Zn ion diffusion.
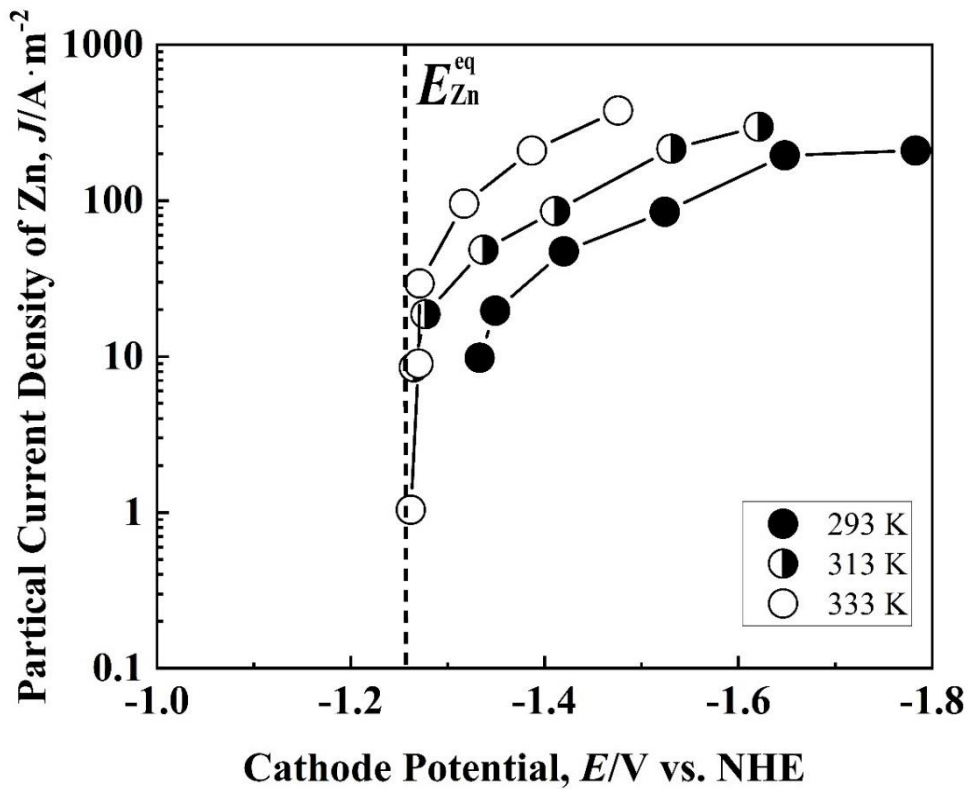

Fig. 3-8. Partial polarization curves for Zn deposition from Zn only alkaline solutions at 293, 313 and 333 K.
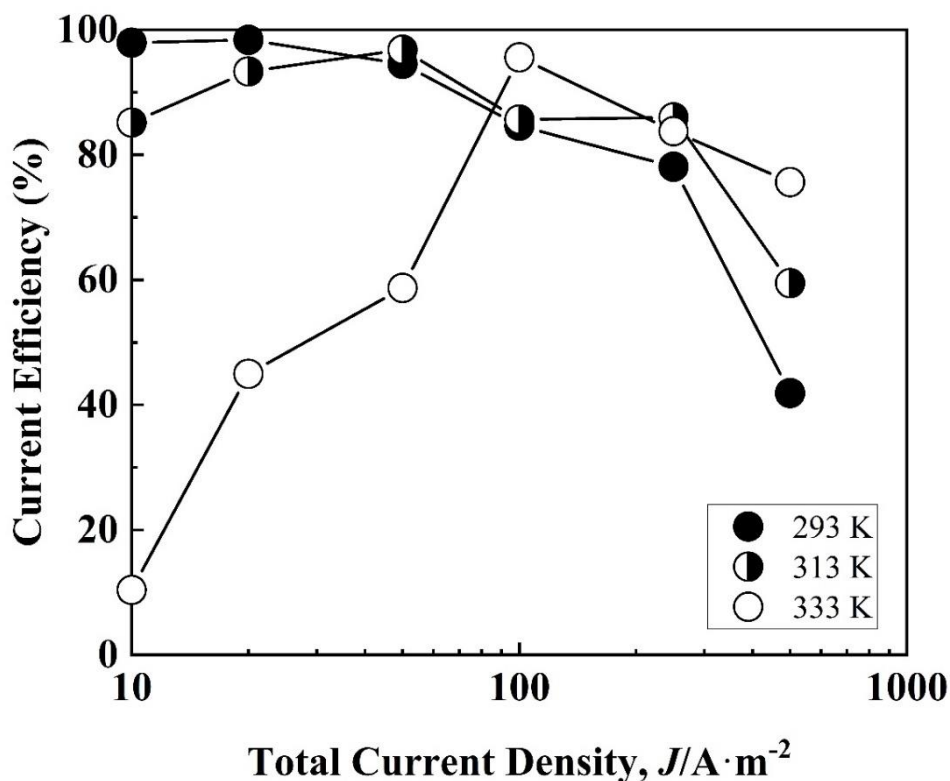
Fig. 3-9. Current efficiencies for Zn deposition from Zn only alkaline solutions at 293, 313 and 333 K.

The effect of solution temperature on the current efficiency for alloy deposition and the composition of the deposited films will be discussed next, based on the results for the solutions that included only Ni or Zn noted above. First, the current efficiency for alloy deposition increased with increasing solution temperature in both the normal ($10–50$ A$\cdot$m^{-2}) and anomalous (500 A$\cdot$m^{-2}) co-deposition regions (Fig. 3-2(a)). In the normal co-deposition region, the Ni content of the deposited films was approximately 90 mass%, revealing that the competition reaction between Ni deposition and H$_2$ evolution mainly occurred in this region. Ni deposition and H$_2$ evolution were both promoted with increasing solution temperature, but the promotional effect on the Ni deposition was stronger, as determined from the results for the Ni solution (Figs. 3-6 and 3-7). As a result, the current efficiency for alloy deposition increased with increasing solution temperature. In the normal co-deposition region of $10–50$ A$\cdot$m^{-2}, the current efficiency for alloy deposition decreased with increasing current density at all solution temperatures. This was attributed to increase in the formation rate of Zn(OH)$_2$ in the multistep reactions of Zn deposition, caused by increasing the current density and the suppression of Ni deposition by Zn(OH)$_2$. Contrastingly, in the anomalous co-deposition region at 500 A$\cdot$m^{-2}, the Ni content in the deposited films was approximately 5 mass%, revealing that the competition reaction between Zn deposition and H$_2$ evolution occurred

- 48 -

mainly in this region. The Zn deposition in this region appeared to proceed under a mixed rate-determining process that included the charge transfer and diffusion of Zn ions (Fig. 3-1(b)). The diffusion of Zn ions was promoted with increasing solution temperature, resulting in an increase in the current efficiency of the alloy deposition. Comparing the current efficiency of Ni deposition from the alloy solution and the single Ni solution, that from the alloy solution was observably higher (Figs. 3-2(c) and 3-7). This suggested that the formation of $Zn(OH)_2$ in the alloy solution suppressed both the H_2 evolution and Ni deposition but that the H_2 evolution was more strongly suppressed.

The Ni content in the deposited films increased with increasing solution temperature in both the normal ($10-50 \text{ A} \cdot \text{m}^{-2}$) and anomalous ($250-500 \text{ A} \cdot \text{m}^{-2}$) co-deposition regions (Fig. 3-3). The Zn and Ni depositions in the alloy deposition appeared to proceed under a rate-determining process comprising the charge transfer in the normal co-deposition region, while they appeared to follow a mixed rate-determining process comprising the charge transfer and diffusion of Zn^{2+} ions in the anomalous co-deposition region. Since Ni deposition was promoted to a greater degree than Zn deposition by increasing the solution temperature in the region where the charge transfer process was rate-limiting, the Ni content in the deposited films seems to increase with solution temperature in both the normal and anomalous co-deposition regions.

As shown in Fig. 3-1(b), in the Zn–Ni alloy deposition, the Zn appeared to have been deposited in a potential region nobler than its equilibrium potential, whereas this phenomenon was not observed in the deposition from a single Zn solution (Fig. 3-8). It was reported that Zn–Ni alloy deposition in the potential range nobler than the equilibrium potential of Zn had been caused by the formation of a stable intermetallic compound, Ni_5Zn_{21}, through deposition, which considerably reduced the activity coefficient of the Zn in the deposited films.[34-36] That is, the co-deposition of Ni is essential for the Zn apparently depositing in the potential region nobler than its equilibrium potential. In the present study, the deposition of Zn in the noble potential region is thought to be increased with temperature because the deposition of Ni was accelerated at a higher solution temperature.

Finally, we discuss the difference between the deposition behavior of the Zn–Ni alloy from the zincate solution in this study and that from a sulfate solution previously reported. The most important difference between the deposition from zincate and sulfate solutions was the cause of $Zn(OH)_2$ formation, which is an inhibitor of Ni deposition and H_2 evolution. In sulfate solutions, $Zn(OH)_2$ is formed by the hydrolysis of Zn^{2+} due to the increase of solution pH by the reduction of H^+ at the cathode. In contrast, in the zincate solution, it is thought to be formed in the intermediate stage of the multistep Zn deposition reactions. In the case of alloy deposition from sulfate solutions, it was reported that the Ni content in the deposited films was approximately 10 mass% in the region where an anomalous-type co-deposition occurred, which was much lower than the CRL (50 mass% Ni^{2+} content in the solution).[21] In the case of the present study, the Ni content in the deposited films from the zincate solution was approximately 5–8 mass% in the region where the anomalous co-deposition occurred (Fig. 3-3), which was below the CRL (8.7 mass%). However, the anomalies were greater in the sulfate solution than in the zincate solution

(Fig. 3-3), indicating that the suppression of Ni deposition by $Zn(OH)_2$ was stronger. The difference in the degree of Ni deposition suppression between the sulfate and zincate solutions may have been due to difference in cause $Zn(OH)_2$ formation. In the sulfate solution, the Ni content in the deposited films increased from approximately 10 mass% to approximately 25 mass% as the solution temperature increased from 303 to 333 K.[31] However, the increase in Ni content may be larger than that in the zincate solutions (Fig. 3-3) because the inhibitory effect of $Zn(OH)_2$ on the Ni deposition is stronger in the sulfate solution.

3-5. Conclusion

The effect of solution temperature on the deposition behavior of Zn−Ni alloys from alkaline zincate solutions was investigated. The transition current density at which the deposition behavior shifted from the normal to anomalous co-deposition was almost identical at solution temperatures of 293 and 313 K but clearly increased at 333 K. The transition current density appeared to increase due to the enhancement of H_2 evolution and Ni deposition at 333 K. The current efficiency for alloy deposition also increased with increasing solution temperature in both the normal ($10-50$ A·m^{-2}) and anomalous (500 A·m^{-2}) co-deposition regions. In the normal co-deposition region, Ni deposition and H_2 evolution mainly occurred, and the promoting effect of increase in the solution temperature on the Ni deposition was greater than that on the H_2 evolution, resulting in an increase in current efficiency alongside solution temperature. In the anomalous co-deposition region at 500 A·m^{-2}, Zn deposition and H_2 evolution mainly occurred, and Zn deposition appeared to proceed under a mixed rate-determining process comprising the charge transfer and diffusion of Zn ions. Since the diffusion of Zn ions is promoted by increasing the solution temperature, the current efficiency also seems to increase. Furthermore, the Ni content in the deposited films increased with the solution temperature at all current densities. In the region where the charge transfer process is rate-limiting, Ni deposition accelerates to a greater degree compared with Zn deposition alongside increasing solution temperature, as a result, Ni content in the deposited films seems to increase. In addition, the γ-phase of the deposited films increased with an increasing solution temperature.

3-6. References

1) H. Fukushima, T. Akiyama, J.-h.Lee, M. Yamaguchi and K. Higashi: *J. Met. Finish. Soc. Jpn.*, **33** (1982), 574 (in Japanese).
2) H. Fukushima, T. Akiyama, M. Yano, T. Ishikawa and R. Kammel: *ISIJ Int.*, **33** (1993), 1009.
3) H. Nakano, S. Kobayashi, T. Akiyama, T. Tsuru and H. Fukushima: *Tetsu-To-Hagane*, **89** (2003), 64 (in Japanese).
4) H. Nakano, M. Matsuno, S. Oue, M. Yano, S. Kobayashi and H. Fukushima: *J. Japan Inst. Metals*, **69** (2005), 548 (in Japanese).
5) El Hajjami, M. P. Gigandet, M. De Petris-Wery, J. C. Catonne, J. J. Duprat, L. Thiery, F. Raulin, N. Pommier, B. Starck and P. Remy: *Appl. Surf. Sci.*, **254** (2007), 480.
6) Conde, M. A. Arenas and J. J. de Damborenea: *Corros. Sci.*, **53** (2011), 1489.
7) H. Nakano, M. Matsuno, S. Oue, M. Yano, S. Kobayashi and H. Fukushima: *Mater. Trans.*, **45** (2004), 3130.
8) G. W. Loar, K. R. Romer and T. J. Aoe: *Plat. Surf. Finish.*, **78** (1991), 74.
9) G. Y. Li, J. S. Lian, L. Y. Niu and Z. H. Jiang: *Surf. Coat. Technol.***191** (2005), 59.
10) Muller, M. Sarret and M. Benballa: *J. Electroanal. Chem.* **519** (2002), 85.
11) H. Y. Lee and S. G. Kim: *Surf. Coat. Technol.* **135** (2000), 69.
12) R. Pfiz and G. Strube: Trans. IMF, **74** (1996). 158.
13) L. S. Tsybulskaya, T. V. Gaevskaya, O. G. Purovskaya and T. V. Byk: *Surf. Coat. Technol.* **203** (2008), 234.
14) H. Nakano, S. Arakawa, S. Oue and S. Kobayashi: *ISIJ Int.*, **53** (2013),1864.
15) S. Haruyama: Hyomen Gizyutsusya no tameno Denkikagaku (Electrochemistry for Surface Engineer) Maruzen, Tokyo (2005), 88, 173 (in Japanese).
16) M. Pourbaix: Atlas of Electrochemical Equilibria in Aqueous Solutions, Pergamon Press, New York, (1966), 406.
17) D. Perrin: Stability Constants of Metal-ion Complexes, Part B: Organic Ligands, Pergamon Press, Oxford, (1979), 466.
18) T. Akiyama, H. Fukushima and K. Higashi: *Tetsu-To-Hagane,* **72** (1986), 918 (in Japanese).
19) S. H. Bae, S. Oue, I. Son and H. Nakano: *ISIJ int.*, **61** (2021), 2256.
20) S. H. Bae, S. Oue, I. Son and H. Nakano: *Tetsu-To-Hagane*, **107** (2021), 229 (in Japanese).
21) T. Akiyama and H. Fukushima: *Shigen-to-Sozai*, **112** (1996), 583 (in Japanese).
22) H. Nakano, S. Oue, D. Yoshihara, H. Fukushima, Y. Saka, S. Sawada and Y. Hattori: *Mater. Trans.*, **52** (2011), 1237.
23) H. Nakano, S. Oue, D. Yoshihara, H. Fukushima, Y. Saka, S. Sawada and Y. Hattori: *J. Japan Inst. Metals*, **75** (2011), 61 (in Japanese).
24) H. Fukushima and H. Nakano: *J. Surf. Sci. Soc. Jpn.,* **22** (2001), 107 (in

Japanese).

25) H. Nakano, T. Ohgai, H. Fukushima, T. Akiyama, R. Kammel: *Metall*, **55**(2001), 676.

26) H. Fukushima, T. Akiyama and K. Kiyotani: *Shigen-to-Sozai*, **109** (1993), 861 (in Japanese).

27) T. Yamashita and S. Toshima: *Nippon Kagaku Kaishi*, **1980** (1980), 1824 (in Japanese). https://doi.org/10.1246/nikkashi.1980.1824

28) K. Aotani: Gokin Mekki VI (Alloy plating VI), Nippon Plating Kyokai, Tokyo, (2005), 133 (in Japanese).

29) T. Yoshida: Saishin Hyomen Shori Gizyutsu Soran (New Engineering Review of Coating), Sangyo Gizyutsu Service Center, Tokyo, (1987), 318 (in Japanese).

30) K. Fukuda, Y. Kashiwa, S. Oue, T. Takasu and Hiroaki Nakano: *ISIJ int.*, **61** (2021), 919.

31) K. Fukuda, Y. Kashiwa, S. Oue, T. Takasu and H. Nakano: *Tetsu-To-Hagane*, **105**(2019), 988 (in Japanese).

32) K. Fukuda, Y. Kashiwa, S. Oue, T. Takasu and H. Nakano: *ISIJ int.*, **59** (2019), 1632.

33) Y. Kashiwa, N. Nagano, T. Takasu, S. Kobayashi, K. Fukuda and H. Nakano: *ISIJ int.*, **59** (2019), 514.

34) H. Nakano, S. Arakawa, Y. Takada, S. Oue and S. Kobayashi: *J. Japan Inst. Metals*, **76** (2012), 443 (in Japanese).

35) H. Nakano, S. Arakawa, S. Oue and S. Kobayashi: *Tetsu-To-Hagane*, **99** (2013), 425 (in Japanese).

36) H. Nakano, S. Arakawa, Y. Takada, S. Oue and S. Kobayashi: *Mater. Trans.*, **53** (2012), 1946.

Chapter 4. Synergistic Effect of Brightener and Solution Temperature on the Electrodeposition Behavior of Zn-Ni Alloy from Alkaline Zincate Solution

4-1. Introduction

Unlike the sulfate and chloride solutions, a brightener is typically added to the zincate solution for Zn–Ni alloy deposition. Although many reports have demonstrated the relationship between the appearance qualities of the deposited films from the zincate solution and the brightener,[1–5] few have reflected the effect of the brightener on the electrochemical reaction.[6,7] Therefore, the authors selected a reaction product of epichlorohydrin and imidazole (IME) as a brightener, reported to have a brightening effect in Zn deposition from a zincate solution in the previous report, and the effect was investigated. When IME is added, the transition current density at which the deposition behavior shifts from normal to anomalous type is reduced due to suppression of hydrogen evolution, and both Zn and Ni deposition are suppressed to reduce the current efficiency of alloy deposition, the Ni content of the deposited films decreases because Ni deposition is more strongly suppressed.[8,9]

Conversely, although the solution temperature affects the deposition overpotential, throwing power, metal salt solubility and solution conductivity, etc.,[10] and is an extremely important factor in electrodeposition, few studies have reported the effect of solution temperature on the deposition behavior of Zn-Ni alloy from zincate solution.

In the region wherein the charge transfer process is rate-determining, Ni deposition is promoted more than Zn deposition when the solution temperature is increased. Therefore, the Ni content of the deposited films increases with the solution temperature.[11] Reportedly, the Ni content increases significantly as the solution temperature increases above 323 K,[12] but the details are unknown. In the electrodeposition from an electrolytic solution with a brightener, the effect of the brightener may differ depending on the solution temperature, with a possible synergistic effect of the brightener and solution temperature on the deposition behavior, but the details are unknown. The synergistic effects of IME and solution temperature on the deposition behavior were investigated based on the partial polarization curves of Zn and Ni deposition, hydrogen evolution, the appearance, and microstructure of the deposited films.

4-2. Experimental

Table 4-1 shows the composition of the zincate solution and the electrolysis conditions for the Zn–Ni alloy deposition. The electrolytic solutions were prepared by dissolving the reagent-grade ZnO (0.15 mol·dm^{-3}), NiSO$_4$·6H$_2$O (0.016 mol·dm^{-3}), N(CH$_2$CH$_2$OH)$_3$ (0.34 mol·dm^{-3}), and NaOH (2.5 mol·dm^{-3}) in distilled and deionized water. The reaction product of epichlorohydrin and IME was prepared as previously reported.[13,14] 6.81 g of IME was placed in 100 ml of pure water, and the temperature was raised to 313~323 K. Then, 9.25 g of epichlorohydrin was gradually added dropwise below 333 K while stirring the solution with a magnetic stirrer. After the epichlorohydrin addition, the temperature was raised to 353 K and refluxed for about 2 h with stirring to obtain IME. The structural formula of IME is shown in Fig. 4-1. Electrolysis was performed by the constant current electrolysis method without stirring at the current density of 10–500 A·m^{-2}, amount of electricity of 5 × 10^4 C·m^{-2}, and solution temperatures of 293 K, 313 K, and 333 K. The amount of electricity of 5 × 10^4 C·m^{-2} corresponds to a film thickness of 2.4 μm assuming the deposition of pure Zn at a current efficiency of 100%. A Cu plate (1 cm × 2 cm) was used as the cathode and Pt plate (1 cm × 2 cm) as the anode. However, when preparing samples for gloss evaluation, scanning electron microscopy (SEM) observation, and XRD analysis, a Fe plate (1 cm x 2 cm) was used as the cathode. The obtained deposited films were dissolved in nitric acid, and Zn and Ni were determined by the ICP optical emission spectroscopy to obtain the composition of the deposited alloy and the current efficiencies of Zn and Ni deposition. Partial current densities for Zn and Ni deposition and hydrogen evolution were calculated by multiplying the total current density by the respective current efficiency (%)/100. An Ag/AgCl electrode (saturated KCl, 0.199 V vs. NHE, 298 K) was used as a reference electrode to measure the polarization curves, but the potentials were converted to the standard hydrogen electrode and displayed. The gloss of the deposited films was evaluated by a spectrophotometer (Konica Minolta, Inc. CM-3610d). The light source was a pulsed xenon lamp with a diameter of 8 mm. The diffuse illumination was performed using an integrating sphere, and the total reflectance (SCI method, including specular reflectance) and diffuse reflectance (SCE method, removing specular reflectance) were measured in the 8° direction. The gloss was evaluated by subtracting the diffuse reflectance (SCE method) from the total reflectance (SCI method).[15]

To quantify the IME codeposited in the deposited films, the emission intensities of C, Cu, Zn, and Ni were measured by the high-frequency glow discharge optical emission spectrometry (rf-GDOES) with the following conditions: analysis diameter: φ2 mm, argon pressure: 600 Pa, power: 40 W, pulse frequency: 2000 Hz, duty cycle: 0.125. The surface morphology of the deposited films was observed by SEM, and the phase identification was performed via an X-ray diffractometer (Cu-Kα, tube voltage 40 kV, tube current 15 mA).

Table 4-1. Solution compositions and electrolysis conditions

ZnO	(mol·dm^{-3})	0.15	Current density (A·m^{-2})	10–500	
NiSO$_4$·6H$_2$O	(mol·dm^{-3})	0.016	Temperature (K)	293, 313, 333	
N(CH$_2$CH$_2$OH)$_3$	(mol·dm^{-3})	0.34	Amount of charge (C·m^{-2})	5×10^4	
NaOH	(mol·dm^{-3})	2.5	Cathode	Cu (1 × 2 cm^2)	
Reaction product of epichlorohy-drin and imid-azole (IME)	(ml·dm^{-3})	0,3,5	Anode	Pt (1 × 2 cm^2)	
			Quiescent bath		
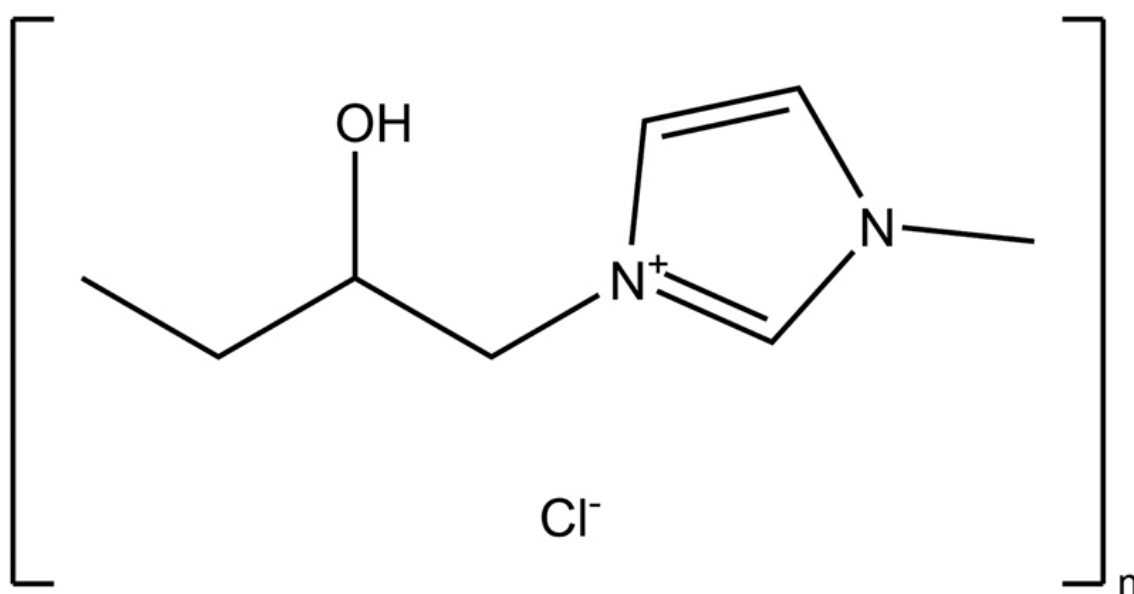
Fig. 4-1. Structural formula of reaction product of epichlorohydrin and imid-azole.

4-3. Results

4-3-1. Effects of IME and Solution Temperature on the Deposition Behavior of Zn–Ni Alloys

Figure 4-2 shows the total and the partial polarization curves of Zn, Ni deposition, and hydrogen evolution when Zn–Ni alloy deposition was performed at a solution temperature of 293 K. The equilibrium potential E_{Zn}^{eq} of Zn deposition (ZnO$_2^{2-}$ + 2H$_2$O + 2e$^-$ → Zn + 4OH$^-$) assuming that pure Zn is deposited at a solution temperature of 298 K is −1.27 V. [16] In addition, the equilibrium potential E_{Ni}^{eq} of the deposition (Ni(TEA)$_2^{2+}$ + 2e$^-$ → Ni + 2TEA) was calculated −0.41 V based on the complex stabilization constant K = 104.74 of triethanolamine (TEA) coordinated to the Ni^{2+} ion assuming that pure Ni is deposited at a solution temperature of 298 K. [17] In the total polarization curve (Fig. 4-

2(a)), without IME, even though increased the current density from 10 to 50 $A \cdot m^{-2}$ in the potential region nobler than the equilibrium potential (-1.27 V) of Zn, the potential rarely changed, while on exceeding 50 $A \cdot m^{-2}$, it moved largely in less noble potential direction, and on reaching the equilibrium potential of Zn, the shift of potential became small even on increasing the current density. During deposition from a solution containing 3.5 $ml \cdot dm^{-3}$ of IME, the total polarization curve shifted to a less noble potential range when the current density exceeded 10 $A \cdot m^{-2}$ and the current density at which the potential began to shift was smaller than that without IME. Even in the solution containing IME, at the equilibrium potential of Zn, the shift of the potential to the less noble side became small despite increasing the current density. The partial polarization curve (Fig. 4-2(b)) of Zn deposition from the solution without IME showed a rise in the potential region nobler than the equilibrium potential of Zn, as in the total polarization curve, followed by a shift toward the less noble potential region, and then a sharp rise at potential less noble than the equilibrium potential of Zn (-1.27 V). In contrast, the partial current density of Zn deposition from the solution containing 3 and 5 $ml \cdot dm^{-3}$ of IME was not detected in the potential region nobler than the equilibrium potential of Zn, and increased in the potential region less noble than the equilibrium Zn potential. Comparing the partial current density of Zn deposition from the solution containing 3 and 5 $ml \cdot dm^{-3}$ of IME with that from IME-free solution at same potential, it was lower with IME than that from IME-free solution. The partial polarization curve of Ni deposition (Fig. 4-2(c)) also showed a similar trend to that of Zn deposition (Fig. 4-2(b)) (suppression of Ni deposition by IME in the region $E < E_{Zn}^{eq}$). The hydrogen evolution (Fig.4-2(d)) from the Zn–Ni alloy deposition solution was observed at potential nobler than the equilibrium potential of Zn in the presence and absence of IME, decreased once despite the shift to a less noble potential, and increased at potential less noble than the equilibrium potential of Zn. The partial current density of hydrogen evolution, which started decreasing despite the shift to the less noble potential, was smaller for the solution containing IME.

Figure 4-3 shows the total and partial polarization curves of Zn and Ni deposition and hydrogen evolution during the Zn–Ni alloy deposition at a solution temperature of 313 K. The total polarization curve (Fig. 4-3(a)) shows a large shift to a less noble potential region when the current density exceeds 50 $A \cdot m^{-2}$ regardless of the presence or absence of IME, and the shift of potential to the less noble direction becomes smaller at the equilibrium Zn potential, despite increasing the current density. For the current density above 50 $A \cdot m^{-2}$, the effect of IME on the total polarization curve was not observed at 313 K, unlike at 293 K (Fig. 4-2(a)). Conversely, the partial current density of Zn deposition (Fig. 4-3(b)) was almost the same at potentials less noble than the equilibrium potential of Zn, regardless of the presence or absence of IME, and showed a different trend from that for 293 K (Fig. 4-2(b)). In contrast, the partial current density of Ni deposition (Fig. 4-3(c)) was lower in the solution containing 3 and 5 $ml \cdot dm^{-3}$ of IME than that in IME-free solution in the potential region less noble than the equilibrium potential of Zn, showing a similar trend to that of the solution at 293 K. Hydrogen evolution from the Zn–Ni alloy electrolytic solution (Fig. 4-3(d)) was observed at potentials nobler than the equilibrium

potential of Zn with or without IME, and as at 293 K (Fig. 4-2(d)), decreased once despite the shift to a less noble potential, and increased at potential less noble than the equilibrium potential of Zn. However, unlike the solution temperature of 293 K, the partial current density of hydrogen evolution, which started to decrease at potentials nobler than the equilibrium potential of Zn, was about 50 A·m^{-2} with and without IME and almost the same for both cases.
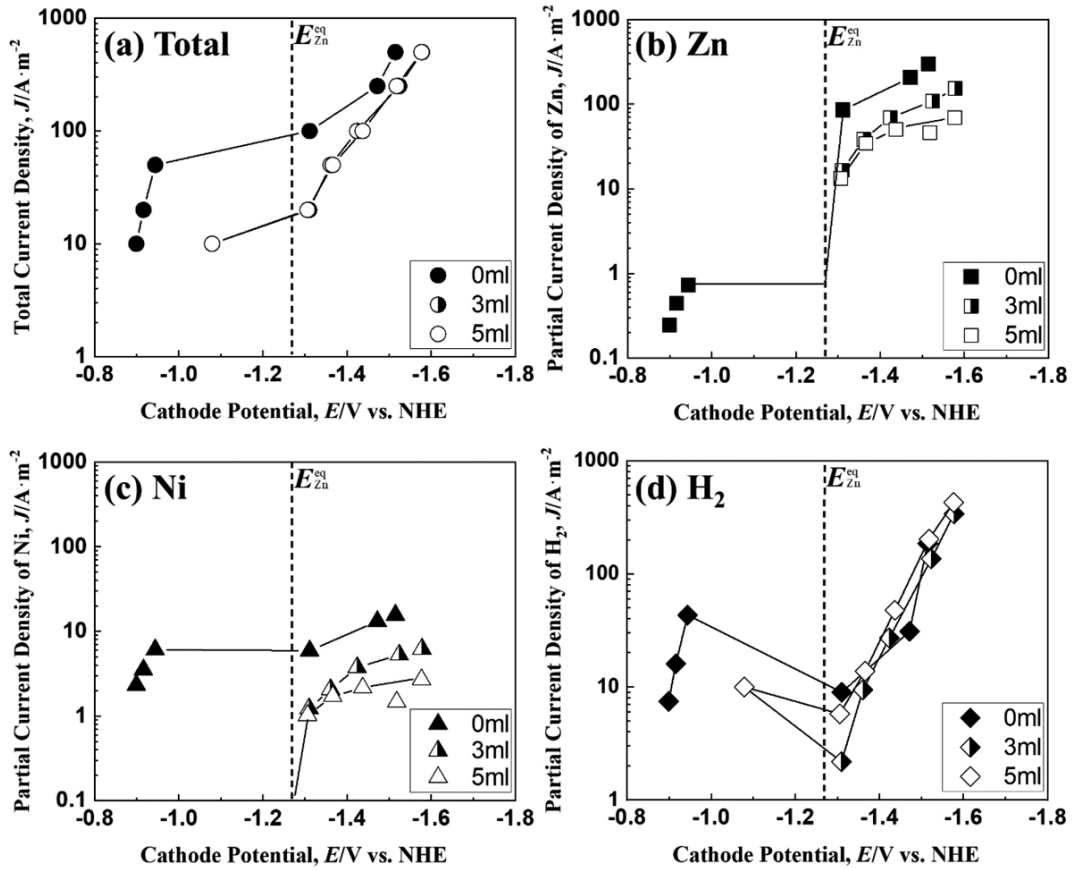

Fig. 4-2. Polarization curves for Zn-Ni alloy deposition at 293 K from the solutions containing various amounts of IME. [Concentration of IME: 0, 3, 5 ml·dm^{-3}, (a) Total polarization curves and partial polarization curves of (b) Zn, (c) Ni and (d) H$_2$]
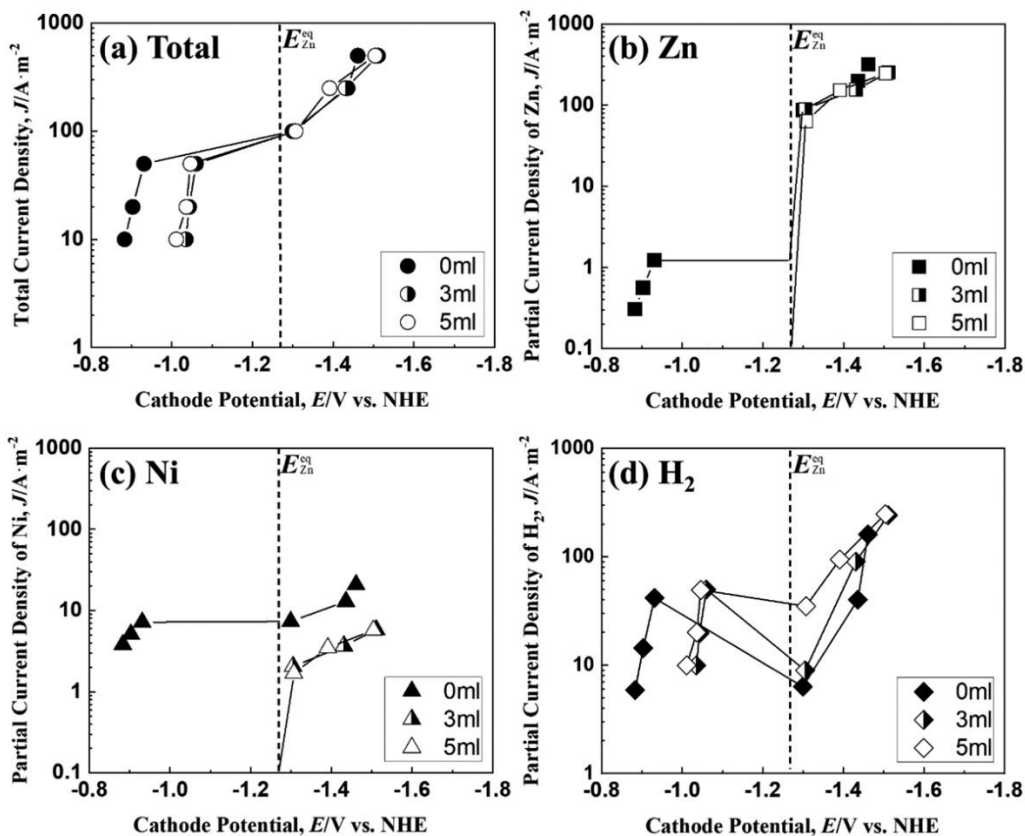
Fig. 4-3. Polarization curves for Zn-Ni alloy deposition at 313 K from the solutions containing various amounts of IME. [Concentration of IME: 0, 3, 5 ml·dm^{-3}, (a) Total polarization curves and partial polarization curves of (b) Zn, (c) Ni and (d) H$_2$]

Figure 4-4 shows the total and the partial polarization curves of Zn and Ni deposition and hydrogen evolution during the Zn–Ni alloy deposition at a solution temperature of 333 K. The total polarization curve (Fig. 4-4(a)) shows a large shift to a less noble potential region when the current density exceeds 100 A·m^{-2} with/without IME, and the shift to the less noble potential became smaller at the equilibrium potential of Zn, despite increasing the current density. For the current density above 100 A·m^{-2}, the effect of IME on the total polarization curve was not observed at 333 K, as with 313 K (Fig. 4-3(a)). The partial current density of Zn deposition (Fig. 4-4(b)) was slightly smaller with 3 ml·dm^{-3} of IME at potentials less noble than the equilibrium potential of Zn, but the degree of decrease with 3 ml·dm^{-3} of IME was slight comparing with that at 293 K (Fig. 4-2(b)) In contrast, the partial current density of Ni deposition (Fig. 4-4(c)) was clearly lower in the solutions containing 3 and 5 ml·dm^{-3} of IME at the potential range less noble than the equilibrium potential of Zn, showing the same trend as the solution temperatures of 293 K and 313 K. Conversely, the partial polarization curve of hydrogen evolution (Fig. 4-4(d)) showed a large shift from the region of noble potential to that of less noble potential, regardless of the presence of IME. The partial current density at which the potential began to shift was almost same to be about 100 A·m^{-2} with/without IME, unlike at 293 K.
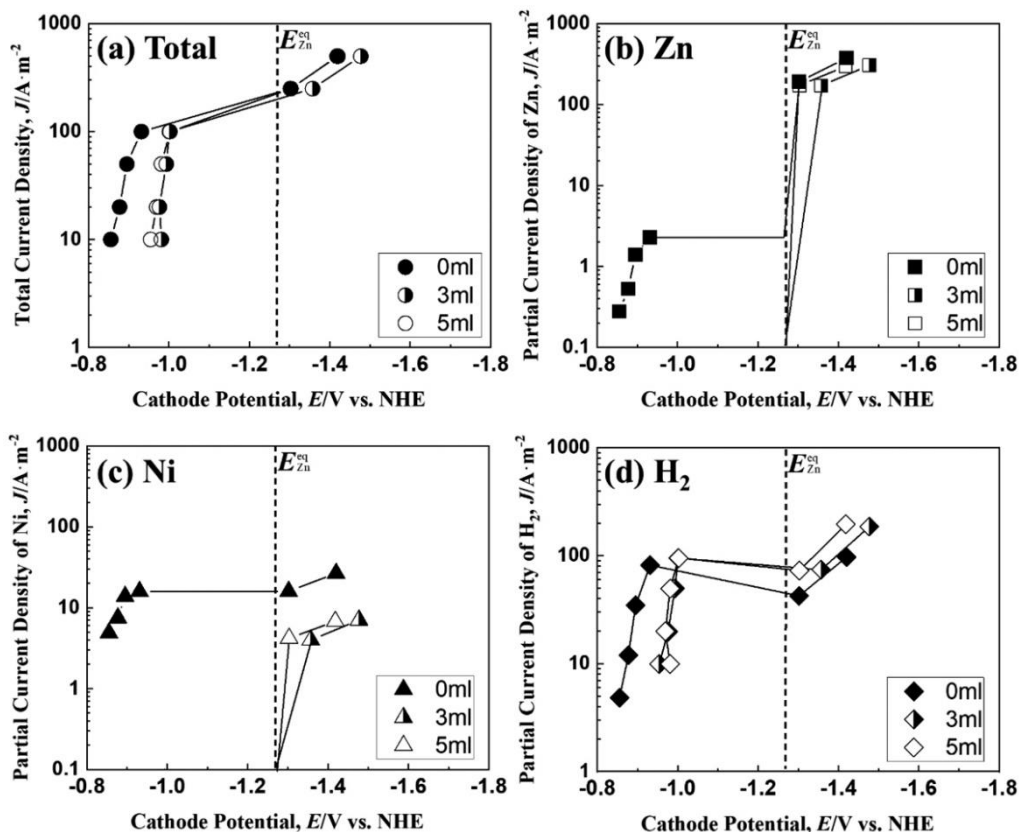
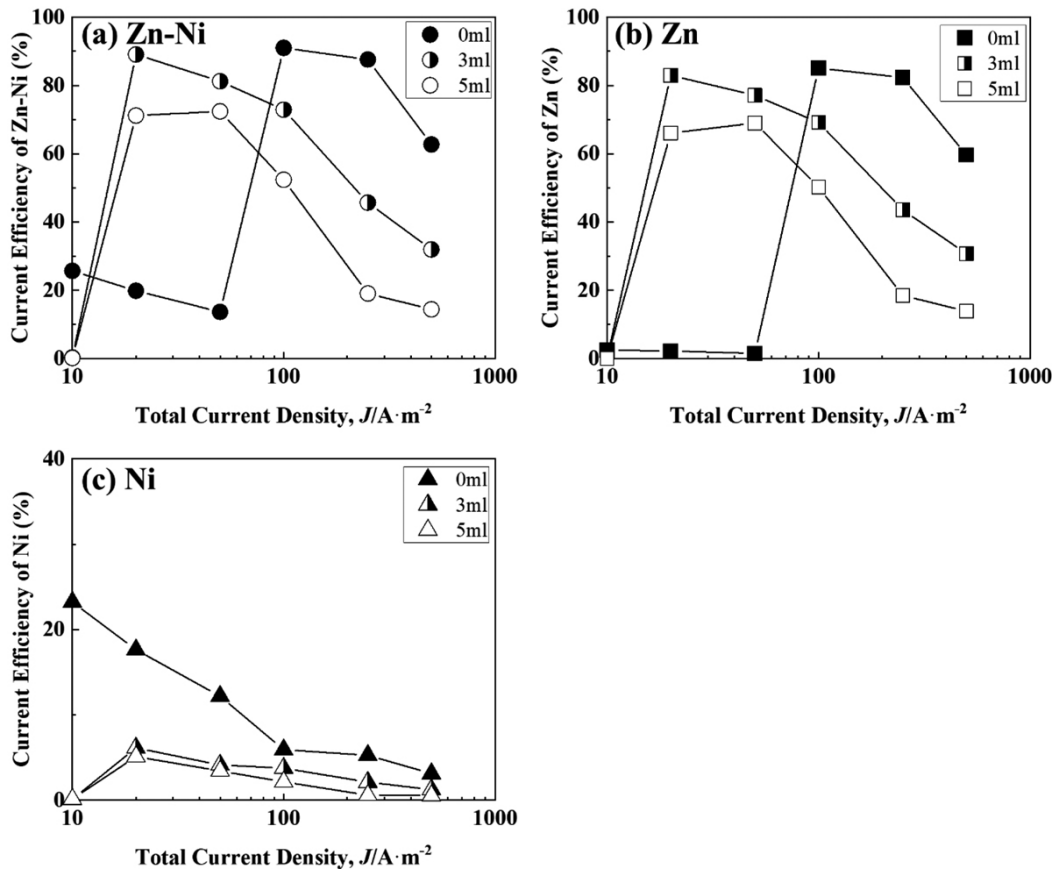Fig. 4-4. Polarization curves for Zn-Ni alloy deposition at 333 K from the solutions containing various amounts of IME. [Concentration of IME: 0, 3, 5 ml·dm^{-3}, (a) Total polarization curves and partial polarization curves of (b) Zn, (c) Ni and (d) H$_2$]

Figure 4-5 shows the correlation between the current density and current efficiency of Zn–Ni, Zn, and Ni depositions during Zn–Ni alloy deposition at a solution temperature of 293 K. The current efficiency of Zn–Ni alloy deposition shown below is the sum of the current efficiencies of Zn and Ni depositions. In IME-free solution, the current efficiency of Zn–Ni alloy deposition (Fig. 4-5(a)) was low (14%–26%) in the low current density range of 10–50 A·m^{-2}, but rapidly increased above 50 A·m^{-2}, became maximum at 100 A·m^{-2}, and then, decreased as the current density increased. In the solution containing 3 or 5 ml·dm^{-3} IME, the current efficiency was almost zero at a current density of 10 A·m^{-2} but rapidly increased above 10 A·m^{-2} and reached its maximum from 20 to 50 A·m^{-2} and significantly decreased above 50 A·m^{-2}. The current efficiency of Zn deposition during the alloy deposition (Fig. 4-5(b)) showed a similar behavior to that of alloy deposition (Fig. 4-5(a)), except for the low current density range of 10–50 A·m^{-2} from the solution without IME. The current efficiency of alloy deposition with and without IME increased rapidly at low to high current density region (Fig. 4-5(a)) because of the increase in the current efficiency of Zn deposition. The current density at which the current efficiency of Zn deposition started increasing was lower in the solution containing 3 or 5 ml·dm^{-3} of IME. For high current densities above 100 A·m^{-2},

the current efficiency of Zn deposition decreased significantly with IME addition. The degree of decrease became larger when IME was increased from 3 to 5 ml·dm^{-3}. Conversely, the current efficiency of Ni deposition (Fig. 4-5(c)) was lower with IME than that without IME for the entire current density range. The current efficiency of Ni deposition decreased with the increasing current density in the solution without IME, whereas it in the solutions containing 3 and 5 ml·dm^{-3} of IME showed a similar current density dependence as that of Zn deposition.
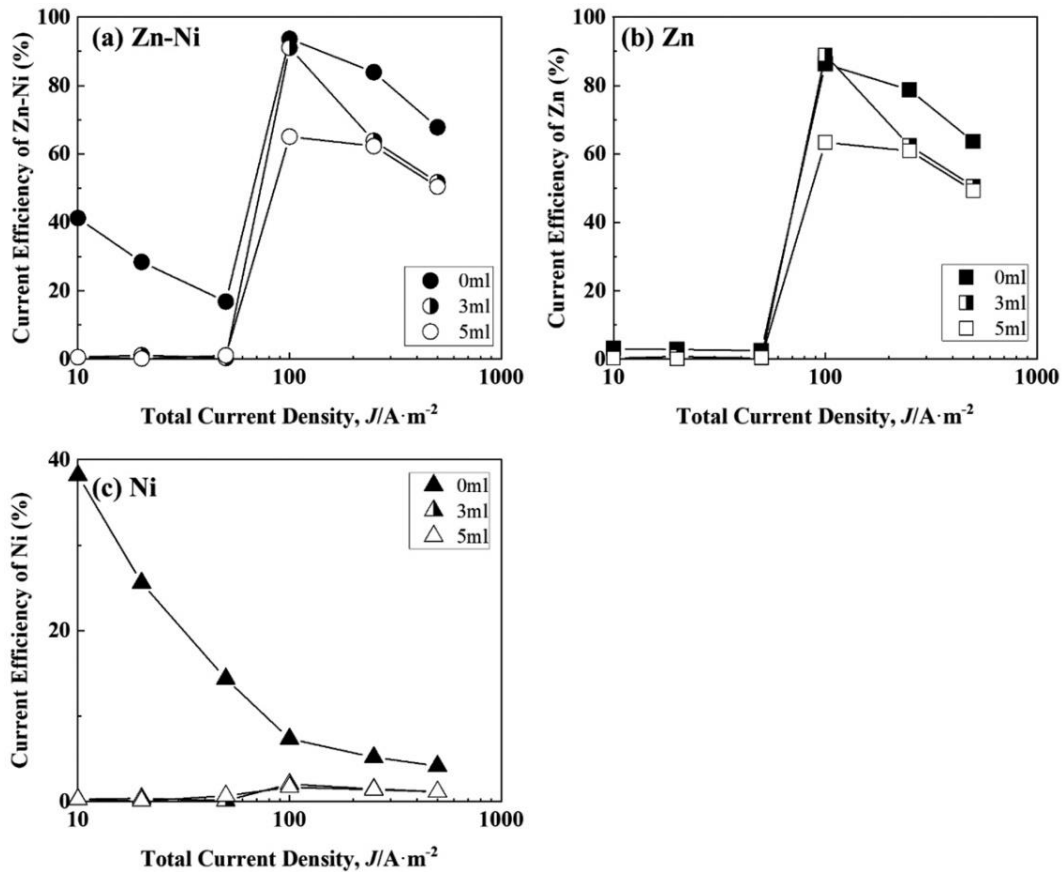

Fig. 4-5. Current efficiency for Zn-Ni alloy deposition at 293 K from the solutions containing various amounts of IME. [Concentration of IME: 0, 3, 5 ml·dm^{-3}, (a)Zn-Ni, (b) Zn and (c) Ni]

Figure 4-6 shows the correlation between the current density and current efficiency of Zn–Ni, Zn, and Ni deposition during Zn–Ni alloy deposition at a solution temperature of 313 K. The current efficiency of Zn–Ni alloy deposition (Fig. 4-6(a)) increased rapidly at current density above 50 A·m^{-2}, regardless of the presence of IME, reached its maximum at 100 A·m^{-2}, and decreased with further increase in the current density. The current efficiency of Zn deposition during the alloy deposition (Fig. 4-6(b)) was similar to that of the alloy deposition (Fig. 4-6(a)), except for the low current density region of 10–50 A·m^{-2} from the solution without IME. In the high current density region above 100 A·m^{-2}, the current efficiency of Zn deposition decreased with the addition

of IME, but the degree of decrease was lower than that at 293 K(Fig. 4-5(b)). In the high current density region above 250 A·m^{-2}, the current efficiency of Zn deposition did not decrease much despite increasing the IME from 3 to 5 ml·dm^{-3}. The current efficiency of Ni deposition (Fig. 4-6(c)) was lower with the addition of IME in the total current density range.

Fig. 4-6. Current efficiency for Zn-Ni alloy deposition at 313 K from the solutions containing various amounts of IME. [Concentration of IME: 0, 3, 5 ml·dm^{-3}, (a)Zn-Ni, (b) Zn and (c) Ni]

Figure 4-7 shows the correlation between the current density and current efficiency of Zn–Ni, Zn, and Ni deposition during Zn–Ni alloy deposition at a solution temperature of 333 K. The current efficiency of Zn–Ni alloy deposition (Fig. 4-7(a)) increased rapidly at the current density above 100 A·m^{-2}, reaching its maximum at 250 A·m^{-2} with/without IME, and further decreased with the increase in the current density. The current efficiency of Zn deposition during alloy deposition (Fig. 4-7(b)) was similar to that of the alloy deposition (Fig. 4-7(a)), except in the low current density region of 10–100 A·m^{-2} from the solution without IME. In the high current density region above 250 A·m^{-2}, the current efficiency of Zn deposition decreased with the addition of IME, but the degree of decrease was lower than that at 293 K (Fig. 4-5(b)). The current efficiency of Zn deposition rarely decreased despite increasing the IME from 3 to 5 ml·dm^{-3}.The current efficiency of Ni deposition (Fig. 4-7(c)) was lower

with the addition of IME for the entire current density range.

The current efficiency of Zn deposition (Figs. 4-5(b), 4-6(b), and 4-7(b)) was compared with the total polarization curves (Figs. 4-2(a), 4-3(a), and 4-4(a)). The current density at which the current efficiency of Zn deposition increased rapidly was consistent with that at which the potential significantly shifted from nobler than the equilibrium potential of Zn to where it was less noble in the total polarization curve. The current density at which the potential significantly shifted from nobler than the equilibrium potential of Zn to less noble was lower with IME at a solution temperature of 293 K (Fig. 4-2(a)), while it almost remained unchanged by the addition of IME at the solution temperatures of 313 K and 333 K (Figs. 4-3(a) and 4-4(a)).
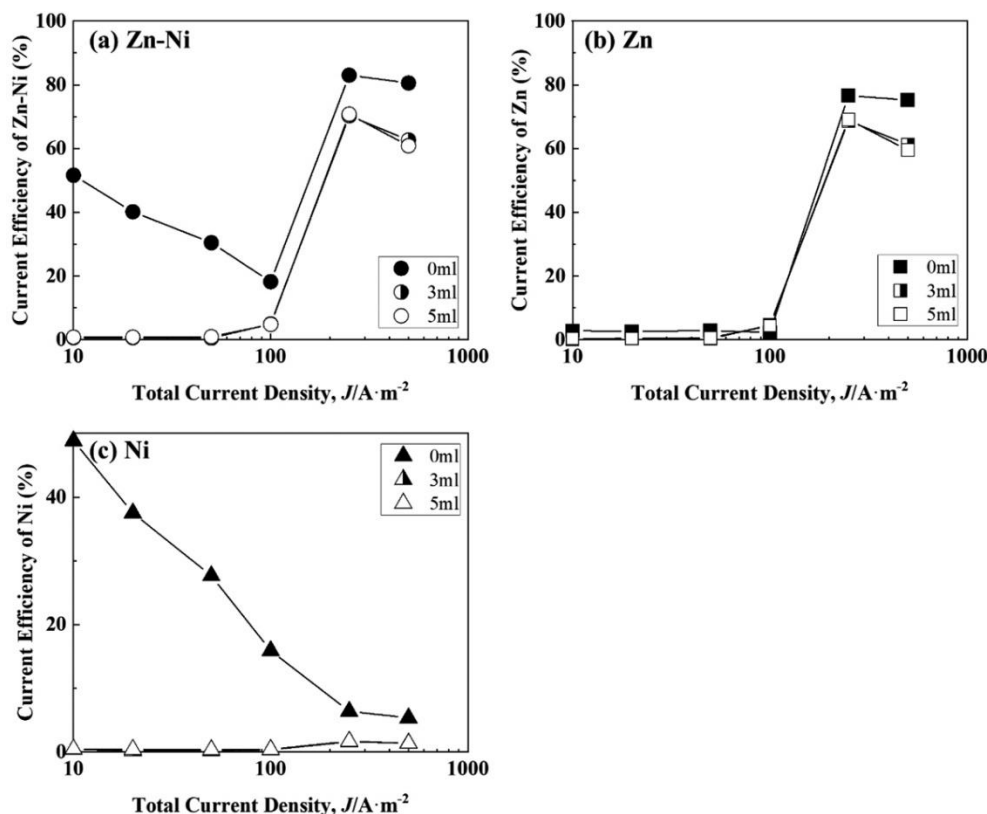

Fig. 4-7. Current efficiency for Zn-Ni alloy deposition at 333 K from the solutions containing various amounts of IME. [Concentration of IME: 0, 3, 5 ml·dm^{-3}, (a)Zn-Ni, (b) Zn and (c) Ni]

Figure 4-8 shows the correlation between the current density and Ni content of Zn–Ni alloy deposited films for each solution temperature. The broken line in the figure shows the composition reference line (CRL) of Ni, which means that the Ni content in the solution is identical to that in the deposited films. When the Ni content in the deposited films is greater than CRL, normal codeposition occurs, in which electrochemically nobler Ni deposited in preference to Zn. In contrast, when the Ni content in the deposited films is lesser than CRL, anomalous codeposition occurs, in which less noble Zn deposited in preference to Ni. As shown in Fig. 4-8(a), in IME-free solution at 293 K, the Ni

content in deposited films significantly changed at current density region of 50-100 $A \cdot m^{-2}$. Below 50 $A \cdot m^{-2}$, the Ni content was above the CRL at around 90 mass%, indicating normal-type codeposition, whereas above 100 $A \cdot m^{-2}$, it was below the CRL, indicating anomalous codeposition. With the addition of 3 and 5 $ml \cdot dm^{-3}$ of IME, the Ni content in deposited films significantly changed at current density range of 10-20 $A \cdot m^{-2}$. Above 20 $A \cdot m^{-2}$, the content was below the CRL, showing anomalous codeposition. The current density at which the deposition behavior shifted from normal to anomalous is called the transition current density.[18-20] This transition current density was consistent with the current density where the potential of the total polarization curve shown in Fig. 4-1(a) shifted abruptly from the nobler than the equilibrium potential of Zn to less noble region, and the current density where the current efficiency of Zn changed significantly (Fig. 4-5(b)). The transition current density evidently decreased with an addition of IME at 293 K. In contrast, at a solution temperature of 313 K (Fig. 4-8(b)), the transition current density ranged from 50 to 100 $A \cdot m^{-2}$ regardless IME, showing a different trend from that at 293 K. Figs. 4-8(d), (e), and (f) show enlarged images of the Ni content in the high current density region where anomalous codeposition occurred. The Ni content in the region of anomalous codeposition decreased with the IME addition at all solution temperatures; the decrease in Ni content was small at 293 K (Fig. 4-8(d)) but became more pronounced as the solution temperature increased to 313 K (Fig. 4-8(e)) and 333 K (Fig. 4-8(f)). At 293 K, the Ni content was lower for 5 $ml \cdot dm^{-3}$ IME than for 3 $ml \cdot dm^{-3}$ IME (Fig. 4-8(d)), whereas the effect of amount of IME on the Ni content was not observed at 313 K and 333 K.
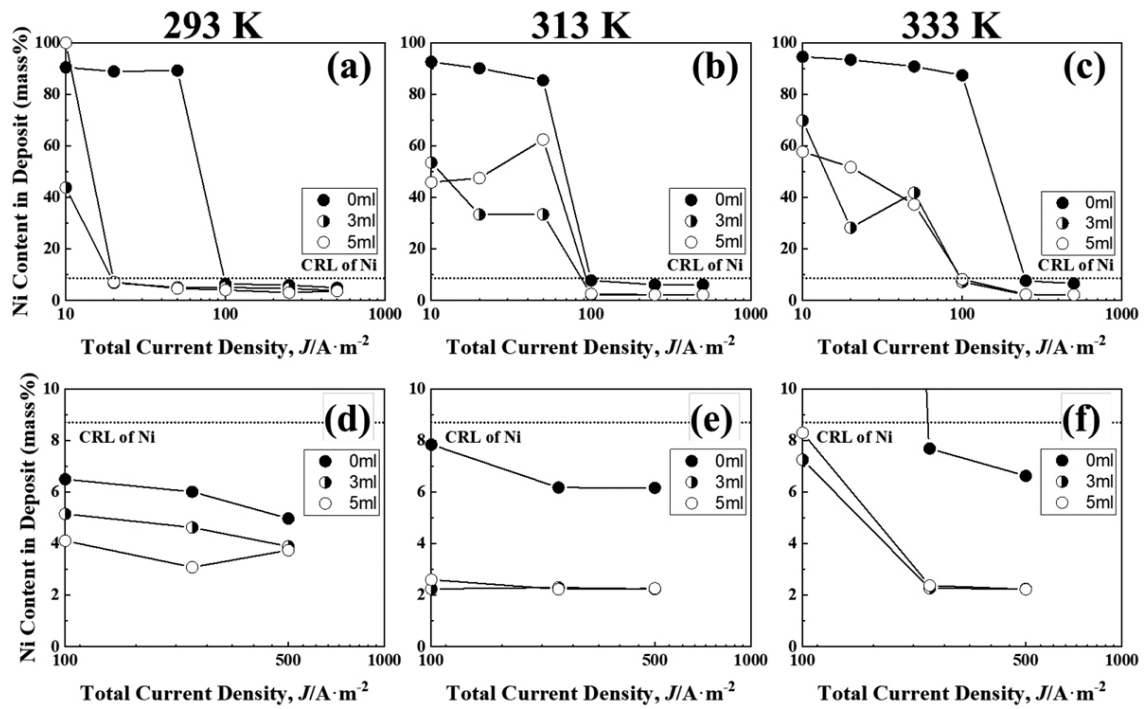
Fig. 4-8. Ni contents in the Zn-Ni alloys deposited at different temperatures from the solutions containing various amounts of IME. (d)-(f) Magnified view of the area of 0–10 mass% of the Ni content. [Concentration of IME: 0, 3, 5 ml·dm^{-3}, (a), (d): 293 K, (b), (e): 313 K, (c), (f): 333 K]

4-3-2. Effects of IME and Solution Temperature on the Appearance and Microstructure of the Deposited Films

Figure 4-9 shows the appearance of the Zn–Ni alloy deposition films obtained at 500 A·m^{-2} from a solution of 293 K, 313 K, and 333 K containing various concentrations of IME. When IME was not included (Fig. 4-9(a), (d), and (g)), the deposited films were gray and matte at any solution temperature, with several bubble traces at 313 K and 333 K. With the addition of 3 and 5 ml·dm^{-3} of IME, it became silvery and glossy in a solution of 293 K (Fig. 4-9(b), (c)). However, as the solution temperature increased to 313 K and 333 K, the gloss decreased (Fig. 4-9(e), (f), (h), and (i)).

Figure 4-10 shows the correlation between the concentration of IME and the glossiness of Zn–Ni alloy films obtained at 250 and 500 A·m^{-2} for each solution temperature. The glossiness of films deposited at 250 A·m^{-2} from IME-free solution was low at all the solution temperatures (Fig. 4-10(a)), however, the addition of 3 ml·dm^{-3} of IME greatly increased the glossiness at solution temperatures of 293 K and 313 K, which was especially pronounced at 293 K. However, when the solution temperature was increased to 333 K, the addition of IME did not increase the glossiness. At solution temperatures of 293 K and 313 K, the increase in IME addition from 3 to 5 ml·dm^{-3} decreased the gloss. Conversely, the gloss of the deposited films obtained at 500 A·m^{-2} (Fig. 4-10(b)) also increased significantly with the IME addition, and the degree of increase in gloss was greater for the deposited films obtained at 500 A·m^{-2} than for that at 250 A·m^{-2}. As described above, the glossiness of the deposited films obtained from the solution containing IME was highest at a solution temperature of 293 K and decreased on increasing it to 313 K and 333 K.
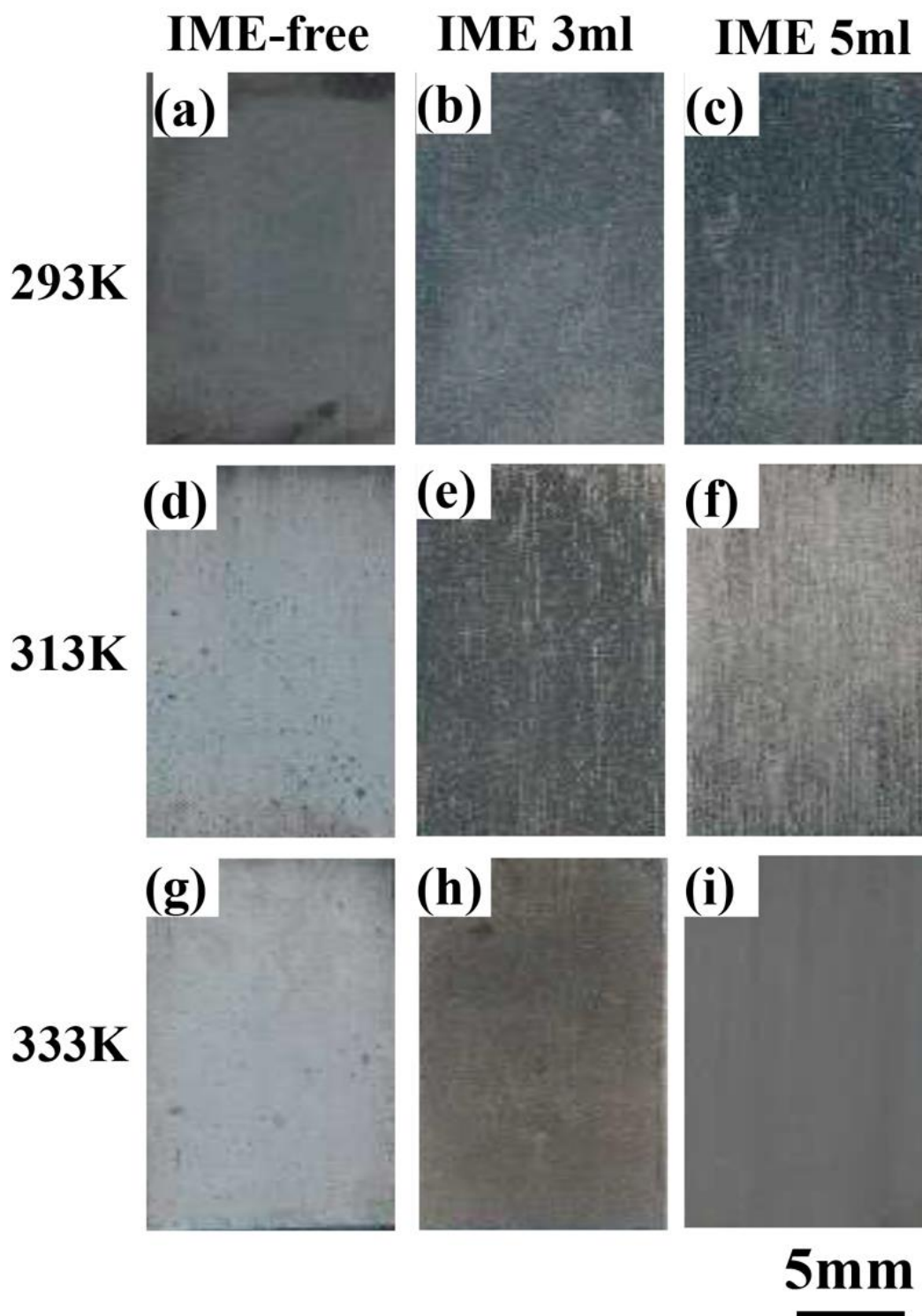
Fig. 4-9. Appearance of Zn-Ni alloy films deposited at 500 A·m^{-2} and different temperatures from the solutions containing various amounts of IME. [Concentration of IME: 0, 3, 5 ml·dm^{-3}, (a): IME-free, 293 K, (b): IME 3 ml·dm^{-3}, 293 K, (c): IME 5 ml·dm^{-3}, 293 K, (d): IME-free, 313 K, (e): IME 3 ml·dm^{-3}, 313 K, (f): IME 5 ml·dm^{-3}, 313 K, (g): IME-free, 333 K, (h): IME 3 ml·dm^{-3}, 333 K, (i): IME 5 ml·dm^{-3}, 333 K]
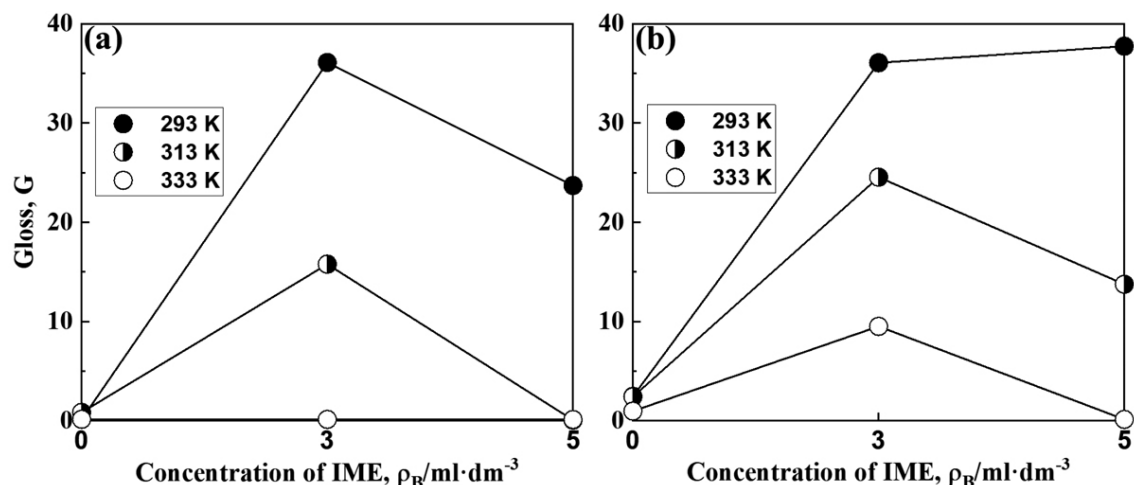
Fig. 4-10. Effect of IME concentration on the gloss of Zn-Ni alloy films deposited at different temperatures. [(a) 250 A·m^{-2}, (b) 500 A·m^{-2}]

Figure 4-11 shows the X-ray diffraction patterns of the deposited films obtained in the solution containing 3 ml·dm^{-3} of IME at different solution temperatures and current densities. At 293 K (Fig. 4-11(a)), the peaks related to the Fe of the substrate and η-Zn phases were detected in the deposited films obtained at 250 A·m^{-2}, whereas at 313 K (Fig. 4-11(b)) and 333 K (Fig. 4-11(c)), the peaks related to the γ-phase (intermetallic compound of Ni_2Zn_{11}) were detected besides the Fe and η-phase. The Ni content of the deposited films was 4.6, 2.2, and 2.3 mass% at 293 K, 313 K, and 333 K, respectively, indicating that the γ phase was formed even though the Ni content of the deposited films decreased with the increasing solution temperature. In contrast, in the deposited films obtained at 500 A·m^{-2}, only the peaks related to Fe and η phases were detected regardless of the solution temperature. At 313 K and 333 K, the Ni contents of the films obtained at the current densities of 250 and 500 A·m^{-2} were almost the same (2.3 mass%). These results indicate that the γ-phase was more easily formed in the deposited films obtained from the solution containing 3 ml·dm^{-3} IME at higher a solution temperature and a lower current density, i.e., lower overpotential for deposition.

Figure 4-12 shows the SEM images of the deposited films obtained in the solution containing 3 ml·dm^{-3} IME at different solution temperatures and current densities. The films deposited at 250 A·m^{-2} were smooth, consisting of fine plate-like crystals at 293 K (Fig. 4-12(a)). However, when the solution temperature increased to 313 K (Fig. 4-12(b)) and 333 K (Fig. 4-12(c)), the crystals became more rounded and lumpier. As mentioned earlier, for the deposition at 250 A·m^{-2} at 293 K, the deposited film (Ni content, 4.6 mass%) consisted of a single phase of η, whereas at 313 K and 333 K, the deposited films (Ni content, 2.2–2.3 mass%) consisted of η and γ phases. The γ phase of deposited Zn-Ni alloys is reported to consists of rounded granular crystals.[21,22] The surface morphology of the deposited films obtained at 250 A·m^{-2} differed greatly depending on the solution temperature, possibly attributed to the difference in the phase structures. Conversely, the films obtained at 500 A·m^{-2}

showed fine plate-like crystals and smooth surface at solution temperatures of 293 K (Fig. 4-12(d)) and 313 K (Fig. 4-12(e)), while the surface became slightly rough at a higher solution temperature of 333 K (Fig. 4-12(f)). The films obtained at 500 A·m^{-2} consisted of η phase with Zn content in films higher than 90 mass% at all the solution temperatures, and the grain size became larger at a higher solution temperature of 333 K because the overpotential for deposition became smaller. By comparing the SEM images of the Zn−Ni alloy deposited films shown in Fig. 4-12 with the gloss levels shown in Fig. 4-10, since the deposited films (Fig. 4-12(a), (d)) obtained in a solution containing 3 ml·dm^{-3} IME at a solution temperature of 293 K had fine crystals and a smooth surface, the glossiness of the films was higher. The glossiness of the films obtained from the solution containing IME was larger for those obtained at 500 A·m^{-2} than for those at 250 A·m^{-2} (Fig. 4-10), probably because the former films consisted of finer crystals (Fig. 4-12).
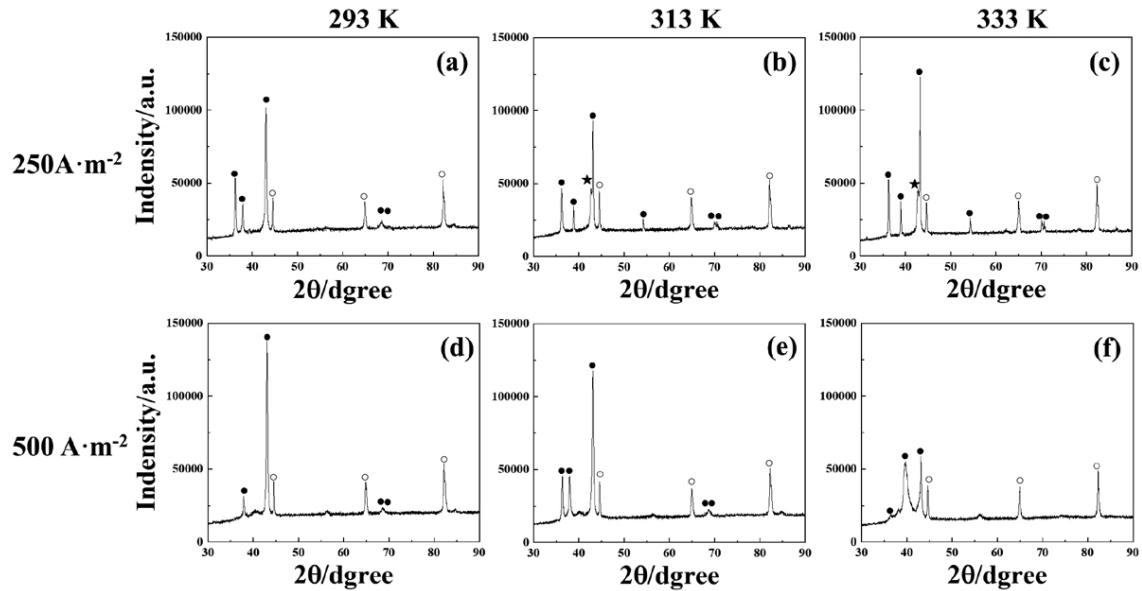

Fig. 4-11. X-ray diffraction patterns of the Zn-Ni alloy films deposited at various current densities and temperatures from the solution containing 3 ml·dm^{-3} of IME. [(a): 250 A·dm^{-2}, 293 K, (b): 250 A·dm^{-2}, 313 K, (c): 250 A·dm^{-2}, 333 K, (d): 500 A·dm^{-2}, 293 K, (e): 500 A·dm^{-2}, 313 K, (f): 500 A·dm^{-2}, 333 K] (○ Fe PDF # 65-4899, ● Zn[η] PDF # 87-0713, and ★ Ni$_2$Zn$_{11}$[γ] PDF # 65-5310)
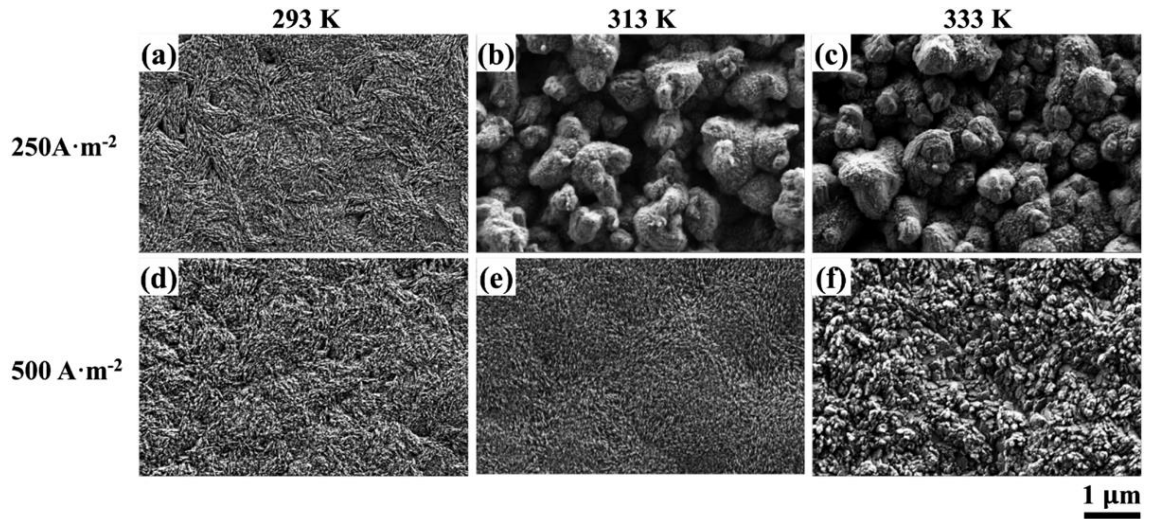
Fig. 4-12. SEM images of the Zn-Ni alloy films deposited at various current densities and temperatures from the solution containing 3 ml·dm^{-3} of IME. [(a): 250 A·dm^{-2}, 293 K, (b): 250 A·dm^{-2}, 313 K, (c): 250 A·dm^{-2}, 333 K, (d): 500 A·dm^{-2}, 293 K, (e): 500 A·dm^{-2}, 313 K, (f): 500 A·dm^{-2}, 333 K]

4-4. Discussion

Table 4-2 summarizes the results of the effect of IME on the deposition behavior of Zn–Ni alloys at 293 K and 333 K from alkaline zincate baths. The effects of IME on the transition current density at which the deposition behavior shifted from normal to anomalous, the current efficiency of alloy deposition, and the composition of the deposited films, varied with the solution temperature. Next, the factors are discussed for each potential range nobler than the equilibrium potential of Zn (normal type codeposition region) and less noble than the equilibrium potential of Zn (anomalous type codepositgion region).

Table 4-2. Effect of IME on the deposition behavior of Zn-Ni alloy at 293 and 333 K.

Potential		$E > E_{Zn}^{eq}$	$E < E_{Zn}^{eq}$
Deposition type		Normal codeposition	Anomalous codeposition
293K	Zn deposition Ni deposition H_2 evolution	— Suppressed Suppressed	Suppressed Suppressed Not affected
	Transition C.D. Current efficiency Ni % in deposit	Decrease Decrease —	— Significantly decrease Slightly decrease
333K	Zn deposition Ni deposition H_2 evolution	— Suppressed Not affected	Not affected Suppressed Not affected
	Transition C.D. Current efficiency Ni % in deposit	Not affected Significantly decrease —	— Slightly decrease Decrease

4-4-1. Electrodeposition Behavior in the Potential Region Nobler than the Equilibrium Potential of Zn (region of normal-type codeposition)

Figure 4-13 shows the relationship between the transition current density and IME concentration in the Zn–Ni alloy deposition for each solution temperature. The transition current density at which the deposition behavior shifted from normal to anomalous corresponded to the current density at which the potential shifted abruptly from a potential range nobler to less noble than the equilibrium potential of Zn in the total polarization curve. The transition current density shown in Fig. 4-13 was evaluated by the current density at which the potential began to shift from nobler to less noble in total polarization curve. As shown in Figs. 4-2, 4-3, and 4-4, hydrogen evolution was dominant in the

region nobler than the equilibrium potential of Zn, therefore, the transition current density could be approximated by the current density of hydrogen evolution when the potential shifts from nobler to less noble. As shown in Fig. 4-13, the transition current density increased with the increasing solution temperature regardless of the presence of IME because the higher the solution temperature, the more hydrogen evolution was promoted. Regarding the effect of IME on the transition current density, at a solution temperature of 293 K, the transition current density decreased significantly with the addition of 3 ml·dm^{-3} of IME, suggesting that IME suppressed the hydrogen evolution in the Zn–Ni alloy deposition in the potential region nobler than the equilibrium potential of Zn at solution temperature 293 K. However, at 313 K and 333 K, the transition current density did not change with the addition of IME, indicating that the suppression effect of IME on hydrogen evolution decreased with increasing the solution temperature.

As shown in Figs. 4-2(b), 4-3(b), and 4-4(b), slight partial current density of Zn deposition from the solution without IME was detected at around −0.9 V, nobler than its equilibrium potential, regardless of the solution temperature possibly due to the underpotential codeposition of Zn. However, no underpotential codeposition of Zn occurred from the solutions containing 3 and 5 ml·dm^{-3} of IME at all the solution temperatures. The underpotential codeposition of Zn in Zn–Ni alloy deposition reportedly occurs due to the formation of a stable intermetallic compound Ni_5Zn_{21} by deposition, considerably reducing the activity coefficient of Zn in the deposited films.[23–26] In other words, Ni codeposition is essential for the occurrence of Zn underpotential codeposition; however, in the current study, Ni deposition was greatly suppressed at all solution temperatures in the solution containing IME, suggesting that Zn underpotential codeposition did not occur because Ni did not deposit in the potential region nobler than the equilibrium potential of Zn.
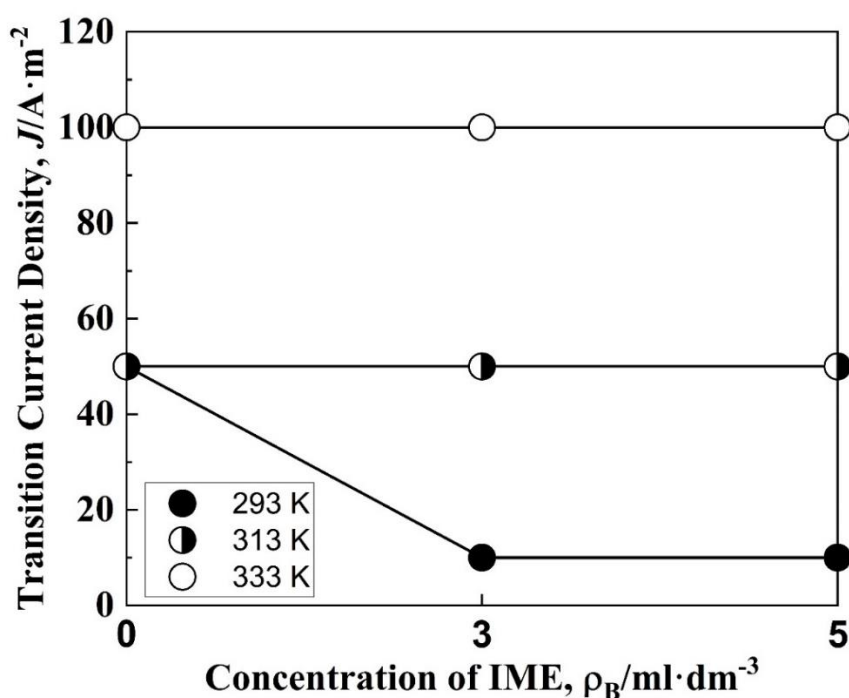
Fig. 4-13. Effect of IME concentration on the transition current density of Zn-Ni alloy deposition at different temperatures.

4-4-2. Electrodeposition Behavior in the Potential Region Less Noble than the Equilibrium Potential of Zn (region of anomalous co deposition)

The inhibitory effect of IME on the Zn and Ni deposition during the alloy deposition was compared for each solution temperature. At a temperature of 293 K, the partial current density of Zn was significantly reduced by the IME addition when the partial current density of Zn was compared at the same potential in the potential range less noble than the equilibrium potential of Zn (Fig. 4-2(b)). Similarly, the partial current density of Ni was clearly decreased by the addition of IME (Fig. 4-2(c)). Conversely, at 313 K and 333 K, the partial current density of Zn did not decrease with IME addition in the potential range less noble than the equilibrium potential of Zn (Figs. 4-3(b) and 4-4(b)), while that of Ni clearly decreased with the IME addition (Figs. 4-3(c), 4-4(c)). The inhibitory effect of IME on Zn and Ni deposition in the potential range less noble than the equilibrium potential of Zn varied with the solution temperature, and the inhibitory effect of IME on Zn deposition decreased with the increasing solution temperature, while maintaining the inhibitory effect on Ni deposition. The current efficiency in the anomalous region of $250-500$ $A \cdot m^{-2}$ showed that the current efficiency of Zn deposition decreased significantly with the addition of IME at a solution temperature of 293 K (Fig. 4-5(b)), while the decrease is smaller at solution temperatures of 313 K and 333 K (Figs. 4-6(b), 4-7(b)). In contrast, the current efficiency of Ni deposition in the anomalous region of $250-500$ $A \cdot m^{-2}$ decreased with the addition of IME to the same

extent regardless of the solution temperature (Figs. 4-5(c), 4-6(c), 4-7(c)). The Ni content in the deposited films in the anomalous range of 250–500 A·m^{-2} decreased significantly with the addition of IME at high solution temperature (Figs. 4-8(d), (e), (f)). These results for the current efficiency of Zn and Ni deposition and the Ni content of the deposited films reflect that the inhibitory effect of IME on Zn deposition decreased with increasing the solution temperature, while maintaining the inhibitory effect on Ni deposition.

To clarify the effect of solution temperature on the Ni content of the deposited films, the results of Fig. 4-8 were summarized for each IME concentration. The Ni content of the deposited films in the anomalous region of 250–500 A·m^{-2} increased with increasing the solution temperature without IME (Fig. 4-14(d)), while it decreased with increasing the solution temperature with 3 or 5 ml·dm^{-3} of IME (Fig. 4-14(e), (f)). The effect of solution temperature on the Ni content of the deposited films showed an opposite trend depending on the presence or absence of IME. Since Ni deposition was more accelerated than Zn deposition at higher solution temperatures for all current densities in the Zn–Ni alloy deposition from solutions without IME, Ni content was reported to increase with the increasing solution temperature,[11,12] and the same result was obtained in this study. Conversely, in the case of IME, the Ni content of the deposited films decreased with the increasing solution temperature, possibly because the inhibitory effect of IME on Zn deposition decreased with increasing the solution temperature, while the inhibitory effect on Ni deposition was maintained.
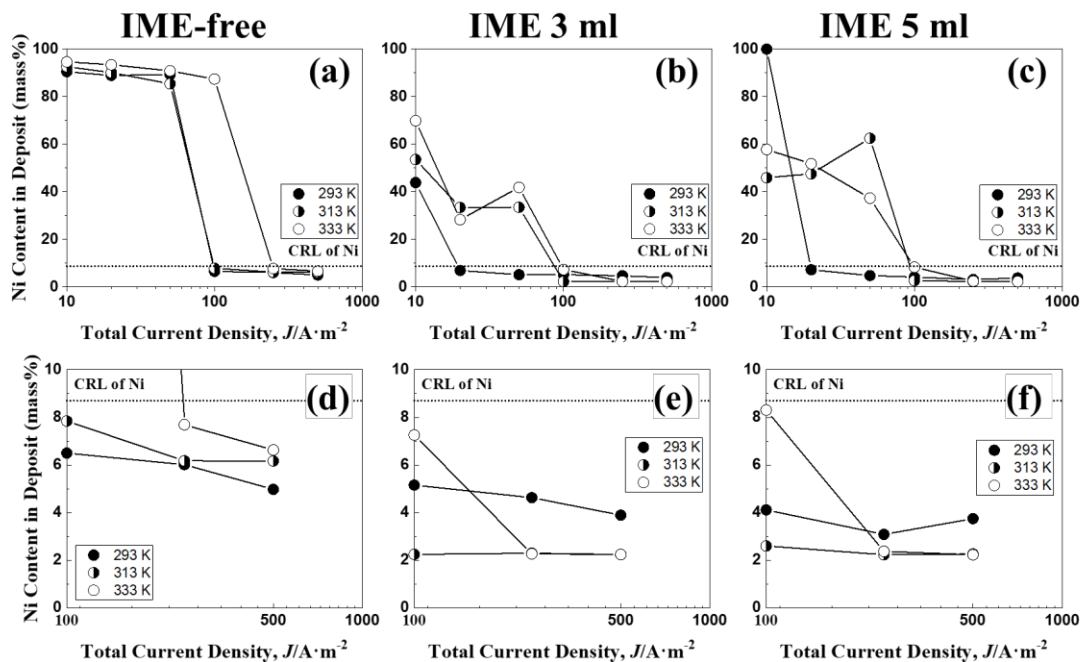

Fig. 4-14. Ni contents in the Zn-Ni alloys deposited at different temperatures from the solutions containing various amounts of IME. (d)-(f) Magnified view of the area of 0–10 mass% of the Ni content. [(a),(d): IME-free, (b),(e): IME 3 ml·dm^{-3}, (c),(f): IME 5 ml·dm^{-3}]

Since the inhibitory effect of IME on Zn deposition decreased with increasing the solution temperature, the adsorption ability of IME on the cathode surface was expected to vary with the solution temperature. In general, in the electrodeposition of metals, the amounts of additive components incorporated into the deposited films is reported to increase as the adsorption ability of the additive to the cathode increases.[27,28] Therefore, to evaluate the adsorption ability of IME on the cathode, the amount of C, which is a component of IME incorporated into the deposited films, was measured by GDOES, whose results are shown in Fig. 4-15. For the deposition from the solution without IME (Fig. 4-15(a), (b), (c)), C was codeposited in the deposited films, possibly due to triethanolamine added as a complexing agent for Ni^{2+}. In the films obtained from the solution containing IME (Fig. 4-15(d), (e), and (f)), the amount of C codeposited clearly increased, suggesting that the components of IME were codeposited. The amount of C codeposited in the deposited films was the highest at a solution temperature of 293 K (Fig. 4-15(d)) and decreased as the temperature increased. Based on this result, it is expected that the adsorption ability of IME on the cathode surface decreases with the increasing solution temperature. Therefore, the inhibitory effect of IME on Zn deposition decreased with increasing the solution temperature.

In contrast, the inhibitory effect of IME on Ni deposition was maintained even when the solution temperature was increased, indicating that IME inhibited the Ni deposition despite the decreasing adsorption ability. Focussing on the difference in inhibitory effect of IME on the Ni and Zn deposition, the Ni content in the films deposited in the anomalous codeposition region decreased with the addition of IME, regardless of the solution temperature, indicating that Ni deposition was more strongly inhibited by IME (Fig. 4-8(d), (e), (f)). Reportedly, the Ni deposition from hydrated ions proceeds with a multistep reduction mechanism via a hydroxyl-containing adsorption intermediate, $NiOH_{ad}$, and the overpotential for deposition was large due to the limited sites at which $NiOH_{ad}$ could be adsorbed.[29−32] In the Zn−Ni alloy deposition, the added IME blocks the adsorption sites of $NiOH_{ad}$ which are restricted inherently, more strongly suppressing the Ni deposition. Even though the adsorption ability of IME decreases with the increasing solution temperature, the inhibitory effect of IME on the Ni deposition seems to be larger than that on Zn deposition. The highest gloss of the Zn−Ni alloy deposited films was observed at 293 K due to the large adsorption ability of IME and fine and smooth grains of the deposited films.
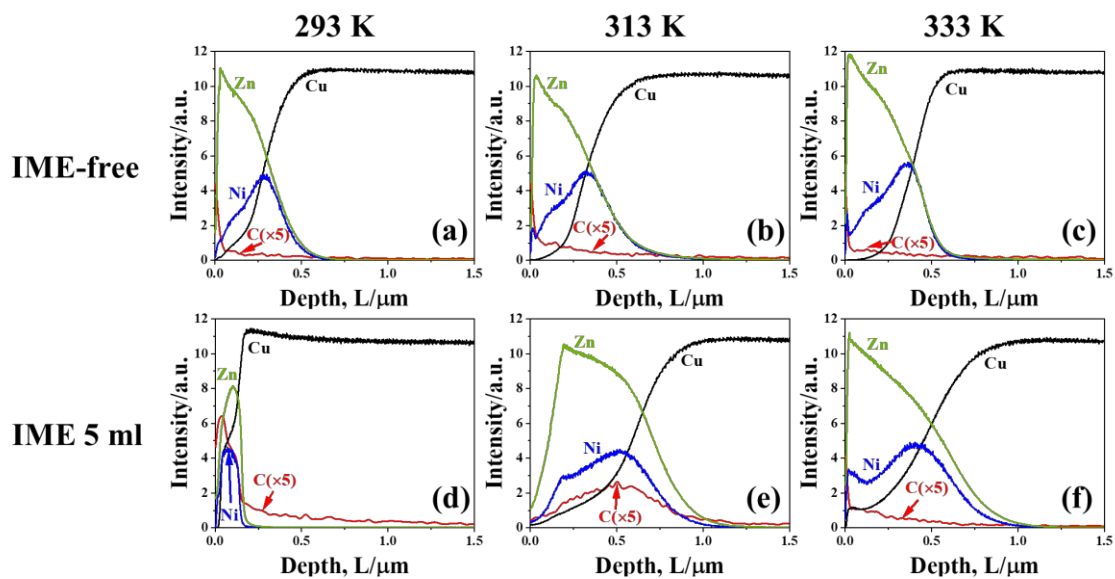
Fig. 4-15. Rf-GDOES depth profiles of Zn-Ni films deposited at 500 A·m^{-2} from the solutions of different temperatures with and without IME. [(a): IME-free, 293 K, (b): IME-free, 313 K, (c): IME-free, 333 K, (d): IME 5 ml·dm^{-3}, 293 K, (e): IME 5 ml·dm^{-3}, 313 K, (f): IME 5 ml·dm^{-3}, 333 K]

4-5. Conclusion

The synergistic effect of IEM and solution temperature on the deposition behavior of Zn–Ni alloy from alkaline zincate solutions was investigated. The transition current density, at which the deposition behavior shifted from the normal to anomalous type decreased with the addition of IME at 293 K but did not change regardless of IME addition at 313 K and 333 K. This indicates that the inhibitory effect of IME on the hydrogen evolution decreases with increasing the solution temperature. The suppression effect of IME on the Zn and Ni depositions during the alloy deposition was observed at 293 K, while at 313 K and 333 K, the suppression effect was decreased on the Zn deposition, though maintained on the Ni deposition. Therefore, Ni content in the deposits significantly decreased with IME as the temperature increased. The current efficiency for Zn deposition significantly decreased with IME at 293 K, while decreasing insignificantly at 313 K and 333 K. The C content in the deposits was the highest at 293 K, and decreased with the increasing solution temperature, indicating that the adsorption ability of IME on the cathode decreases with the increasing temperature. As a result, the suppression effect of IME on the Zn deposition seems to decrease with increasing the temperature. The gloss of the deposited films was the highest at 293 K, attributed to the adsorption ability of IME being large at 293 K and deposited films with fine crystals becoming smooth.

4-6. References

1) Z.Feng, Q.Li, J.Zhang, P.Yang and M.An: *RSC Adv.*,**5**(2015), 58199.
2) L.M.Muresan, J.Eymard, D.Blejan and E.Indrea: *Stud. Univ. Babes-Bol-yai Chem.*, (2010), No.1, 37.
3) G.Y.Li, J.S.Lian, L.Y.Niu and Z.H.Jiang: *Surf. Coat. Technol.*, **191**(2005), 59.
4) S.H.Mosavat, M.E.Bahrololoom and M.H.Shariat: *Appl. Surf. Sci.*, **257**(2011), 8311.
5) Z.Feng, L.Ren, J.Zhang, P.Yang and M.An: *RSC Adv.*, **6**(2016), 88469.
6) Z.Feng, D.Li, Q.Sun, L.Wang, P.Xing and M.An: *J. Alloy Compd.*, **765**(2018), 1026.
7) Z.Feng, D.Li, L.Wang, Q.Sun,P.Lu, P.Xing and M.An: *Ionics,***25**(2019), 1857.
8) S.Bae, S.Oue, I.Son and H.Nakano: *TETSU TO HAGANE*, **107**(2021), 229. (in Japanese).
9) S.Bae, S.Oue, I.Son and H.Nakano: *ISIJ Int.*, **61**(2021), 2256.
10) S.Haruyama: Hyomen Gizyutsusya no tameno Denkikagaku (Electro-chemistry for Surface Engineer) , Maruzen , Tokyo , (2005), 173 (in Japanese).
11) S.Bae, S.Oue, Y.-k.Taninouchi, I.Son and H.Nakano: *TETSU TO HA-GANE*, **108**(2022),120 (in Japanese).
12) H.Y.Lee and S.G.Kim: *Surf. Coat. Technol.*, **135**(2000), 69.
13) H.Nezu, S.Fujii, N.Kaneko and N.Ofuchi: *J. Met. Finish. Soc. Jpn.*, **32**(1981), 17 (in Japanese).
14) S.Konishi, S.Eguchi, N.Ozeki and M.Uesugi: *J. Met. Finish. Soc. Jpn.*, **20**(1969), 263 (in Japanese).
15) M.Vidal, M.Ostra, N.Imaz, E.Garcia-Lecina and C. Ubide: *Chemom. In-tell. Lab. Syst.*, **149**(2015), Part A, 90.
16) M.Pourbaix: Atlas of Electrochemical Equilibria in Aqueous Solutions, Pergamon Press, New York, (1966), 406.
17) D.D.Perrin: Stability Constants of Metal-ion Complexes, Part B: Or-ganic Ligands, Pergamon Press, Oxford, (1979), 466.
18) T.Akiyama, H.Fukushima and K.Higashi: *Tetsu-To-Hagane,* **72**(1986), 918 (in Japanese).
19) H.Nakano, S.Shibata, S.Arakawa, S.Oue and S.Kobayashi: *ISIJ int.*, **53**(2013), 1858.
20) H.Nakano, S.Shibata, S.Arakawa, S.Oue and S.Kobayashi: *Tetsu-To-Ha-gane,* **99**(2013), 346 (in Japanese).
21) N.Lotfi, M.Aliofkhazraei, H.Rahmani and G.B.Darband: *Prot. Met. Phys. Chem. Surf.*, **54**(2016), 1102.
22) S.Fashu and R.Khan: *Anti-Corros. Methods Mater.*, **66**(2019), 45.
23) H.Nakano, S.Arakawa, Y.Takada, S.Oue and S.Kobayashi: *Mater. Trans.*, **53**(2012), 1946.
24) H.Nakano, S.Arakawa, Y.Takada, S.Oue and S.Kobayashi: *J. Japan Inst. Metals*, **76**(2012), 443 (in Japanese).

25) H.Nakano, S.Arakawa, S.Oue and S.Kobayashi: *Tetsu-To-Hagane*, **99**(2013), 425 (in Japanese).

26) H.Nakano, S.Arakawa, S.Oue and S.Kobayashi: *ISIJ int*., **53**(2013),1864.

27) K.Fuchi, S.Oue, Y.Kikuchi, S.Akamatsu, Y.Kashiwa and H.Nakano: *Mater. Trans*., **59**(2018), 1767.

28) K.Fuchi, S.Oue, Y.Kikuchi, S.Akamatsu, Y.Kashiwa and H.Nakano: *J. Jpn. Inst. Met. Mater*., **82**(2018), 281 (in Japanese).

29) K.Fukuda, Y.Kashiwa, S.Oue, T.Takasu and H.Nakano: *ISIJ int*., **61**(2021), 919.

30) K.Fukuda, Y.Kashiwa, S.Oue, T.Takasu and H.Nakano: *Tetsu-To-Hagane*, **105**(2019), 988 (in Japanese).

31) K.Fukuda, Y.Kashiwa, S.Oue, T. Takasu and H. Nakano: *ISIJ int*., **59**(2019), 1632.

32) Y.Kashiwa, N.Nagano, T.Takasu, S.Kobayashi, K.Fukuda and H.Nakano: *ISIJ int*., **59**(2019), 514.

Chapter 5. Effect of Brightener on the Corrosion Resistance of Zn−Ni Alloy Electrodeposited Steel Sheet from Zincate Solution

5-1. Introduction

In Zn-Ni alloy electrodeposition using a zincate solution, unlike sulfate and chloride solutions, typically, a brightener is added. Many studies have explored the relationship between the appearance of electrodeposited films obtained from a zincate solution and brighteners[1-15]; however, few reports have explored the effect of brighteners on the corrosion resistance.[16,17] When a brightener synthesized by condensing salicylaldehyde and cysteine hydrochloride[18] and another by vanillin and glycine[19] are added to a sulfate solution, the corrosion current density at an early stage of the Zn-Ni alloy plating film reportedly decreases, especially in a chloride ion environment. However, the effect of brightener on the corrosion resistance after the corrosion products are formed is unknown.

Studies have also reported that the formation of zinc chloride hydroxide ($Zn_5(OH)_8Cl2 \cdot H_2O$) with high film resistance as a corrosion product is the reason for the superior corrosion resistance of Zn-Ni alloy-coated steel sheets compared to Zn-coated steel sheets in a chloride ion environment.[20] To better explain the effect of brightener on the corrosion resistance after the corrosion product is formed, it is important to investigate the effect of brightener on the formation behavior of corrosion products.

Hence, we selected a reaction product (IME) of epichlorohydrin and imidazole as a brightener. In this chapter, to investigate the corrosion behavior of Zn-Ni alloy plating film in a relatively simple corrosion environment, a dipping test was conducted in an aqueous NaCl solution, which is a typical chloride ion environment. The effect of IME on the formation of zinc chloride hydroxide that is a corrosion product was investigated.

5-2. Experimental

The electrolyte composition and experimental conditions are presented in Table 5-1. As described in the previous chapter, the sample was prepared using an equal amount of electricity. In this chapter, however, the film thickness of deposited films was kept constant at 40 μm, while the Ni content of the films was 4.98, 3.88, 3.89, and 3.75 mass% for IME added amounts of 0, 1, 3, and 5 ml·dm^{-3}, respectively. Table 5-2 lists the conditions for the corrosion tests. In a 3 mass% aqueous NaCl solution, the potential was shifted from less noble to noble at a rate of 10 mV·s^{-1} using the potential sweep method. A polarization curve was generated to obtain the corrosion current density and corrosion potential. The 3 mass% aqueous NaCl solution was pre-pumped with air for several hours, and the experiments were conducted under air-saturated conditions. Each specimen was immersed in the 3 mass% aqueous NaCl solution (saturated with air) at a constant solution temperature of 25 °C and left standing for 24 h. For these films, polarization curves were obtained using LSV to evaluate the corrosion resistance after the formation of the corrosion products. The

structure of the corrosion products was identified using X-ray diffraction (XRD). Low-voltage scanning electron microscopy (SEM) was used to observe the microstructures of the samples' surfaces. Temperature (K)

Table 5-1 Solution composition and electrolysis conditions

ZnO (mol·dm^{-3})	0.15	Current density (A·m^{-2})	500
NiSO$_4$·6H$_2$O (mol·dm^{-3})	0.016	Temperature (K)	293
N(CH$_2$CH$_2$OH)$_3$ (mol·dm^{-3})	0.34	Thickness	40 μm
NaOH (mol·dm^{-3})	2.5		
IME (ml·dm^{-3})	0,1,3,5	Cathode	Fe (1 × 2 cm^2)
Quiescent solution		Anode	Pt (1 × 2 cm^2)

Table 5-2 Corrosion test conditions

	Temperature (K)	313
	Cathode	Pt (1 × 2 cm^2)
3 mass% NaCl	Anode	Sample (1 × 2 cm^2)
	Scan speed	10 mV·s^{-1}

5-3. Results

5-3-1. Effect of IME on the Initial Corrosion Resistance of Deposited Zn-Ni Alloy Films

Figure 5-1 shows the polarization curves of the Zn-Ni alloy deposits in the 3 mass% aqueous NaCl solution. The corrosion potential of the deposit obtained from the solution without IME was approximately -0.86 V, but the corrosion potential shifted to the noble side when IME was added. The oxidation reaction (a dissolution reaction of the deposited films) was suppressed with IME, causing the corrosion potential to shift to the noble side. In contrast, the reduction of dissolved oxygen (cathodic reaction of the corrosion reaction) was almost unchanged with or without IME, resulting in negligible effects of IME addition on the corrosion current density.
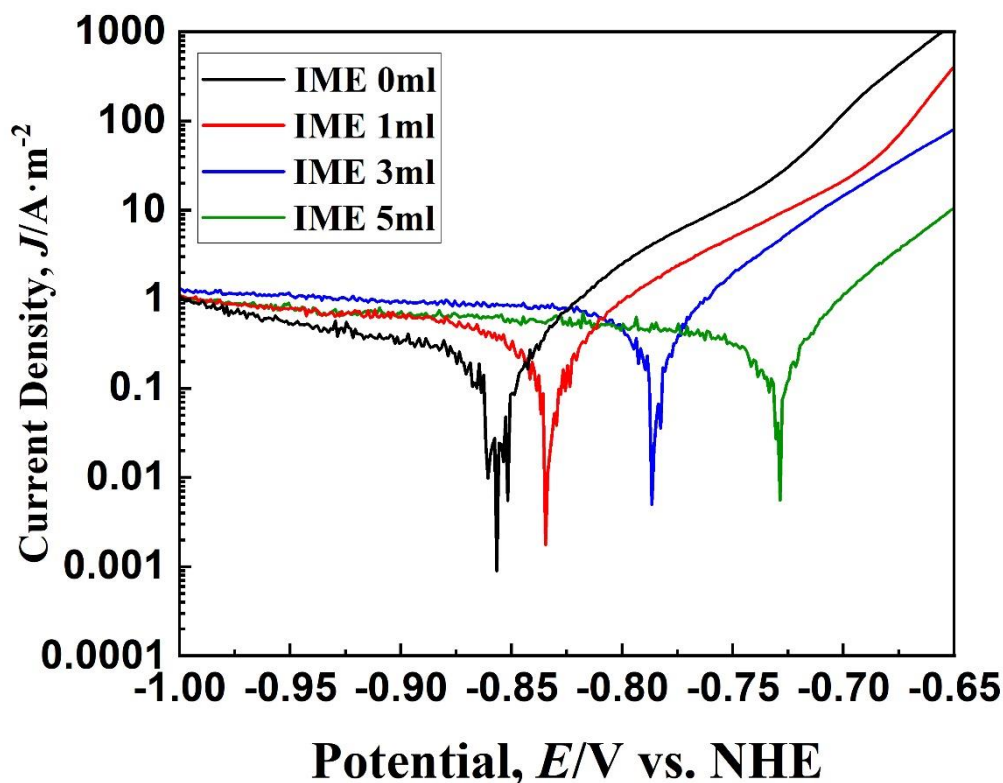
Fig. 5-1. Polarization curves of Zn-Ni alloy deposits in a 3 mass% NaCl solution.

Figure 5-2 shows the anodic current density (at a constant potential of -0.8 V) of the Zn-Ni alloy deposited films immersed in the 3 mass% aqueous NaCl solution. Anodic current density, that is, the dissolution current density of Zn-Ni alloy deposited films, increased with time irrespective of the presence of IME. The anodic current density decreased as IME concentration increased from 0 to 5 ml·dm^{-3}, except at the initial time. The anodic current density at a constant potential reflects the polarization curve of the anodic reaction, revealing that the anodic reaction of corrosion was suppressed when the IME concentration increased from 0 to 5 ml·dm^{-3}. The increase in the anodic current density with time was attributed to the increase in the true surface area as the electrodeposited films dissolved.
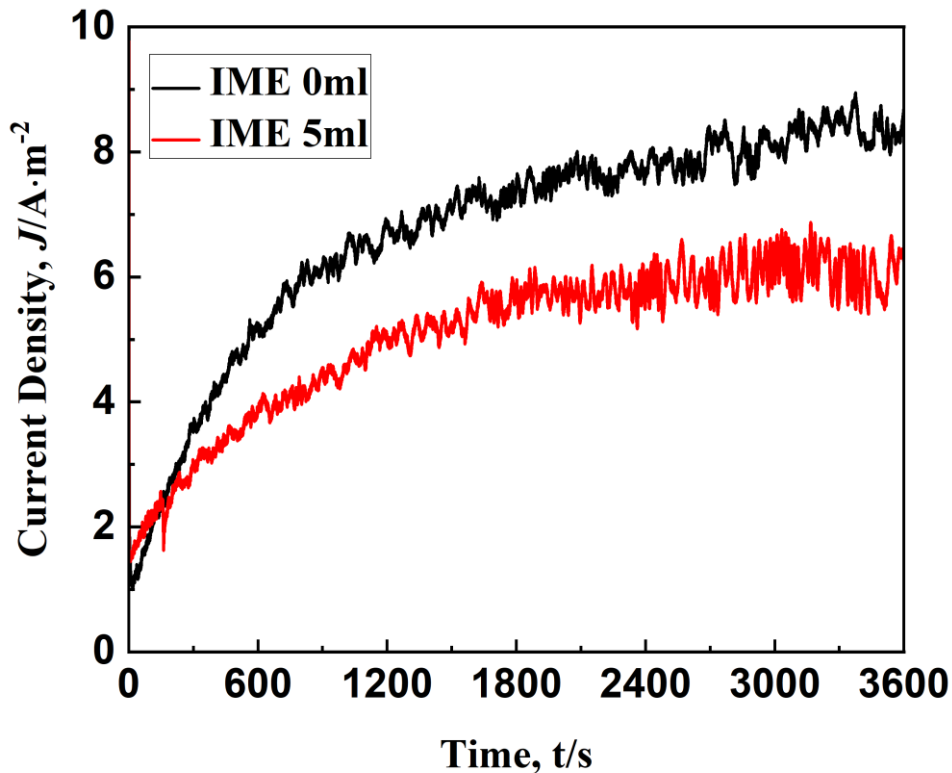
Fig. 5-2. Anodic current density at a constant potential of -0.8 V of the deposited Zn-Ni alloy films in a 3 mass% NaCl solution.

5-3-2. Effect of IME on the Appearance of Deposited Zn-Ni Alloy Films after Corrosion Tests

Figure 5-3 shows the appearance of Zn-Ni alloy films obtained at 500 A·m^{-2} from a 293 K solution containing different IME concentrations. The films deposited from IME-free solution were gray and dull lustre (Fig. 5-3(a)), while the films deposited from solutions containing 1 and 3 ml·dm^{-3} of IME showed somewhat gloss (Fig. 5-3(b), (c)). The samples were shiny silver and showed significant gloss after adding 5 ml·dm^{-3} IME (Fig. 5-3(d)).

Figure 5-4 shows the appearance of the Zn-Ni alloy deposited films after measuring the polarization curve in the 3 mass% aqueous NaCl solution. The films deposited from IME-free solution partialy dissoved and Fe substrate appeared (Fig.5-4(a)), while the films deposited from solutions containing 1 and 3 ml·dm^{-3} of IME were dark gray (Fig. 5-4(b) and (c)), and at 5 ml·dm^{-3} of IME, they lost their luster and turned gray (Fig. 5-4(d)).

Figure 5-5 shows the appearance of the deposited Zn-Ni alloy films after immersion in the 3 mass% aqueous NaCl solution for 24 h. Regardless of the presence of IME, no red rust of Fe substrate appeared after immersion in the 3 mass% aqueous NaCl solution for 24 h. However, white precipitates, that is, corrosion products of the deposited films, were observed on the surface.

Figure 5-6 shows the appearance of the deposited Zn-Ni alloy films after 24

h immersion and subsequently measuring the polarization curve in the 3 mass% aqueous NaCl solution. In the absence of a brightener (Fig. 5-6(a)) and with 1 ml·dm^{-3} of IME (Fig. 5-6(b)), red rust of Fe substrate appeared due to corrosion. In the case of 3 and 5 ml·dm^{-3} IME, no red rust of Fe substrate was observed (Fig. 5-6(c) and (d)). White precipitates from the deposited films appeared on the surface.
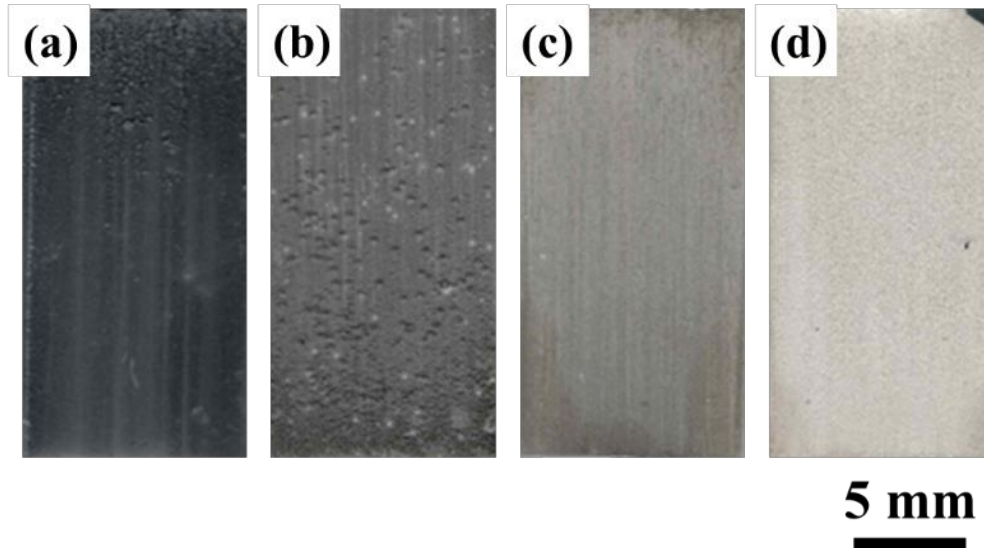

Fig. 5-3. Effect of IME addition on the appearance of the deposited Zn-Ni Alloy films.
[(a) IME-free, (b) IME 1 ml·dm^{-3}, (c) IME 3 ml·dm^{-3}, (d) IME 5 ml·dm^{-3}]
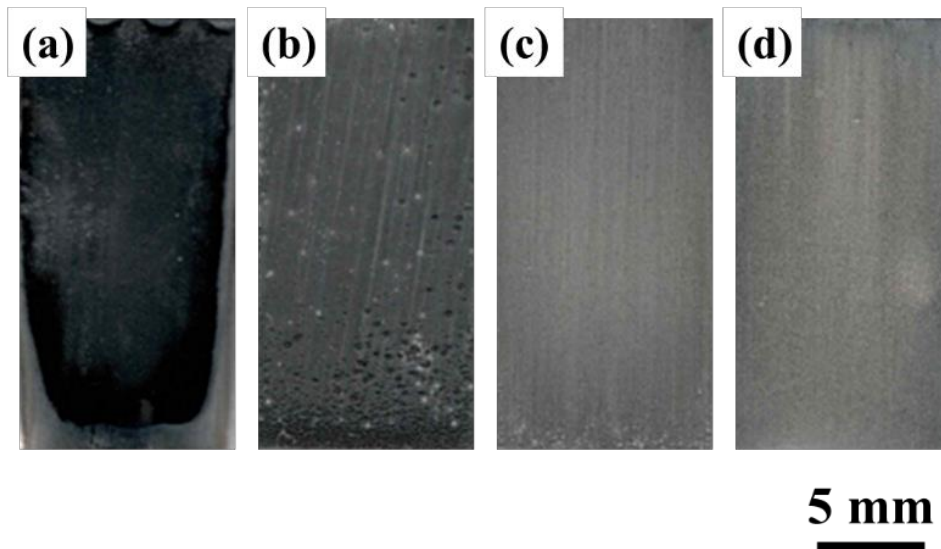
Fig. 5-4. Appearance of the deposited Zn-Ni alloy films after measuring the polarization curve in the 3 mass% NaCl solution.
[(a) IME-free, (b) IME 1 ml·dm^{-3}, (c) IME 3 ml·dm^{-3}, (d) IME 5 ml·dm^{-3}]
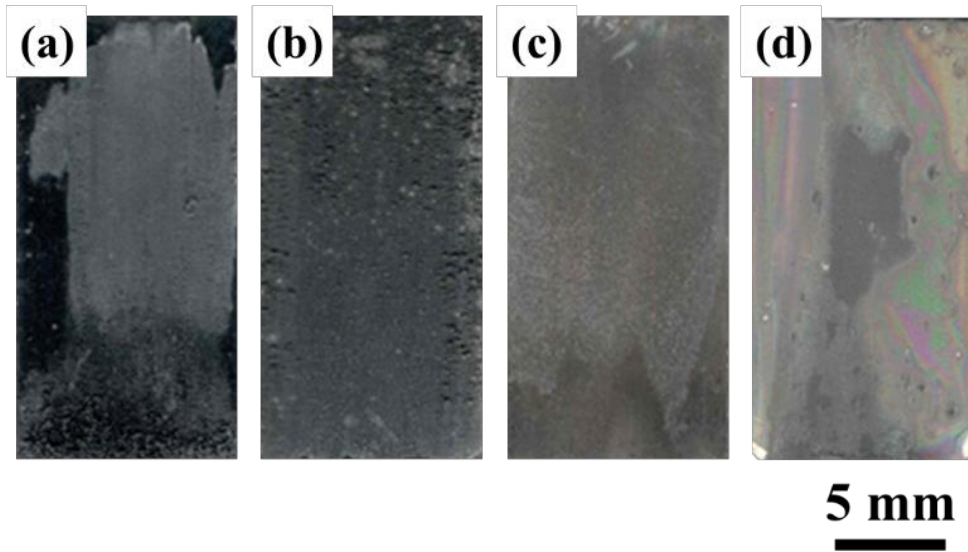
Fig.5-5. Appearance of the deposited Zn-Ni alloy films after 24 h immersion in the 3 mass% NaCl solution.
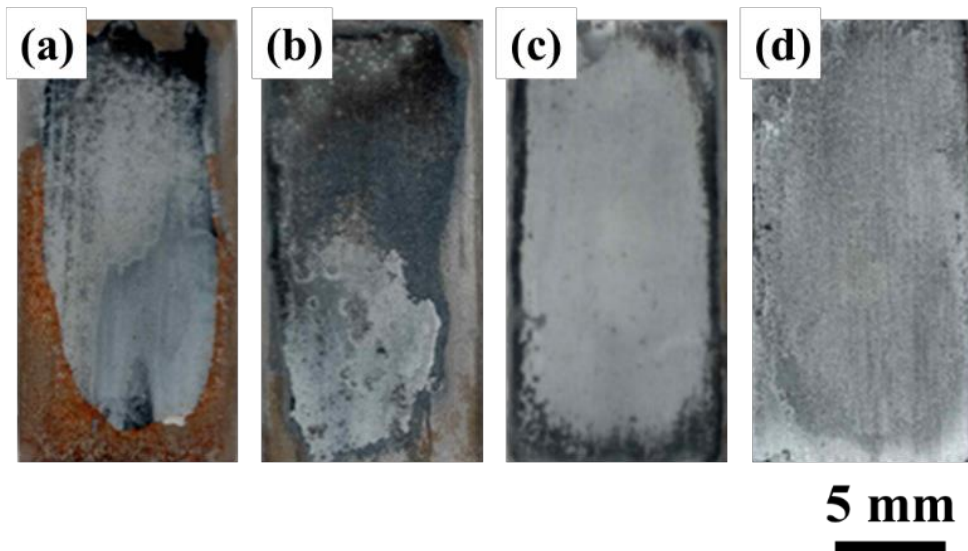[(a) IME-free, (b) IME 1 ml·dm^{-3}, (c) IME 3 ml·dm^{-3}, (d) IME 5 ml·dm^{-3}]

Fig. 5-6. Appearance of the deposited Zn-Ni alloy films after 24 h immersion and subsequently measuring the polarization curve in the 3 mass% NaCl solution.
[(a) IME-free, (b) IME 1 ml·dm^{-3}, (c) IME 3 ml·dm^{-3}, (d) IME 5 ml·dm^{-3}]

5-3-3. Effect of IME on the Corrosion Product Structures of Deposited Zn-Ni Alloy Films

Figure 5-7 shows the XRD patterns of the Zn-Ni alloy films obtained at 500 A·m^{-2}. Only η-Zn phase (solid solution of Ni in the Zn) and γ phase (intermetallic compound Ni$_2$Zn$_{11}$) were detected regardless of the presence of IME. The formation of the γ phase increased when IME was added. The peak resulting from Fe substrate was not detected because Zn-Ni plating was performed at thickness of 40 μm.

Figure 5-8 shows the XRD patterns of the deposited Zn-Ni alloy films after 24 h immersion in the 3 mass% aqueous NaCl solution. In addition to η-Zn and γ phases (Ni$_2$Zn$_{11}$ intermetallic compound), peaks for zinc chloride hydroxide (Zn$_5$(OH)$_8$Cl2·H$_2$O) and Zn(OH)$_2$ were detected. In comparison with the XRD patterns in Fig. 5-7, the η-Zn and γ phases' peaks decreased after immersion in the NaCl solution. This is attributed to the formation of Zn$_5$(OH)$_8$Cl$_2$·H$_2$O and Zn(OH)$_2$ which are the corrosion products of the deposited Zn-Ni alloy films during 24 h immersion in the 3 mass% aqueous NaCl solution.
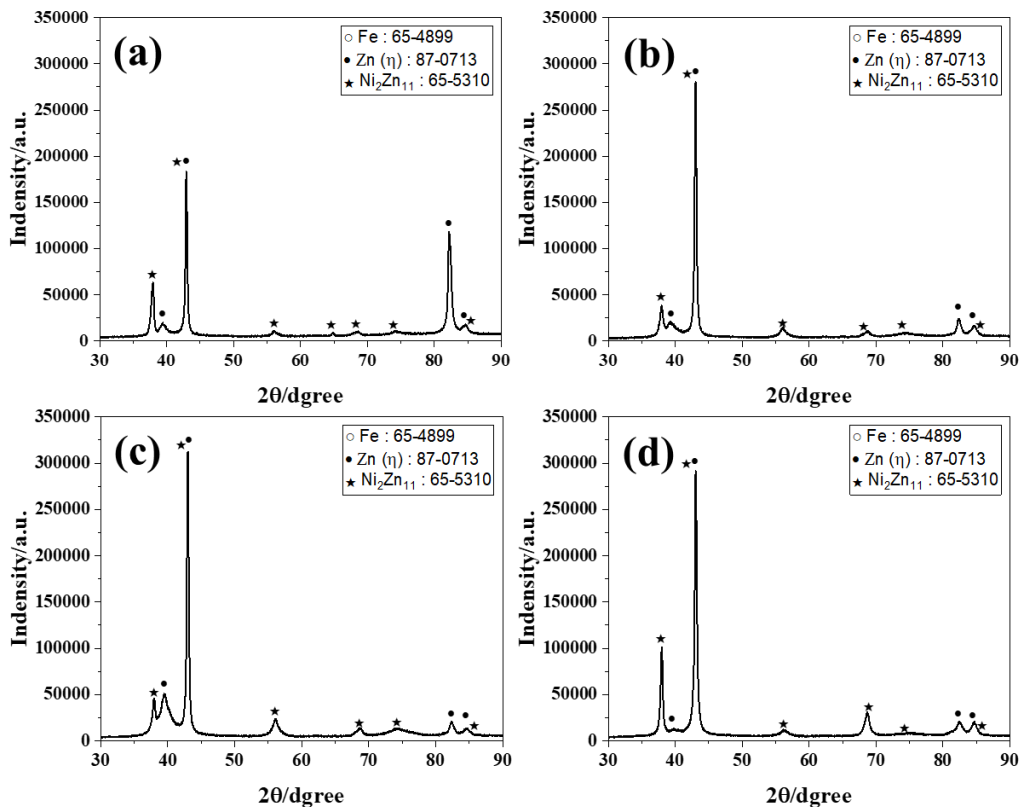

Fig. 5-7. X-ray diffraction patterns of the deposited Zn-Ni alloy films.
[(a) IME-free, (b) IME 1 ml·dm^{-3}, (c) IME 3 ml·dm^{-3}, (d) IME 5 ml·dm^{-3}]
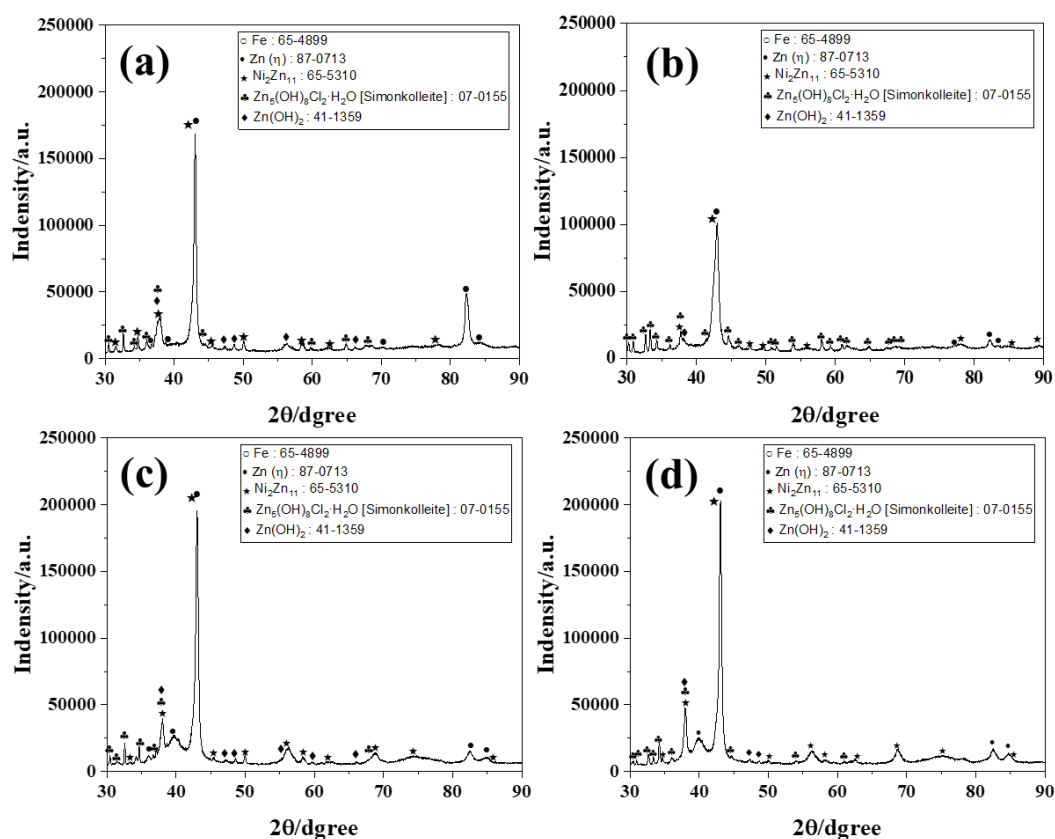
Fig. 5-8. X-ray diffraction patterns of the deposited Zn-Ni alloy films after 24 h immersion in the 3 mass% NaCl solution. [(a) IME-free, (b) IME 1 ml·dm^{-3}, (c) IME 3 ml·dm^{-3}, (d) IME 5 ml·dm^{-3}]

Figure 5-9 shows the SEM images of the surface of Zn-Ni alloy films obtained at 500 A·m^{-2} from solutions with varying IME concentrations. The films obtained from the solution without IME exhibited a vertically grown triangular pyramid (Fig. 5-9 (a)). In the films deposited with 1 and 3 ml·dm^{-3} IME, the plate-like crystals disappeared, transforming into the rounded agglomerations consisting of fine crystals (Fig. 5-9 (b), (c)). With 5 ml·dm^{-3} of IME, the surface became smooth overall (Fig. 5-9 (d)). At high IME concentration, the γ phase was predominant (Fig. 5-7), and the phase structure affected the morphology of the surface.

Figure 5-10 shows the SEM image and point analysis by EDX of the Zn-Ni alloy films deposited from IME-free solution after 24 h immersion in the 3 mass% aqueous NaCl solution. Massive crystals ((b) in Fig. 5-10 (a)) and hexagonal plate crystals ((c) in Fig. 5-10 (a)) were observed on the surface of the deposited films. Zn, O, and Ni were detected in the massive crystals ((b) in Fig. 5-10 (a)), indicating that they were mainly composed of the η-Zn and γ phases (Ni$_2$Zn$_{11}$ intermetallic compound). In contrast, Zn, O, Na, C, Cl, and Ni were detected in the hexagonal plate-shaped crystal ((c) in Fig. 5-10 (a)), in conjunction with a result of Fig.5-8(a), showing the formation of zinc chloride hydroxide (Zn$_5$(OH)$_8$Cl$_2$·H$_2$O) which are the corrosion products.
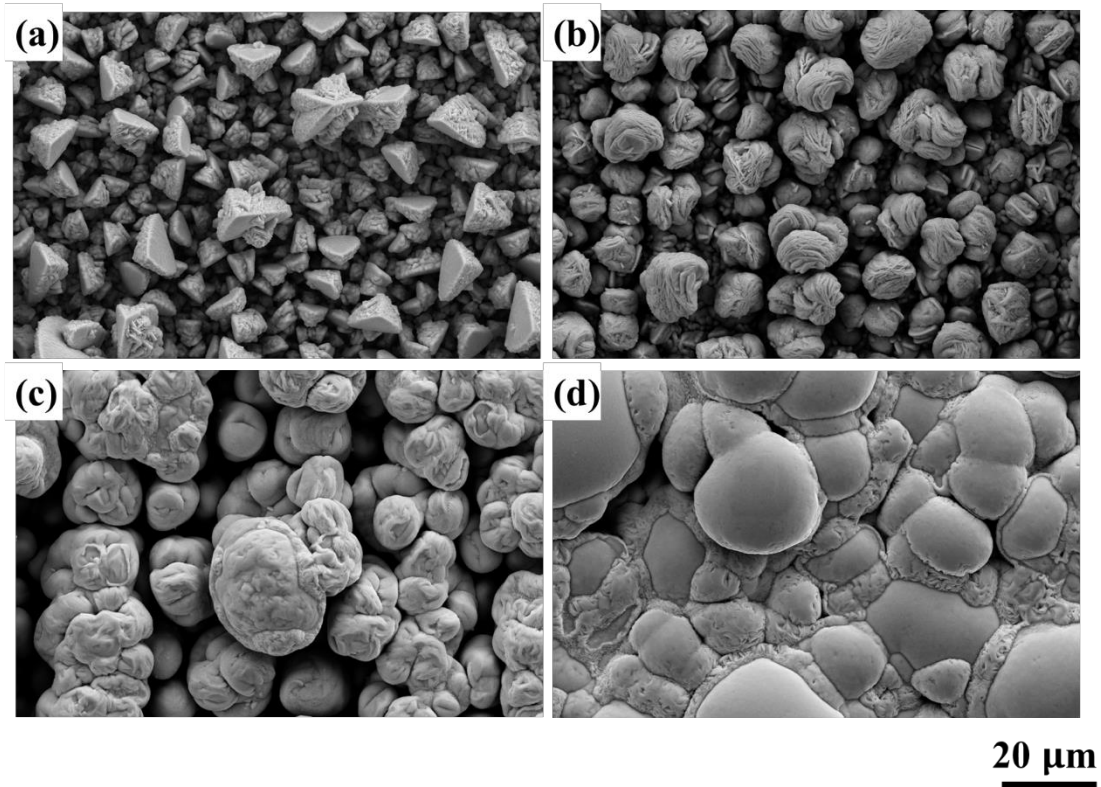
Fig. 5-9. SEM images of the surface of Zn-Ni alloy films obtained at 500 A·m^{-2} from solutions with varying IME concentrations. [(a) IME-free, (b) IME 1 ml·dm^{-3}, (c) IME 3 ml·dm^{-3}, (d) IME 5 ml·dm^{-3}]
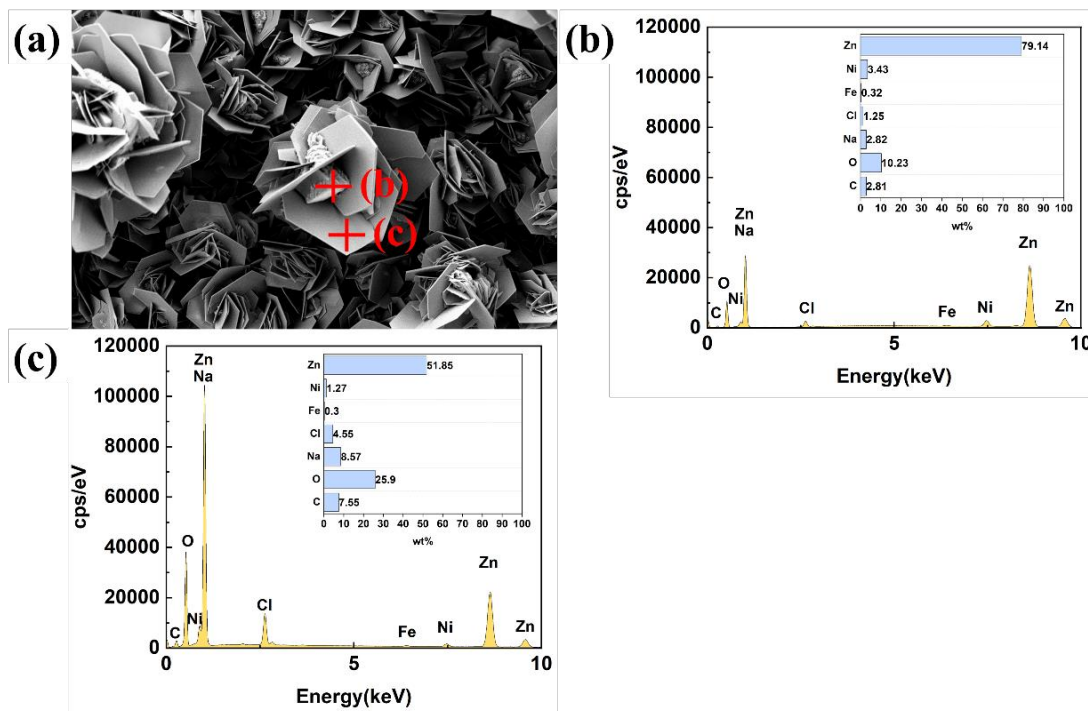

Fig. 5-10. SEM image and point analysis by EDX of the Zn-Ni alloy films deposited from IME-free solution after 24 h immersion in the 3 mass% aqueous NaCl solution.

Figure 5-11 shows the SEM image and point analysis by EDX of the Zn-Ni alloy films deposited from solution containing 5 ml·dm^{-3} of IME after 24 h immersion in the 3 mass% aqueous NaCl solution. Plate-like crystals were observed over the entire surface of the deposited films. Zn, O, Na, C, Cl, and Ni were detected in this plate-like crystal ((b) in Fig. 5-11 (a)), in conjunction with a result of Fig.5-8(d), indicating the formation of zinc chloride hydroxide $(Zn_5(OH)_8Cl_2 \cdot H_2O)$, which are corrosion products.

Figure 5-12 shows SEM images of the surface of deposited Zn-Ni alloy films after 24 h immersion in the 3 mass% aqueous NaCl solution. Hexagonal plate-like crystals, which are corrosion products, were observed after immersion in the aqueous NaCl solution, regardless of the presence of IME. These plate-like crystals seem to be grown zinc chloride hydroxide $(Zn_5(OH)_8Cl_2 \cdot H_2O)$ from the SEM-EDS results shown in Figs. 5-10 and 5-11. In the films obtained from the IME-free solution (Fig. 5-12 (a)), the size and distribution of the plate-like crystals were non-uniform. However, when IME was added, the plate-like crystals grew finely and uniformly over the entire surface with increasing the concentration of IME (Fig. 5-12 (d)).
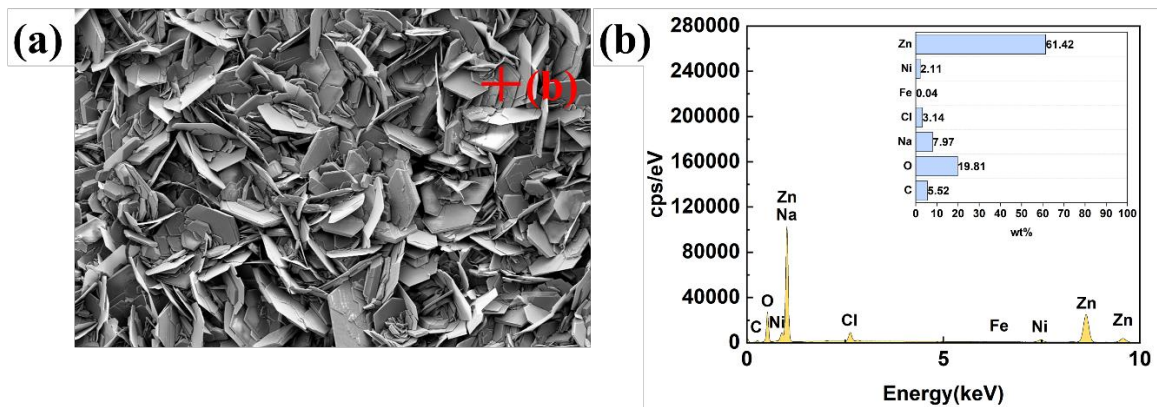

Fig. 5-11. SEM image and point analysis by EDX of the Zn-Ni alloy films deposited from solution containing 5 ml·dm^{-3} of IME after 24 h immersion in the 3 mass% aqueous NaCl solution.
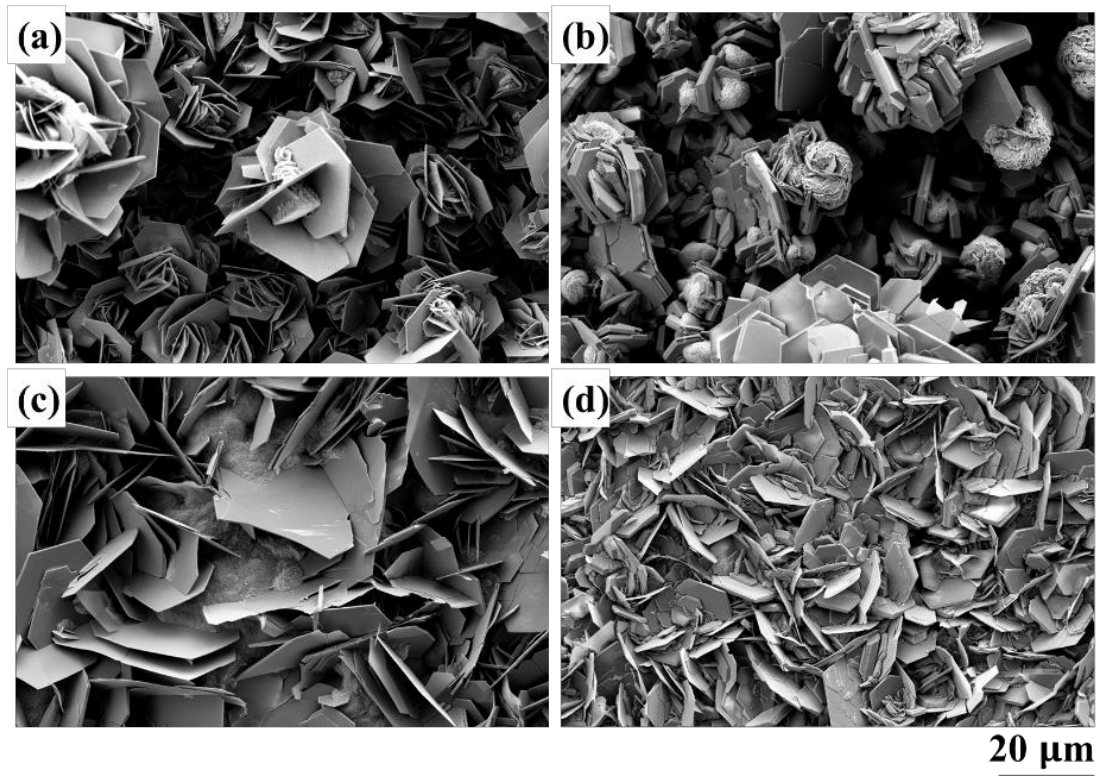
Fig. 5-12. SEM images of the surface of deposited Zn-Ni alloy films after 24 h immersion in the 3 mass% aqueous NaCl solution.
[(a) IME-free, (b) IME 1 ml·dm^{-3}, (c) IME 3 ml·dm^{-3}, (d) IME 5 ml·dm^{-3}]

5-3-4. Effect of IME on the Corrosion Resistance of Deposited Zn-Ni Alloy Films after Forming Corrosion Products

Figure 5-13 shows the polarization curve of deposited Zn-Ni alloy films after 24 h immersion in the 3 mass% aqueous NaCl solution. The corrosion potential of the films obtained from the solution without IME was approximately -1.07 V, but when IME was added, it greatly shifted to the noble one. This shows that the anodic reaction (dissolution reaction of films) is greatly suppressed by the addition of IME, even after 24 h immersion in the aqueous NaCl solution. In the films obtained from the solution containing 5 ml·dm^{-3} of IME, plate-like crystals of zinc chloride hydroxide ($Zn_5(OH)_8Cl_2 \cdot H_2O$) grew finely and uniformly on the entire surface after 24 h immersion in the 3 mass% aqueous NaCl solution (Fig. 5-12 (d)), which contribute toward suppressing the dissolution reaction of the deposition films.
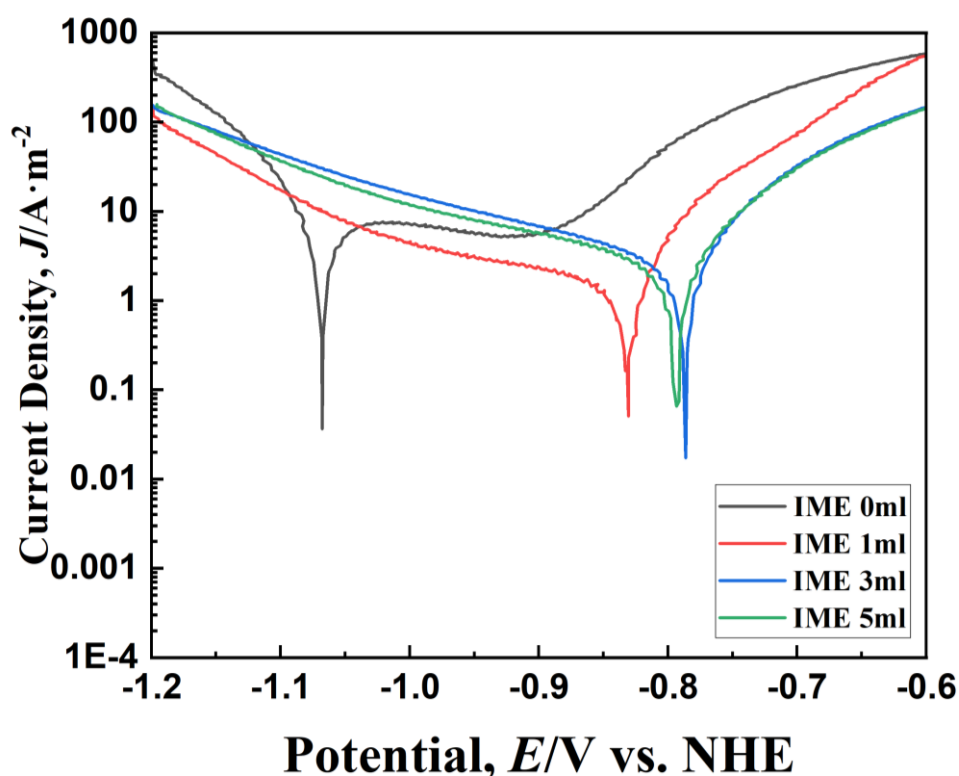
Fig. 5-13. Polarization curve of the deposited Zn-Ni alloy films after 24 h immersion in the 3 mass% aqueous NaCl solution.

5-4. Discussion

Based on these results, the effect of IME addition on the corrosion resistance of the deposited Zn-Ni alloy films was discussed. As shown in Figs. 5-1 and 5-2, the anodic reaction (dissolution reaction) of deposited Zn-Ni alloy films, in which no corrosion products were formed, was suppressed with IME addition. On the other hand, in the films obtained from the solutions containing IME, C resulting from IME codeposited as mentioned in chaper 4. The amount of co-deposited C was confirmed to increase with increasing the concentration of IME. The co-deposition of C was expected to increase the resistance of the films, as a result, it may have suppressed the anodic reaction of the deposited films.

In contrast, even in the films on which the corrosion products were formed after 24 h immersion in the 3 mass% aqueous NaCl solution, the anodic reaction was suppressed by IME addition (Fig. 5-13). This may be due to the formation of uniform corrosion products (zinc chloride hydroxide ($Zn_5(OH)_8Cl_2 \cdot H_2O$)) on the surface (Fig. 5-12(d)), in addition to the co-deposition of C. Zinc chloride hydroxide was uniformly formed on the films obtained from the solution containing 5 $ml \cdot dm^{-3}$ of IME because the surface of the films before immersion in the 3 mass% aqueous NaCl solution was smooth (Fig. 5-9(d)), and the anodic reaction was suppressed by the co-deposited C.

5-5. Conclusion

The effect of IME addition on the corrosion resistance of the deposited Zn-Ni alloy films was investigated using immersion tests in a 3 mass% aqueous NaCl solution, which is a typical environment containing chloride ions. In the deposited Zn-Ni alloy films without 24 h immersion in the 3 mass% aqueous NaCl solution, the anodic reaction was suppressed with IME and the corrosion potential shifted to noble direction. Even in the films on which the corrosion products were formed after 24 h immersion in the 3 mass% aqueous NaCl solution, the anodic reaction was suppressed by IME addition and the corrosion potential shifted to the noble side. The corrosion products which were zinc chloride hydroxide ($Zn_5(OH)_8Cl_2 \cdot H_2O$), were formed after 24 h immersion in the 3 mass% NaCl solution of Zn-Ni alloy films deposited with and without IME. The plate-like crystals of zinc chloride hydroxide formed on the Zn-Ni alloy films, which was obtained from the solution containing 5 ml·dm^{-3} of IME, were fine and uniform over the entire surface. In the films on which the corrosion products were formed after 24 h immersion in the 3 mass% aqueous NaCl solution, the suppression of anodic reaction with IME is attributed to the formation of uniform corrosion products (zinc chloride hydroxide) on the surface, in addition to the co-deposition of C.

5-6. References

1) V.Narasimhamurthy and L.H.Shivashankarappa: *J.Adv. Electrochem.*, **6**(2020), 188.
2) S.Anwar, Y.Zhang and F.Khan: *RSC Adv.*, **8**(2018), 28861.
3) C.Cachet, B.Saidani, and R.Wiart: *J. Electrochem. Soc.*, **138**(1991), 678.
4) A.Abibsi, J.K.Dennis and N.R.Short: *Trans. Inst. Met. Finish.*, **69**(1991), 145.
5) M.G.Hosseini, H.Ashassi-Sorkhabi and H.A.Y.Ghiasvand: *Surf. Coat. Technol.*, **202**(2008), 2897.
6) A.Brenner: Electrodeposition of Alloys, Vol. 2, Academic Press, New York, (1963), 194.
7) H.Fukushima, T.Akiyama, J.-h.Lee, M.Yamaguchi and K. Higashi: *J. Met. Finish. Soc. Jpn.*, **33**(1982), 574 (in Japanese).
8) H.Fukushima, T.Akiyama, M.Yano, T.Ishikawa and R.Kammel: *ISIJ Int.*, **33**(1993), 1009.
9) H.Nakano, S.Kobayashi, T.Akiyama, T.Tsuru and H Fukushima: *Tetsu-to-Hagane*, **89**(2003), 64 (in Japanese).
10) H.Nakano, M.Matsuno, S.Oue, M.Yano, S.Kobayashi and H.Fukushima: *J. Jpn. Inst. Met.*, **69**(2005), 548 (in Japanese).
11) Z.Feng, Q.Li, J.Zhang, P.Yang and M.An: *RSC Adv.*,**5**(2015), 58199.
12) L.M.Muresan, J.Eymard, D.Blejan and E.Indrea: *Stud. Univ. Babes-Bolyai Chem.*, (2010), No.1, 37.
13) G.Y.Li, J.S.Lian, L.Y.Niu and Z.H.Jiang: *Surf. Coat. Technol.*, **191**(2005), 59.
14) S.H.Mosavat, M.E.Bahrololoom and M.H.Shariat: *Appl. Surf. Sci.*, **257**(2011), 8311.
15) Z.Feng, L.Ren, J.Zhang, P.Yang and M.An: *RSC Adv.*, **6**(2016), 88469.
16) Z.Feng, D.Li, Q.Sun, L.Wang, P.Xing and M.An: *J. Alloy Compd.*, **765**(2018), 1026.
17) Z.Feng, D.Li, L.Wang, Q.Sun,P.Lu, P.Xing and M.An: *Ionics,***25**(2019), 1857.
18) S. Kavirajwar, S.Basavanna and K. Devendra: *Elctrochem. Sci. Adv.*, (2021)
19) S. Basavanna and Y. Arthoba Naik: *J. Appl. Electrochem.,* **41** (2011),535
20) A. Sakoda , N. Usuki, S. Wakano and M.Nishihara: *J. Surf. Finish. Soc. Jpn.*,**40**(1980) 164.

Chapter 6. Conclusion

Electrodeposited Zn–Ni alloy coatings are used for automobile parts, electric household products, and building materials owing to their superior corrosion resistance. Zn–Ni alloys are usually deposited in a sulfate or chloride solution; however, considering the throwing power on small parts, the use of a zincate solution is preferable. The brightening agents are usually added to zincate solutions for the electrodeposition of Zn-Ni alloys, unlike for sulfate and chloride solutions. In contrast, the solution temperature is an extremely important factor in electrodeposition, but the effect of solution temperature on the electrodeposition behavior of Zn-Ni alloys from zincate solutions has rarely been reported. Therefore, in this study, Zn-Ni alloy electrodeposition was performed in zincate solutions at different solution temperatures using IME as a brightener, and the respective and synergistic effects of IME and solution temperature on the electrodeposition behavior were discussed based on the partial polarization curves of Zn and Ni depositions and hydrogen evolution, appearance, and microstructure of the electrodeposited films.

In Chapter 1, with respect to the background of this study as mentioned above, the previous studies on the deposition behavior of Zn-Ni alloys, and the mechanism of brightening agents, and the purpose and structure of this thesis were described.

In Chapter 2, the effect of the reaction product of epichlorohydrin and imidazole (IME) on the deposition behavior of Zn–Ni alloys was investigated using polarization curves for the Zn and Ni depositions and hydrogen evolution. The IME was used as the brightener. The transition current density at which the deposition behavior shifted from the normal type to anomalous was $50-100$ $A \cdot m^{-2}$ in the IME-free solution; it became $10-20$ $A \cdot m^{-2}$ with the addition of the IME, indicating that the IME greatly decreased the transition current density. The transition current density corresponds to the current density at which the potential of the total polarization curve significantly shifts from the more noble region than the equilibrium potential of Zn to the less noble region. With the addition of the IME, the decrease in transition current density was attributed to the suppression of hydrogen evolution, and the current efficiency for the alloy deposition in the high-current-density region decreased due to the suppression of both the Zn and Ni depositions. The Ni content of the deposited films decreased with the IME, indicating that Ni deposition was more suppressed by the IME than Zn deposition. With increasing current density, the crystals of the films deposited from the IME-containing solution became smooth and showed significant brightness. The oxidation reaction of the films deposited from the IME-containing solution was suppressed. Consequently, the corrosion potential shifted to the noble direction with the IME.

In Chapter 3, the effect of solution temperature on the deposition behavior of Zn–Ni alloys from alkaline zincate solutions was investigated. The

transition current density at which the deposition behavior shifted from the normal to anomalous co-deposition was almost identical at solution temperatures of 293 and 313 K but clearly increased at 333 K. The transition current density appeared to increase due to the enhancement of H_2 evolution and Ni deposition at 333 K. The current efficiency for alloy deposition also increased with increasing solution temperature in both the normal ($10-50$ A$\cdot$m^{-2}) and anomalous (500 A$\cdot$m^{-2}) co-deposition regions. In the normal co-deposition region, Ni deposition and H_2 evolution mainly occurred, and the promoting effect of increase in the solution temperature on the Ni deposition was greater than that on the H_2 evolution, resulting in an increase in current efficiency alongside solution temperature. In the anomalous co-deposition region at 500 A$\cdot$m^{-2}, Zn deposition and H_2 evolution mainly occurred, and Zn deposition appeared to proceed under a mixed rate-determining process comprising the charge transfer and diffusion of Zn ions. Since the diffusion of Zn ions is promoted by increasing the solution temperature, the current efficiency also seems to increase. Furthermore, the Ni content in the deposited films increased with the solution temperature at all current densities. In the region where the charge transfer process is rate-limiting, Ni deposition accelerates to a greater degree compared with Zn deposition alongside increasing solution temperature, as a result, Ni content in the deposited films seems to increase. In addition, the γ-phase of the deposited films increased with an increasing solution temperature.

In Chapter 4, the synergistic effect of IEM and solution temperature on the deposition behavior of Zn–Ni alloy from alkaline zincate solutions was investigated. The transition current density, at which the deposition behavior shifted from the normal to anomalous type decreased with the addition of IME at 293 K but did not change regardless of IME addition at 313 K and 333 K. This indicates that the inhibitory effect of IME on the hydrogen evolution decreases with increasing the solution temperature. The suppression effect of IME on the Zn and Ni depositions during the alloy deposition was observed at 293 K, while at 313 K and 333 K, the suppression effect was decreased on the Zn deposition, though maintained on the Ni deposition. Therefore, Ni content in the deposits significantly decreased with IME as the temperature increased. The current efficiency for Zn deposition significantly decreased with IME at 293 K, while decreasing insignificantly at 313 K and 333 K. The C content in the deposits was the highest at 293 K, and decreased with the increasing solution temperature, indicating that the adsorption ability of IME on the cathode decreases with the increasing temperature. As a result, the suppression effect of IME on the Zn deposition seems to decrease with increasing the temperature. The gloss of the deposited films was the highest at 293 K, attributed to the adsorption ability of IME being large at 293 K and deposited films with fine crystals becoming smooth.

In Chapter 5, the effect of IME addition on the corrosion resistance of the deposited Zn-Ni alloy films was investigated using immersion tests in a 3 mass% aqueous NaCl solution, which is a typical environment containing chloride

ions. In the deposited Zn-Ni alloy films without 24 h immersion in the 3 mass% aqueous NaCl solution, the anodic reaction was suppressed with IME and the corrosion potential shifted to noble direction. Even in the films on which the corrosion products were formed after 24 h immersion in the 3 mass% aqueous NaCl solution, the anodic reaction was suppressed by IME addition and the corrosion potential shifted to the noble side. The corrosion products which were zinc chloride hydroxide ($Zn_5(OH)_8Cl_2 \cdot H_2O$), were formed after 24 h immersion in the 3 mass% NaCl solution of Zn-Ni alloy films deposited with and without IME. The plate-like crystals of zinc chloride hydroxide formed on the Zn-Ni alloy films, which was obtained from the solution containing 5 ml·dm^{-3} of IME, were fine and uniform over the entire surface. In the films on which the corrosion products were formed after 24 h immersion in the 3 mass% aqueous NaCl solution, the suppression of anodic reaction with IME is attributed to the formation of uniform corrosion products (zinc chloride hydroxide) on the surface, in addition to the co-deposition of C.

Acknowledgments

令和4年

BAE SEONGHWA (裵聖和)